PETROGRAPHIC AND MICROFACIES ANALYSIS OF THE SHUBLIK FORMATION, NORTHERN ALASKA: IMPLICATIONS FOR AN UNCONVENTIONAL RESOURCE SYSTEM

By

April Rae Knox, B.S.

A Thesis Submitted in Partial Fulfillment of the Requirements

for the Degree of

MASTER OF SCIENCE

in

Geology

University of Alaska Fairbanks

August 2018

APPROVED:

Dr. Michael Whalen, Committee Chair

Dr. Catherine Hanks, Committee Member

Marwan Wartes, Committee Member

Dr. Paul McCarthy, Chair

Department of Geosciences

Dr. Anupma Prakash, Interim Dean

College of Natural Science and Mathematics

Dr. Michael Castellini

Dean of Graduate School

Abstract

The North Slope of Alaska includes a world-class conventional petroleum system that has been producing for approximately 40 years. While the regional stratigraphy includes multiple proven source and reservoir rocks, the Middle to Upper Triassic Shublik Formation (Fm.) is the most prolific. The decline in conventional hydrocarbon production on the North Slope and the presence of high quality source rocks inspire the evaluation of the Shublik Fm. as an unconventional petroleum system where oil or gas are produced directly from source rocks.

The Shublik Fm. is a heterogeneous calcareous shale and limestone interval that has been interpreted to indicate deposition influenced by marine upwelling. Lithofacies observed in outcrop consist of intervals of non-resistant organic-rich packages that are interbedded with resistant coarsening upward rhythmic depositional successions of phosphatic and carbonate parasequences.

The heterogenous characteristics of the microfacies is one of the challenges in the unconventional exploration of the Shublik Fm. Detailed microfacies descriptions, as part of this study, document the complex lithologies and identify patterns in the occurrence of the microfacies. Microfacies descriptions are the building blocks to identify stacking patterns that define the parasequences. The parasequences observed in core, outcrop, and petrographic analysis are calibrated to well logs to map relevant stratigraphic intervals on a regional scale.

A targeted interval for the unconventional exploration of the Shublik Fm. is identified using a relative brittleness index. Flat clam and phosphatic parasequences are the

primary packages present within the targeted interval. The parasequences are comprised of small-scale brittle and ductile couplets.

High resolution pore imaging and mechanical stratigraphy characteristics are documented within the interval. Pore types and networks provide potential storage and migration pathways within unconventional resource systems. Pore types were imaged at a high resolution using scanning electron microscopy. Pore types that are present within the Shublik Fm. include interparticle, intraparticle, porous floccules, moldic, microfracture, and microchannel. The phosphatic limestone facies contains the greatest amount of porosity including interparticle, intraparticle, and moldic within the phosphate nodules and matrix and fractures surrounding phosphate nodules. Microfracture, microchannel, and intraparticle porosity are the primary pore types within the flat clam facies.

Mechanical stratigraphy has a direct impact on the success of hydraulic fracturing. The microfacies descriptions identify laminae scale mechanical stratigraphy characteristics which include erosional surfaces, laminations, graded bedding, mineralogical variation, and textural anisotropy and isotropy.

A regional correlation of the targeted interval was developed building upon previous work and utilizing sequence stratigraphic models. Significant parasequence surfaces are readily identified in the well log signatures.

The challenge of the heterogeneity of the Shublik Fm. is simplified first by identifying a targeted interval consisting of brittle and ductile packages enriched in TOC. Then recognizing the parasequences contained as part of the interval which include

significant characteristics pertaining to pore networks and mechanical stratigraphy. Combining methods and results of this study provides an important component to evaluating the Shublik Fm. as a potential unconventional resource system.

Table of Contents

List of Figures

List of Tables

List of Appendices

Acknowledgements

This project would not have been possible without guidance and financial support from the following individuals and organizations. Foremost, I would like to thank my academic advisor Dr. Michael Whalen for his dedication, academic support, and intellectual guidance while I completed the requirements for my graduate degree and thesis. Also, my committee members Dr. Cathy Hanks and Marwan Wartes for their continued patience and availability. This project was funded in part by The University of Alaska Fairbanks (UAF) by way of teaching assistantship and by the Department of Natural Resources, Alaska's Division of Geological and Geophysical Surveys (DGGS) who provided funding for helicopter supported fieldwork and a research assistantship. This project would not have been possible without UAF's Advanced Instrumentation Laboratories (AIL). Thank you, Karen Spaleta and Ken Severin for teaching me how to approach the questions that I wanted to answer and designing a successful analytical routine. Thank you to Great Bear Petroleum, Ed Duncan, and Allegra Hosford Scheirer for allowing access to the Merak core for description and thin sections. I'd also want to thank David Houseknecht, Kate Whidden, Julie Dumoulin, and William Rouse of the United States Geological Survey (USGS) for providing thin sections, collaboration, spectral gamma ray, and being available. Thanks to Eric Hutton who passed on the data he had compiled during his thesis study of the Shublik Fm. Thank you to Dr. Nilesh Dixit for technical support with the SMT Kingdom program. I am honored to have received grants and scholarships awarded by the following organizations, American Association of Petroleum Geologists (AAPG) Grants in Aid, Alaska Geologic Society, Association of Women Geoscientists, and Pacific Section AAPG. Finally, this project

would not have been possible without the unending support from my children and family. Thank you.

Chapter 1

Introduction

Northern Alaska includes one of the most prolific petroleum provinces in the United States (Houseknecht and Bird, 2005), and has been producing petroleum conventionally for approximately 40 years (Scheirer et al., 2014). In recent years, North Slope production has declined. In northern Alaska, there are multiple proven source and reservoir intervals, primarily in Paleozoic and Mesozoic rocks (Peters et al., 2006; Houseknecht and Bird, 2005). This decline in conventional hydrocarbon production and the presence of high quality source rocks have led to the evaluation of these intervals as possible unconventional petroleum systems (Scheirer et al., 2014). Not all unconventional systems are shale resource plays.

The primary source rocks on the North Slope include the Triassic Shublik Formation (Fm.); Jurassic Kingak Shale; and two Cretaceous units, the Kalubik Fm., also informally called the pebble shale, and the Hue Shale (Figure 2) (Scheirer et al., 2014; Houseknecht et al., 2012). In 2012, the USGS completed an assessment of potential undiscovered shale-oil and shale-gas on the North Slope and reported the possibility of 0-2 billion barrels of oil (Houseknecht et al., 2012).

The Shublik Fm. is a heterogeneous, calcareous, organic-rich interval, and has been interpreted as having been deposited under the influence of marine upwelling (Parrish et al., 2001a; Parrish et al., 2001b; Kelly et al., 2007). Shublik Fm. lithofacies include phosphatic silt and sandstones, nodular phosphorites, organic-rich mudstones, packstones, grainstones, and glauconitic and non-glauconitic sandstones (Kelly et al.,

2007), all with varying levels of organic content and different mechanical properties. The facies are commonly stacked in coarsening upward packages or parasequences. Considering the complexity of the heterogenous lithologies in the Shublik Fm., it is necessary to identify the optimal shale-oil producible facies based on source and reservoir rock characteristics.

The goal of this paper is to evaluate the Triassic Shublik Fm.as an unconventional resource system by identifying a target interval for hydraulic fracturing. This study provides new information on the types of pores and pore networks that are present within the target. A thorough examination of the complex microfacies provide building blocks for the parasequences and detailed descriptions of the variety of mechanical stratigraphy characteristics and pore types and networks present within the target interval. The parasequences are successfully identified in well log signature and correlated in a regional context.

Starting with the “big picture”, this project identifies an interval to focus on and transitions to higher level of detail within that interval which is ultimately applied to create a detailed regional correlation.

Chapter 2[1]

The Shublik Formation, northern Alaska: Implications for an Unconventional Resource System

2.1 Geologic Setting

Alaska has a complex geologic history (Moore et al., 1994). Together the Brooks Range and the North Slope encompass northern Alaska (Figure 1). The Brooks Range is a fold and thrust belt that extends east to west along the southern margin of northern Alaska with highest elevation in the east. The North Slope includes the arctic coastal plain and foothills. The gently rolling arctic foothills border the Brooks Range to the south and decrease in elevation towards the north where they meet the arctic coastal plain. The arctic coastal plain is marshy and slopes to the Arctic Ocean. The Barrow Arch (Figure 1) is a structural high that trends northwest/southeast near the northern coast of Alaska.

Northern Alaska is composed of two lithotectonic terranes: the Angayucham and Arctic Alaska terranes. The North Slope subterrane, as described by Moore et al. (1994), is the largest of the six subterranes within Arctic Alaska and has undergone the least amount of deformation. It is the most thoroughly studied because of its petroleum resources. The North Slope subterrane includes mainly sedimentary rocks and can be divided into three depositional sequences: the Ellesmerian, Beaufortian, and the Brookian sequences that document distinct plate tectonic episodes (Figure 2) (Hubbard

[1] To be submitted as Knox, A. R., and Whalen, M. T., 2018, Petrographic and microfacies analysis of the Shublik Fm. northern Alaska: Implications for an unconventional resource system: AAPG Bulletin.

et al., 1987; Moore et al., 1994). These rocks sit atop Proterozoic to Devonian metasedimentary and metavolcanic rocks of the Franklinian basement.

The Ellesmerian sequence (355-215 Myr) (Figure 2) contains the primary petroleum systems of northern Alaska (Bird and Molenaar, 1987; Peters et al., 2006). The Ellesmerian sequence records deposition on a subsiding, south facing continental margin (present day coordinates). This sequence is extensive across the full east-west extent of the North Slope and thins toward the south (Moore et al., 1994). It contains three, 2nd order, transgressive-regressive cycles, recording both marine and non-marine environments, is up to 900 m thick in the Sadlerochit Mountains, and is divided into lower, middle, and upper megasequences (Bird and Molenaar, 1987; Moore et al., 1994). The lower Ellesmerian stratigraphy (Figure 2) in the northeastern Brooks Range comprises the Mississippian to Carboniferous Endicott and Lisburne groups, the middle Ellesmerian includes the Permo-Triassic Sadlerochit Group., and the upper Ellesmerian contains the Triassic Shublik Fm. and the Karen Creek Sandstone (Bird and Molenaar, 1987).

The overlying Jurassic and Lower Cretaceous Kingak Shale, Kemik Sandstone, and Pebble Shale unit make up the Beaufortian plate sequence (Hubbard et al., 1987). According to Hubbard et al., (1987), the Beaufortian plate sequence (215-113 Myr) (Figure 2) records a rifting episode that ultimately led to the opening of the Canada Basin. Opening of the Canada basin cut off the northern landmass that was the source of sediments during deposition of the Ellesmerian sequence. The overlying Cretaceous Brookian sequence was sourced from the rising Brooks Range to the south. Deposits of

the Brookian and Beaufortian sequences buried the Ellesmerian into the hydrocarbon generation window (Houseknecht and Bird, 2006).

2.2 Shublik Formation

The Shublik Fm. is Middle to Upper Triassic in age and part of the upper Ellesmerian megasequence (Figure 2) (Detterman et al., 1975; Hubbard et al., 1987). The Shublik Fm. outcrops in a narrow strip on the north flank of the Brooks Range in the Sadlerochit and Shublik Mountains where it is exposed in structurally uplifted thrust sheets (Figure 1) (Moore et al., 1994). The Shublik Fm. thickness varies from 1-173 m in the subsurface to 36-161 m in outcrop (Detterman et al., 1975; Detterman, 1989; Kupecz, 1995; Peters et al., 2006; Kelly et al., 2007).

At Fire Creek, (Figure 3) the Shublik Fm. is 145 m thick, conformably overlies the Fire Creek Siltstone, and is conformably overlain by the Karen Creek Sandstone (Detterman et al., 1975). The upper Shublik Fm. true thickness is difficult to measure at Fire Creek because of an extensive covered interval and folding resulting in structural thickening (Hutton, 2014). The Fire Creek outcrop is unique because both upper and lower contacts are exposed (Detterman et al., 1975). At Prudhoe Bay, the Shublik Fm. overlies the Eileen Sandstone which is the equivalent of the Fire Creek Siltstone and is overlain by the Sag River Sandstone equivalent of the Karen Creek Sandstone (Hulm, 1999; Parrish et al., 2001b).

The Shublik was sourced from the north along a passive continental margin interpreted as a zone of coastal upwelling (Moore et al., 1994; Kupecz, 1995; Parrish et al., 2001a; Kelly et al., 2007). The formation exhibits lateral and vertical facies variation (Kelly et al.,

2007) (Figures 1&3). To the north and east it's lithology is dominated by siltstone and sandstone, and across the central and southern area transitions to limestone and mudstones (Parrish et al., 2001a). The Shublik nearly pinches out over the Barrow Arch, dips south and thickens toward the foothills of the Brooks Range (Parrish et al., 2001a; Parrish et al., 2001b; Kelly et al., 2007).

The Shublik Fm. (Figure 3) contains lithofacies that are observed in modern zones of upwelling (Parrish et al., 2001a; Parrish et al., 2001b). Upwelling zones are characterized by high biological productivity where organic-rich deposits are preserved and may form petroleum source rocks (Parrish, 1982; Kupecz, 1995; Parrish et al., 2001b; Piper and Link, 2002).Depositional facies that are characteristic of modern upwelling zones are organic-rich facies, phosphatic deposits and "fringed" by glauconitic facies (Figure 1) (Parrish et al., 2001a). The Miocene Monterey Fm. of California and the Permian Phosphoria Fm. are both interpreted as ancient upwelling zone deposits that record this type of depositional pattern (Parrish et al., 2001a).

2.2.1 Shublik Formation Zones

Kupecz (1995) divided the Shublik Fm. In the subsurface of Prudhoe Bay into the four zones, A-D (Figure 3), based on lithological characteristics and gamma ray response. Starting at the base of the Shublik Fm., zone D is characterized within the Prudhoe Bay area as massive bedded, fine-medium grained phosphatic sandstone. Outside of the Prudhoe Bay area, zone D is composed of phosphatic sandstone and siltstone, calcareous shale, and bioclastic limestone, with phosphatic components (Kupecz, 1995; Hulm, 1999; Parrish et al., 2001b; Kelly et al., 2007).

In the subsurface, zone C is characterized as fossiliferous, organic-rich black shale grading up into dark to light gray limestone (Kupecz, 1995; Parrish et al., 2001b) dominated by the flat clam *Halobia* (Dingus, 1984). Toward the northeast, zone C contains greater amounts of siliciclastics (Hulm, 1999). At Fire Creek, zone C is dominated by siltstones, sandy phosphorites, lime wackestones and packstones, and silty micrite (Kelly et al., 2007).

Zone B in the subsurface contains nodular and pelletal phosphorite (Hulm, 1999), phosphatic carbonates interlaminated with shale, phosphatic shales and siltstones, and oolitic packstones and grainstones (Kupecz, 1995). At Fire Creek, zone B is composed of phosphatic and bioclastic wackestone and packstones, silty argillaceous limestones, and siltstones (Kelly et al., 2007). Zone B is easily distinguished from zones A and C on gamma ray logs because it is phosphatic and uranium rich (Kupecz, 1995).

Zone A is similar to zone C and is characterised as black shale at the base that grades up to dark gray limestone (Kupecz, 1995; Parrish et al., 2001b). The flat clam *Monotis* is present in Zone A as compared to *Halobia* in Zone C (Dingus, 1984). Zone A coarsens and becomes more siliciclastic toward the northeast (Hulm, 1999).

2.2.2 Sequence Stratigraphy

Sequence stratigraphic evaluation of the Shublik Fm. began with Kupecz (1995) and was refined by Robison et al. (1996), Hulm (1999), Kelly et al. (2007), and Hutton (2014). Kupecz (1995) utilized subsurface well and core data from the Prudhoe Bay field unit to interpret the depositional setting, sequence stratigraphy, diagenesis, and reservoir potential for the Shublik Fm.

Kupecz (1995) interpreted 2 depositional sequences. The base of sequence 1 is marked by the contact between the Ivishak and Shublik Fm. The upper contact is within zone C at the transition from shale to interbedded shale and limestone. The upper contact of sequence 2 is the contact of the Shublik Fm. and the Sag River Sandstone (Karen Creek Sandstone equivalent). Robinson et al. (1996) used a detailed core investigation of the Tenneco Phoenix #1 well in the sequence stratigraphic analysis of the Shublik. This core is a continuous core through the Shublik Fm. and also includes the Eileen Sandstone (Fire Creek Siltstone equivalent) and the Ivishak Fm. Robinson et al. (1996) interpreted the entire succession as a single depositional sequence. The contact between the Ivishak Fm. and Eileen Sandstone is the lower boundary and the upper boundary is the contact of the Shublik Fm. and the Sag River Sandstone (Robinson et al., 1996).

A more detailed sequence stratigraphic interpretation was later developed by Hulm (1999). He utilized subsurface data, conventional core description, thin sections, and facies architecture to build a stratigraphic framework and interpretation of the sequence stratigraphy of the Shublik Fm., Eileen Sandstone (Fire Creek Siltstone equivalent), and Sag River Sandstone (Karen Creek Sandstone equivalent) in a regional context. Hulm (1999) interpreted two complete 3rd ordered depositional sequences and a partial third sequence that included a lowstand and transgressive system tract.

Kelly (2004) and Kelly et al. (2007) built upon Hulm's (1999) subsurface investigation and extended it to the Fire Creek outcrop and the Shublik Fm.'s distal equivalent, the Otuk Fm. at Tiglukpuk Creek and Atigun Gorge to the west (Figure 1). Kelly et al. (2007)

interpreted three full 3rd order depositional sequences including the Fire Creek Siltstone, Shublik Fm., Karen Creek Sandstone and Otuk Fm. equivalents.

Kelly et al. (2007) suggested the possibility of an additional sequence nested within sequence 2 and Hutton (2014) built on that, subdividing sequence 2, resulting in a total of four depositional sequences (Figure 3). Hutton (2014) combined subsurface and outcrop lithostratigraphy, sequence stratigraphy, chemostratigraphy, and petrography from high-resolution sampling conducted at the Fire Creek outcrop to refine the previous sequence stratigraphic interpretations. He correlated the four sequences and generated regional isochore maps (Figure 4) of the 4 sequences using data from 97 industry wells.

Kelly et al. (2007) and Hutton (2014) interpreted the sequence stratigraphy by identifying transgressive systems tracts (TST) and highland systems tracts (HST) through analysis of facies stacking patterns. The sequence boundaries are defined by abrupt facies changes with transgressive surfaces where the coarser grained HST is abruptly overlain by a TST with finer grained deposits indicating deepening events. The maximum flooding surfaces were chosen based on change from fining upward to coarsening upward trends. Identification of systems tract boundaries is less obvious in more distal localities as facies changes become less pronounced.

Sequence 1 is composed of the Fire Creek Siltstone and zone D (Figure 3) and ranges in thickness from 0 to 90 m (Figure 4A) (Kelly et al., 2007; Hutton 2014). Sequence 1 thins over the Mikkelson high and pinches out over the Barrow high, is generally thin (5-10 m) proximal to the Colville High, Fish Creek Platform, and along the Barrow arch and thickens towards the south-southwest (Hutton, 2014).

The base of sequence 1 overlies the Ledge Sandstone and is documented by an erosional surface overlain by a chert pebble conglomerate interpreted as a transgressive lag deposit (Kelly et al., 2007). The Fire Creek Siltstone represents the TST and two shoaling upward parasequences are observed within the HST within zone D of the Shublik Fm. and are interpreted as subtidal shelf deposits (Kelly et al., 2007). The upper sequence boundary is a transgressive surface interpreted as a regional flooding surface.

According to Hutton (2014), sequence 2 contains zone C and part of zone D (Figure 3), and the thickness varies from 0 - ~40 m (Figure 4B). Over the Barrow and Mikkelson Highs, sequence 2 pinches out; and becomes thinner at the Fish Creek Platform, Collville High, Prudhoe Bay, and to the southwest. The thickest occurrence of sequence 2 is south of Prudhoe Bay along a northwest/southeast trend.

The TST of sequence 2 is interpreted as reworked inner shelf sediments. The base of sequence 2 contains fining upward packages that indicate deepening. The MFS is identified by a positive shift in gamma ray and overlain by massive carbonate and sandstone deposits of the HST marking the initiation of a carbonate ramp (Kelly et al., 2007). The upper sequence 2 boundary is identified by a positive shift in the gamma ray, and the deposition of organic rich mudstones (Kelly et al., 2007).

Sequence 3 (Figure 4C) exhibits a general thickness of ~15-30m and contains the remaining Zone C (Figure 3) (Hutton, 2014). This sequence is the thickest in the northwest, up to ~30m, and thins to zero at Mikkelson High. In contrast to sequences 1 and 2, sequence 3 thickens over the Fish Creek Platform (Hutton, 2014).

Two progradational parasequences containing phosphatic and organic rich facies are documented in sequence 3 at the Fire Creek outcrop and have been interpreted as distal deposits on an outer-ramp (Hutton, 2014). The upper sequence boundary is characterized by an immediate depositional change from phosphatic limestone to laminated siltstone (Kelly, 2004). At Fire Creek, the boundary between sequence 3 and 4 is observed by a change in grain size indicating a deepening and a TST (Kelly et al., 2007).

Sequence 4 (Figure 4D) varies in thickness (0- ~ 180 m) and consists of Zone A of the Shublik Fm. and the Karen Creek Sandstone (Figure 3). Sequence 4 is thickest southeast of the Barrow High and becomes significantly thinner to the east-southeast. At Fire Creek, sequence 4 is ~45 m and ~60 m in the Phoenix well. It pinches out over the Mikkelson High (Hutton, 2014). The TST of sequence 4 contains condensed intervals indicating episodes of non-deposition (Kelly et al., 2007). The HST and deposition of the Karen Creek Sandstone records a significant marine regression (Hutton, 2014). The upper boundary of Sequence 4 is a transgressive surface at the top of the Karen Creek Sandstone overlain by the Jurassic Kingak Shale.

2.3 Data

A combination of new and existing data was collected and integrated respectively for this study. New data includes field stratigraphic data, detailed core logging, thin section descriptions, X-ray fluorescence spectrometry (XRF) elemental analysis, and high-resolution backscatter electron (BSE) imaging. Existing data includes well logs, organic and inorganic geochemistry (Appendix A-F), and sequence stratigraphy.

Rock-Eval data is available from Tenneco Phoenix #1 well (Appendix F), Merak #1V and Alcor #1, and one sample from Fire Creek where 67 samples were collected for total organic carbon (TOC) analyses (Kelly, 2004)(Appendix A). Hutton (2014) outlined results from 34 additional TOC analyses from his high-resolution sampling at Fire Creek

33 industry wells were utilized for regional correlation (Table 3).

2.4 Methods

2.4.1 Field Sampling/Core Description

During the 2014 field season (Figure 1) three stratigraphic sections of the Shublik Fm. were examined in the northeastern Brooks Range. High-resolution sampling was conducted at Fire Creek, in the Shublik Mountains, within Arctic National Wildlife Refuge (ANWR) (Figure 1C; Table 1), and at two new sections: Last Creek (Figure 1D; Table 1) in ANWR and Kavik Creek (Figure 1E; Table 1) outside of ANWR to the west. At Last Creek (Figure 1D; Table 1) the Shublik Fm. conformably overlies the Fire Creek siltstone, is truncated by the Lower Cretaceous unconformity (LCu) and is unconformably overlain by the Kemik Sandstone (SS). At Kavik Creek (Figure 1E; Table 1) the Shublik Fm. is structurally complex and is not a complete section.

A Jacob's staff was used to measure stratigraphic sections and samples were collected to document rock type, bedding, mineralogy, and other significant characteristics. Intervals that exhibited greater heterogeneity were sampled at a higher resolution (< 1m) and homogeneous sections more coarsely. The hand samples were used to make thin sections and for geochemical analyses. Detailed field and core descriptions documented lithology, grain size, color, sedimentary structures, fossils, biogenic

evidence, rhythmic bedding packages, and color variations. The weathering profile was documented from outcrop sections. The descriptions were used to draft new stratigraphic sections for Kavik Creek, Last Creek (Figure 12D), and the Merak core (Figure 12B).

Industry cores examined for this project include the Phoenix Tenneco #1(Figure 1A; Table 1) and two, previously undescribed, cores from Great Bear Petroleum, Merak #1, and Alcor #1 (Figure 1B; Table 1). These cores are important because they record both upper and lower contacts of the Shublik Fm.

Merak #1V is located 34km south of Prudhoe Bay (Figure 1B; Table 1). 52.27 meters of core was described through the Eileen Sandstone, Shublik Fm., and Sag River Sandstone as part of this study.

The Phoenix well (Figure 1A; Table 1) was drilled in 1986 by the Tenneco Oil Company and is located on the north side of the Barrow Arch.

2.4.2 Petrography

Petrographic techniques used to analyze thin sections included traditional approaches integrated with electron microscopy at UAF's Advanced Instrumentation Laboratory (AIL). 174 thin sections from the base of the Eileen SS through the Sag River SS were described using standard thin section petrography for the microfacies analysis and interpretation of the depositional environments. 21 of the described thin sections were selected within the targeted interval and were further analyzed with the scanning electron microscope (SEM) for high-resolution pore imaging, mineralogy, and elemental phase mapping.

Proportions of individual components in thin section were estimated using the comparison charts of Baccelle and Bosellini (1965). Observations were also recorded concerning organic material, pore type and location, matrix, cement, sedimentary structures, and textures. Bioturbation was documented and assigned an ichnofabric index (ii) with a range of 1-5 depending on the amount that the sedimentary fabric was disrupted by bioturbation (Droser and Bottjer, 1986,1989). The carbonate rocks were classified based on Dunham (1962) and Embry and Klovan (1971) schemes. The phosphatic components were classified according to Föllmi (1996) and using a modified Dunham (1962) and Embry and Klovan (1971) classification. The fine-grained mudrock facies were described according to the approach of MacQuaker and Adams (2003).

2.4.3 Electron Microscopy

Back-scatter electron images (BSE) and elemental phase maps were generated with the JEOL JXA8530F Electron Microprobe at the AIL. The microprobe has a field emission electron source making it ideal for scanning election microscopy (FE-SEM). The microprobe is equipped with a Thermo Noran System 7 SDD- Energy dispersive detector (EDS). Spectral and Electron Imaging were acquired using the EDS system.

Ultra-thin sections (~20 µm thick), polished to an analytical surface, were examined at a high-resolution Samples were examined using an accelerating voltage of 15-20 kV, with a working distance of approximately 11.00 mm, and magnifications of up to x3300. Pores were identified by the value of darkness with respect to the grey scale of the BSE with the blackest areas interpreted as pore space. Areas that appeared to have been mechanically plucked out as a result of polishing and sampling were disregarded and

not considered pore space. The classification of pores was based on approaches by Loucks et al. (2012), Slatt and O'Brien (2011), and Slatt (2013).

X-ray maps differentiate the chemical composition of individual grains and provide a visual tool for identifying grains that are difficult to be imaged using the SEM alone. This type of microscopic technique helps to image the distribution of mineral components in a thin section (White et al., 1984; Milliken and Reed, 2010; Milliken et al., 2012).

2.4.4 Geochemical Analyses

Hand samples collected in the field were analyzed for whole rock major element data on fresh surfaces using a handheld Oxford X-MET5100 XRF at Alaska's Division of Geological and Geophysical Survey (DGGS). 42 samples were analyzed from Last Creek and 68 from Kavik Creek (Appendix C&D). The results from Last Creek aided in the correlation process.

2.4.5 Relative Brittleness Index (RBi)

Successful unconventional resource exploration requires targeting relatively thin, laterally extensive stratigraphic horizons that exhibit fracture-prone and organic-enriched qualities (Wright et al., 2010; Ratcliffe et al., 2012). Fracture-prone brittle intervals are necessary to provide the migration pathways for the hydrocarbons (Slatt, 2013). Jarvie et al., (2007) utilized proportions of total clay, quartz, and carbonate to identify likely intervals for brittle and ductile prone facies. Ratcliffe et al. (2012) demonstrated that whole rock inorganic geochemical data can be used to approximate the relative brittleness of a stratigraphic succession. The RBi is used as a visual tool to identify where the more facture prone intervals are located within the stratigraphic

column (Ratcliffe et. al., 2012). Ductility is controlled by the clay content and brittle prone facies are enriched with respect to calcite and silica (Jarvie et al., 2007; Ratcliffe et al., 2012). A RBi was generated (Figure 5) for this project using existing geochemical data from Phoenix #1 well (Appendix E) and Fire Creek outcrop (Appendix A&B).

2.4.6 Well Log Correlation

33 industry wells (Table 3) were incorporated into this study for regional correlation of the target interval. IHS Kingdom software was used to interpret the well logs. Alaska's Geologic Materials Center (GMC) *Formation Tops Inventory by Well* document was used to identify the top of the Sag River Sandstone, Shublik Fm., Fire Creek Siltstone, and the Ledge Sandstone (Johnson et al., 2010). Bird's picks from 2006 were applied unless the formation tops had been updated in 2010 by Alaska Oil and Gas Conservation Commission (AOGCC)(Johnson et al., 2010). Each of the 4 depositional sequences (Hutton, 2014) was then interpreted in all wells using their gamma ray signatures. The targeted interval gamma ray characteristics were correlated regionally from the Merak #1 well to other industry wells (Figure 19).

2.5 Unconventional Resource System

Unconventional resource systems include shale-oil and gas, tight sand, and coal-bed methane (Haskett and Brown, 2005). The following overview of a shale-oil unconventional resource system is according to Jarvie (2012b). A shale-oil resource system consists of organic-rich, fine-grained sedimentary rocks that have generated and stored oil. The oil may have migrated to a bed that is not organic-rich and is interbedded or next to the organic-rich interval. Organic-rich, carbonate, siliceous, and

calcareous fine-grained intervals usually serve as both the source and reservoir components. There are three classifications for shale-oil resource systems with criteria based on organic richness and lithological characteristics; tight shale, fractured shale, and hybrid shale. Tight shale systems are characterized by fine-grained, organic-rich rocks that lack open fractures, while fractured shale systems contain an open network of natural fractures. Hybrid systems contain both organic-rich and organic-lean facies that are interbedded. The Mississippian Barnett Shale produces nearly exclusively from tight organic-rich mudstone while the Miocene Monterey Formation produces from shale that has open fractures. The Cretaceous Eagle Ford Shale system is predominately a hybrid system, and the Devonian Bakken Shale is classified as both a hybrid and fractured shale-oil system due to the distribution and characteristics of the source rock intervals and interbedded lithofacies. For over 100 years, fractured shale-oil systems have been exploited and produced. The greatest untapped resource potential is thus within the more complex hybrid and tight shale systems.

Unconventional reservoirs have traditionally been treated as homogenous or assumed to lack lithologic variability. The assumption that an unconventional rock formation lacks variability leads to less effective horizontal well placement and recovery (Donovan et al., 2012). The success of horizontal-well placement within heterogeneous unconventional plays is directly related to the ability to identify important surfaces and predict the distribution and variations of source rock characteristics within the reservoir (Donovan et al., 2012).

This concept can be directly applied to exploration of the Shublik Fm. Hutton (2014) correlated the revised depositional sequences over a regional subsurface area. Similar

to the Eagle Ford, the Shublik Fm. exhibits variation on the parasequence level. Successful exploration of the Shublik Fm. as an unconventional reservoir will be increased by the identification and prediction of significant surfaces and depositional packages as ideal targets for horizontal well placement. An understanding of the depositional setting represented by specific facies is key to interpreting relative sea level change through time and its influence on the distribution of potential reservoir and source rocks (Burchette and Wright, 1992; Bohacs et al., 2005; Passey et al., 2010).

2.5.1 Pore Types and Networks Overview

Pore types and networks are an important rock property for the development of unconventional resource systems (Jarvie, 2012b). Unconventional resource systems are characterized by low permeability and low porosity (Slatt, 2011; Jarvie, 2012a). Micropore networks are an important reservoir property and contribute to the potential storage and flow capacity of unconventional systems (Slatt and Obrien, 2011; Loucks et. al, 2012).

Micropores that contribute to reservoir development come in three categories (Loucks et al., 2012). Their classification depends on pore location including both interparticle and intraparticle pores. The latter are located within grains, minerals, and organic matter. Pores exist within rings of clay minerals that are electrostatically joined as porous floccules; within pieces of organic matter as organopores; within fecal pellets, fossil fragments, and mineral grains; and as microchannels and microfractures (Slatt and Abousleiman, 2011; Slatt, 2013). Phosphatic pellets, ooids, and intraclasts also contain pores within their structure (Slatt and O'Brien, 2011). Slatt and O'Brien (2011) propose that the most beneficial pores for increasing permeability are floccules, organopores,

microfractures, and microchannels. Organic porosity is created by the decomposition of organic matter (Jarvie, 2012a). Pores within organic matter may account for greater than 50% of the total porosity (Passey et al., 2010). Petroleum can become trapped within these isolated pore spaces (Jarvie, 2012b).

2.5.2 Mechanical Stratigraphy Overview

Hydraulic fracturing is required to open pathways to create hydrocarbon flow in shale resource systems (Slatt, 2011). The fabric and texture resulting from deposition, rhythmic bedding, variable grain types, diagenesis, and pore structure have a direct impact on the geomechanics of the formation and how the rock will respond to hydraulic fracturing (Slatt and Abousleiman, 2011; Hart et al., 2013). The type of lamination and bedding exhibiting brittle-ductile couplets creates anisotropy and planes of weakness along bedding planes (Slatt and Abousleiman, 2011). Anisotropy varies in fine-grained rocks and is present at the lamina and bed scale and is controlled by deposition and diagenesis (Hart et al., 2013). Regardless of laminae orientation and presence, brittle units will break more readily when stress is applied as compared to ductile units (Slatt, 2011).

2.6 Microfacies Analysis

The name assigned to each microfacies is chosen to simplify the complicated rocks with an attempt to separate the facies types but also acknowledge variation within each microfacies.

2.6.1 Organic-rich, Silty, Bioclastic Mudstone

This Shublik mudstone consists of 70-80% clay sized material, 1-10% very fine silt to very fine sand sized detrital quartz grains, and up to 10% pyrite (Figure 6A). Carbonate grains include *Halobia* or *Monotis* fragments that make up to 5% of the facies. Calcite and silica cements are observed as intergranular or fracture-fills, <2%. TOC values for this facies are highest in the Phoenix core, with up to 10.04% but only reach 1.01% at Fire Creek (Kelly, 2004). Bioturbation varies from ii 1-5.

The mudstone is present in all four of the Shublik sections but varies in occurrence and lithology. At Last Creek (Figure 12D), the facies is present in all 4 sequences, but is only observed in sequence 4 at Fire Creek (Figure 12C). The lithology is siltier in the more proximal cores compared to the outcrops, with the greatest quartz content and coarsest grains documented in the Phoenix #1 core (Figure 12A). The mudstone is present in sequences 2, 3, and 4 in the Merak #1 core (Figure 12B) and in sequences 2 and 3 in the Phoenix core.

The mudstone occurs in rhythmic successions with flat clam (Figure 10C&D; Figure 13) and phosphatic facies (Figure 13). Phosphatic bioclastic nodular wackestone/floatstone and phosphate pebble/nodule rudstone are commonly below the mudstone. Both flat clam and phosphatic wackestone/packstones are most common above and interbedded with the mudstone facies.

2.6.2 Organic-rich, Calcareous Siltstone

The siltstone comprises 40-90% medium to fine-grained, sub-angular to sub-rounded, poorly to well sorted detrital quartz sand, 20-40% intergranular drusy calcite cement, and 15-20% euhedral and sub-planar dolomite (Figure 6B&C). Minor components

include <1% preferentially aligned mica grains and 1-5% pyrite present replacing quartz grains and as matrix. The siltstone is laminated (Figure 6C) and exhibits low angle cross lamination (Figure 6B) and hummocky cross stratification (HCS) (Figure 10A). Both normal (Figure 6B) and reverse graded bedding (Figure 6C) are observed with evidence of basal scours and erosional surfaces (Figure 6B). The siltstone facies in the Phoenix core is organic-rich with a maximum TOC value of 6.45% but organic-lean at the Fire Creek outcrop with TOC of 0.33%. Bioturbation varies from ii 1-3.

The siltstone lithofacies occurs within the Fire Creek Siltstone (lower part of sequence 1) in both of the outcrop sections (Figure 12C&D) and in the Eileen Sandstone in the Merak and Phoenix cores (Figure 12 A&B). The lithology is consistent and similar between the sections.

This facies is most common directly above sandstone facies and is overlain by the chert pebble conglomerate (Figure 9D) at the base of the Fire Creek Siltstone.

2.6.3 Limestone

Three types of limestone occur in the Shublik Fm. including bioclastic, the flat clam facies and phosphatic. Each type can be further subdivided into microfacies.

2.6.3.1 Bioclastic Limestone

Bioclastic limestone can be divided into three distinct microfacies; 1) organic-rich, bioclastic wacke/packstone; 2) organic-rich, bioclastic packstone/grainstone; and 3) silt-bearing wacke/packstone/floatstone; (Figure 6D,E,&F). The bioclastic limestone is present within sequences 2, 3, and 4 in Fire Creek, Merak IV, and Phoenix (Figure 12A,B,&C), but is only present in sequences 2 and 3 at Last Creek (Figure 12D).

The limestone is most commonly interbedded with flat clam, thin mudstone, and phosphatic facies (Figure 13).

The organic-rich, bioclastic wackestone/packstone microfacies contains 30-60% calcite as micrite, microspar, and psuedospar interpreted as matrix. Micrite is microcrystalline calcite with a grain size limit of <5μm, microspar crystal size ranges from 5-30μm, and psuedospar crystals range from 30-50μm (Folk, 1959; Folk, 1965; Flügel, 2004). Carbonate grains account for 10-40% of the facies and include *Halobia* or *Monotis*, other bivalves, echinoderms, and peloids. Dark, amorphous, clay sized material (possibly organics) is observed as 10-15% of the facies. Minor components include 3-7% sub-rounded, detrital quartz silt and <1% pyrite. This facies contains 0.95% TOC at Fire Creek (Kelly, 2004) and, bioturbation is common with ii 2-4.

The organic-rich, bioclastic packstone/grainstone microfacies (Figure 6D) contains approximately 70-80% carbonate grains similar to those described in the organic-rich, bioclastic wackestone/packstone microfacies; bioclasts are dominantly ≤1.0mm with rare examples up to 5.0mm in size. Approximately 10% drusy calcite cement and 3-7% silt to very fine sand sized, angular to sub-rounded, detrital quartz grains are present. The facies is bioturbated (ii 2-5) and burrows contain concentrated areas of up to 20% dark amorphous organic material.

The silt-bearing wackestone/packstone/floatstone microfacies (Figure 6E) contains 30-60% carbonate grains which include *Halobia* or *Monotis*, other bivalves, and brachiopod fragments. Detrital quartz silt grains vary in abundance from 5-50%, are sub-angular to sub-rounded, and moderately sorted. Micrite and microspar matrix is present at 3-30%,

and 2-10% equant and drusy calcite cement. Minor components include approximately 5-10% pyrite, and 4-5% phosphate that replaces other grains.

This facies is present at Last Creek and more commonly in the Phoenix core where it contains greater amounts of quartz. The facies is limited to sequences 2 and 3 at Last Creek (Figure 12D) and present in sequences 2, 3, and 4 in the Phoenix #1 core (Figure 12A).

2.6.3.2 Flat Clam Facies

The flat clam facies is defined as both a phosphatic and bioclastic limestone facies that contains at least 30% of the flat clams *Halobia* or *Monotis* (Figure 7A,B,C,&D). The facies can be divided and categorized into five microfacies based on the presence, size, and abundance of representative grains and the ratio with respect to matrix material and type. The microfacies include the following: 1) Silt bearing, organic-rich, flat clam packstone/rudstone (Figure 7C); 2) Silt and echinoderm bearing flat clam packstone/grainstone/rudstone; 3) Phosphatic, organic rich, flat clam mudstone/wackestone/packstone/rudstone (Figure 7A&B); 4) Phosphatic, silt bearing, organic rich flat clam packstone/grainstone; and 5) Flat clam coquina (Figure 7D).

In general, this facies contains 30- 90%, paper thin (0.25 mm) flat clams. Carbonate grains other than the flat clams include up to 5% echinoderm, peloids, and bioclast fragments, and phosphate replaces up to 15% of the grains and matrix. The facies contains 15-40% clay sized and organic material, 10-15% silt to very fine sand size detrital quartz grains, and 1-2% pyrite. Calcite is observed as equant and drusy cement contributing up to 15% and 5% micrite, microspar, and psuedospar matrix. The flat clams produce the laminations associated with this facies. Bioturbation varies from ii 1-

4 with more disruption of laminae with increasing bioturbation. The beds where bioturbation is lacking exhibit cycles of concentrated layers of preserved clams interbedded with mud (Figure 10D). The rhythmic flat clam beds are observed as coarsening upward packages (Figure 10C and Figure 13) and also include smaller scale fining upward packages (Figure 10C), both in outcrop (Figure 10B) and core.

The flat clam facies is present in sequences 2, 3, and 4 in the Merak #1 core and Last Creek outcrop (Figure 12B&D). In Merak, most of the facies is present at the top of sequence 2 through over half of sequence three, then appears again in sequence 4. The Merak #1 core flat clam facies has a greater abundance of phosphate grains and echinoderms as compared to the other sections of this study. At Last Creek, the facies is most abundant in the upper two thirds of sequence 4. In the Phoenix #1 core and Fire Creek outcrop (Figure 12A&C), the flat clam facies is present in sequences 2 and 3 with the greatest concentration in the Phoenix core being in sequence 3 and a more equal distribution in the Fire Creek outcrop. Generally, the Phoenix flat clam facies contains more silt as compared to the other sections (Figure 7C).

Mudstone is commonly at the base of the flat clam facies with nodular phosphatic beds directly above the facies (Figure 10C).

2.6.3.3 Phosphatic Limestones

The phosphatic limestone facies can be divided into four distinct microfacies. The first three are organic-rich and silt bearing and include: 1) Bioclastic, phosphatic mudstone/wackestone/packstone; 2) Flat clam, coated grain, phosphatic, bioclastic packstone/grainstone; 3) Bioclastic, phosphatic nodular wackestone/floatstone and 4)

Phosphate pebble/nodule rudstone. Phosphatic limestones are present in all four of the sections examined, generally within sequences 2 and 3. The Phoenix #1 core contains this facies in sequence 3 (Figure 12A); in the Merak #1 core the facies is present in sequences 1, 2 and 3 (Figure 12B); and in Fire Creek and Last Creek within sequences 2 and 3 (Figure 12C&D).

The phosphatic limestones occur in rhythmic successions and coarsens upward (Figure 13, 14A). A mudstone commonly overlies the phosphatic facies and also is present at the base along with flat clam facies (Figure 14A).

The phosphatic mudstone/wackestone/packstone comprises 15-70% phosphate as coated grains, replaced grains, and displasive nodules (0.5-15mm)(Figure 7E). Skeletal grains compose 5-30% of the facies and include; *Halobia* or *Monotis* and other bivalves, brachiopods, echinoderms, bryozoa, and foraminifera. This facies contains 2-10% drusy and equant calcite cement and 10-50% micrite or microspar matrix. This facies contains 5-30% very fine silt to sand sized, subangular to subrounded detrital quartz grains, minimal to 20% clay sized material, and up to 2.52% TOC in the Merak core and 1.72% at Fire Creek. Bioturbation varies in this facies from ii 1-4.

The phosphatic packstone/grainstone comprises 10-45% coated or replaced phosphate grains, displasive nodules (1-20mm), and as matrix (Figure 7B&D). Carbonate grains at 20-70% are similar to those described in the phosphatic wackestone/packstone facies with the addition of peloids. Equant and drusy calcite cement accounts for 5-50% of this facies with 15-40% matrix as micrite and microspar. Detrital silt sized quartz grains, sub angular to sub rounded, are observed at 5-30% and approximately 3% pyrite is present. This facies contains up to 2.74% TOC at Fire Creek and bioturbation varies from ii 1-5.

The nodular phosphatic bioclastic wackestone/floatstone facies comprises 30-50% phosphate as coated grains, replaced grains, displasive nodules (4mm-4.5cm), and as matrix replacement (Figures 7F, 8A, and 11B). Carbonate grains account for 15-20% of the facies and include bivalves, brachiopods, and echinoderms. The facies contains up to 25% equant and drusy calcite cement, 40% microspar matrix, 2-15% detrital silt sized quartz grains, 3-5% pyrite observed replacing bioclasts, and 1.41% TOC at Fire Creek.

The phosphate pebble/nodule rudstone comprises 40-70% sub to well-rounded phosphate pebbles and nodules (1mm-2.5 cm), and 20-30% sand sized, sub-angular, well sorted detrital quartz grains (Figure 8C and 11A). Calcite cement accounts for 10-15% of the facies, and pyrite is present within the pebbles and around the quartz grains, 5%.

This phosphatic facies occurs within the phosphatic limestone as thin beds or hardgrounds and at the top of the coarsening upward packages (Figure 14A). A phosphatic wackestone/packstone is usually directly above and below the thin pebble/nodule beds.

2.6.4 Organic-rich, Calcareous, Phosphatic, Siltstone

The phosphatic siltstone contains 30-90% silt to fine sand size, sub-angular to sub-rounded, moderately to well-sorted detrital quartz grains (Figure 8E & F), and 15-60% phosphate as displasive nodules (1-6mm), coated grains (Figure 8F), and as matrix. Drusy and equant calcite cement at 10-40%, and clay sized and organic material account for 5-7% of the facies. Minor components include, 2% silt-sized pyrite, 1-2% mica, and <1% bioclasts. This facies contains normally graded, laminated bedding and HCS. TOC at Fire Creek is up to 2.58% and bioturbation varies from ii 1-4.

Phosphatic siltstone is present in all of the Shublik sections and is found in the upper part of sequence 1 directly above the Fire Creek Siltstone (Figure 12A,B,C,&D). It is limited to sequence 1 with the exception of Last Creek, where it is present in sequences 1 and 2.

The phosphatic siltstone facies exhibits rhythmic packages that vary in the abundance of fine-grained material within the siltstone. The chert pebble conglomerate (Figure 9D) is at the base of the phosphatic siltstone.

2.6.5 Phosphatic, Organic-rich, Bioclastic, Calcareous Sandstone

The phosphatic sandstone facies comprises 60-80% very fine silt to medium sand size, sub-angular to sub-rounded, moderately to well sorted, detrital quartz grains, 10% phosphate within the matrix and as displasive nodules, 3-5% calcite cement, and up to 5% clay sized particles (Figure 9A&B). In the Phoenix #1well, the sandstone contains up to 20% bioclasts. The facies exhibits normal grading, laminated bedding, and erosional surfaces (Figure 9B,).

The sandstone facies is present in all four of the study sections (Figure 12A,B,C,&D), most common in sequence 1 as part of the Eileen Sandstone and Fire Creek Siltstone and sequence 4 as part of the Sag River and Karen Creek sandstones. The TOC of the Sag River is up to 2.87% in the Phoenix #1 core.

The sandstone facies as part of the Eileen Sandstone and Fire Creek Siltstone, occurs with siltstone and wispy occurrences of mudstone facies. The sandstone facies as part of the Sag River and Karen Creek Sandstones is underlain by limestone and most commonly overlain by glauconitic sandstone (Figure 9C).

2.6.6 Organic-rich Glauconitic Sandstone

The glauconitic sandstone facies contains 15-80%, fine sand sized, moderately sorted, glauconite grains and 1-60% silt to very fine sand sized, sub-angular to sub rounded detrital quartz grains, 5% equant calcite cement, and 10% micrite matrix (Figure 9C). Additional components include 5-10% pyrite, 5-10% clay sized materials, and carbonate grains (<2%) including *Halobia* or *Monotis*, other bivalves, and brachiopods. TOC is measured at 1.61% in the Phoenix core. The glauconite facies is only observed in core sections of this study (Figure 12A&B) and occurs at the base of sequence 4 in the Phoenix core, and at the base and top of sequence 4 in the Merak core.

The glauconitic sandstone occurs (Figure 13; Figure 14A) above nodular phosphatic facies and limestone facies and is commonly overlain by mudstone.

2.6.7 Calcareous, Silt-bearing, Chert Pebble Conglomerate

The chert pebble conglomerate facies comprises 30-80%, sub-angular to sub-rounded, poorly sorted chert pebbles (2-9mm), 30-40%, silt to sand size, sub-angular to sub-rounded, poorly sorted detrital quartz grains (Figure 9D), up to 15% pyrite replacing chert pebbles, microcrystalline quartz filling fractures within the pebbles, 5% calcite cement, 5% microspar matrix, and up to 5% clay sized material. This facies occurs in sequence 1 at Fire Creek (Figure 12C), at the base of the Fire Creek Siltstone; at Last Creek (Figure 12D), located at the top of the Fire Creek Siltstone; in the Merak # core (Figure 12B), at the top of the Eileen Sandstone; and in the Phoenix #1 core (Figure 12A) with multiple occurrences within the Eileen Sandstone.

2.7 Results

2.7.1 Target Interval

RBis for the Phoenix #1 well (Figure 5) and Fire Creek (Figure 5) were generated from existing mineralogy, TOC, and whole rock geochemical data to identify a targeted interval to be the focus for unconvetional exploration. This interval is targeted because of the presence of source rock and brittle prone beds that would make a likely target for an unconventional resource system. Mineralogical and whole rock geochemical data (Appendices A,B,&E) of total clay% (Al_2O_3), quartz (SiO_2), and calcite (CaO) were plotted along with TOC% to construct the RBi (Figure 5). First, an interval enriched in TOC was identifed; then brittle and ductile prone intervals were determined using Al_2O_3 as a proxy for clay and SiO_2 and CaO as proxies for brittle intervals

The zone of interest was identified in the Pheonix #1 well (Figure 5) and Fire Creek outcrop (Figure 5) and was then correlated to Merak and Last Creek based on gamma ray signatures (Figure 12).

The targeted interval is observed in the core locations within sequence 3 and the outcrops within sequences 2 and 3 (Figure 12A,B,C,&D). The thickness of the interval is the greatest in the outcrop sections and thinnest in the Merak #1 core. Table 2 summarizes the location, thickness, and lithofacies present within the target interval for each of the sections.

To simplify the target interval zone, sequences 2 and 3 are combined as the focus of this paper for the interval to target for unconventional exploration. Parasequences present within sequences 2 and 3 are identified and important characteristics are

documented including mappable surfaces, microfacies, pore types and networks, and some mechanical stratigraphic properties.

2.7.2 Facies Associations/Parasequences

Shublik facies commonly occur in repetitive or rhythmic packages bounded by flooding surfaces. The facies stacking pattern provides information about relative facies migration and sea level change. Flooding surface bounded packages are interpreted as parasequences or genetically related, relatively conformable successions of bedsets (Van Wagnor et al., 1990; Mitchum and Van Wagoner, 1991). Bedsets are the fundamental sedimentary bodies and are composed of laminae, laminae sets, and beds, and are bounded by depositional surfaces (Campbell, 1967). Parasequence bounding flooding surfaces are useful for correlating packages from log and cores, but the boundaries are more difficult to identify in a basinward direction (Van Wagoner et al., 1990).

A detailed description of the nearly complete Merak #1 core provided the most comprehensive view of facies stacking patterns that were used to help define parasequences present within the targeted interval. The targeted interval is located at 10753.3-10811.7' (3277.61- 3295.41m) in the Merak core (Figure 12B; Figure 13). Generally, two distinct types of lithofacies are present, the flat clam facies (Figure 10C) which dominate the lower portion of the interval and the phosphatic limestone facies (Figure 14A) which are present in the upper portion of the interval. Flat clam and phosphate depositional overviews are summarized followed by the description of the parasequences.

2.7.2.1 Flat Clam Overview

The term flat clams refers to the Mesozoic bivalves *Halobia*, *Monotis*, and related taxa because the morphology of the shell is very thin with a "narrow valve convexity" (McRoberts, 2010). According to McRoberts (2011), the clams "exhibit high rates of origination and extinction." Historically, flat clams were interpreted to be planktonic dwellers within the water column that would experience episodes of mass die off and would settle to the sea floor (Wingall and Simms, 1990; McRoberts 2011). However, more recent evidence supports the interpretation that the clams were *in situ* benthic dwellers living in relatively deep water, below fairweather wave base, near the oxygen minimum zone (McRoberts, 2010). They are also locally associated with pelagic limestones deposited in fully oxygenated environments (McRoberts et al., 2008). The cyclical deposition of beds of the flat clams indicates that the clams were sensitive to changes in the depositional environment but possessed the ability to reestablish quickly if the conditions were favorable. The flat clams are interpreted to be opportunistic organisms, typically interbedded with organic-rich sediments deposited under oxygen deficient conditions (McRoberts, 2010).

2.7.2.2 Flat Clam Parasequence

Flat clam parasequences (Figure 10, B&C; Figure 13 A-A') create the laminated intervals observed in the core and coarsen upward from a black phosphatic, organic rich, flat clam mudstone to a medium to light grey flat clam packstone/rudstone. The previously described flat clam microfacies are all associated with the flat clam parasequences. Phosphate is present as sand size grains some of which are encrusted or coating quartz grains and others are rounded grains of phosphate. Some of the flat

clam parasequences are capped by phosphatic bioclastic nodular wackestone/floatstone (Figure 10C).

2.7.2.3 Phosphate Overview

Phosphate deposition has been episodic through geologic time and phosphorus is a crucial nutrient that controls primary productivity (Filippelli, 2011; Berndmeyer et al., 2012). Modern marine environments of phosphorite accumulation exhibit common depositional characteristics which include the following; current dominated sedimentary structures, low sedimentation rate, high primary productivity, a low oxygen zone with organic matter decomposition, and iron and manganese redox cycles (Föllmi, 1996; Filippellii, 2011). The general characteristics of a depositional setting of phosphorite are; a continental shelf or slope with high primary productivity, low rate of terrigenous sedimentation, and a repeated process of sedimentation, phosphogenesis, and winnowing or reworking (termed "Baturin cycles")(Föllmi, 1996;Filippellii, 2011). Marine waters contain the largest reservoirs of phosphate supplied by air and water, oxidized inorganic phosphate, and hydrothermal activity which is then brought into the photic zone by the process of upwelling (Föllmi, 1996; Berndmeyer et al., 2012). The second largest reservoir is in the photic zone within the organic layer (Berndmeyer et al., 2012). Phosphorus is part of the organic matter cycle and is recycled at the sediment water interface (Filippellii, 2011). Phosphogenesis is controlled by oxygen, microbial processes, bioturbation, rate of mineralization, and the availability of suitable nucleation surfaces (Föllmi, 1996; Filippellii, 2011).

According to Föllmi (1996), phosphate can be pristine, condensed, or allochthonous. Pristine phosphate is autochthonous and has experienced only one cycle of

phosphogenesis with no evidence of transport or reworking. Pristine phosphates include coated grains, coprolites, fossils and fossil debris, peloids and phosphatized burrow systems. Condensed phosphates are somewhat autochthonous and have experienced one or more Baturin cycle and may have experienced more than one stage of phosphogenesis (Figure 14B). Characteristics of condensed phosphates (Figure 14B) include; internal boundaries or the inclusion of detrital material, small scale unconformities, scour marks, heterogenous phosphate particles, and fossil assemblages of different environment or age. Condensed phosphates are deposited along the inner shelf to the inner shelf margin and transition to allochthonous phosphates at the margin to the outer shelf. Allochothnous phosphate is a result of sedimentary reworking of pristine or autochthonous phosphate resulting in a mix of phosphatic and non-phosphatic particles. Phosphorites are associated with transgressive systems tracts and relative sea-level rise (Föllmi, 1996).

2.7.2.4 Phosphatic Parasequence

Phosphatic facies parasequences (Figure 13D-D'; Figure 14A) in the Merak core generally begins with a black phosphatic mudstone/wackestone and coarsens upward and lightens in color to a nodular phosphatic floatstone. The abundance and size of the phosphate nodules increases upward. The phosphate pebble/nodule rudstone facies occurs as winnowed lag deposits. Phosphate facies present in the Merak core include all four of the previously described phosphatic limestones: bioclastic, phosphatic mudstone/wackestone/packstone (Figure 8D); flat clam, coated grain, phosphatic, packstone/grainstone; nodular phosphatic bioclastic wackestone/floatstone (Figure 8A); and the phosphate pebble/nodule rudstone (Figure 8C&11A). Some laminations from

the flat clams are preserved. Evidence of current, reworking, and bioturbation (ii 1-4) is observed. According to Föllmi (1996), these types of facies would be deposited along the inner shelf to the inner shelf margin near the oxygen minimum zone.

2.7.3 Target Interval Parasequences

The target interval in the Merak #1 core (Figure 12B; Figure13) consists of parasequences and parasequence sets within sequence 3. A sharp contact is present at 10811.75' (3295.42 m) noted by a distinct change in facies from a phosphatic packstone to the first occurrence of a flat clam parasequence. The first parasequence set (10811.7'- ~10807.6')(3295.41- 3294.16 m)(Figure 13, A-A') consists of four repetitive, coarsening upward flat clam parasequences and is overlain by 0.5' interval of black mudstone. The flat clams are well preserved (Figure 10D) with rare bioturbation. The uppermost beds of this parasequence set are nodular phosphatic wackestone/floatstone (Figure 11A). They appear to be distinctly different than the underlying flat clams.

The next parasequence set is at (10807.6'-10782.8') (3295.41-3286.6m) (Figure 13, B-B'). In general, this interval contains multiple parasequences of black flat clam facies that lighten in color and coarsen upward to a light grey bioclastic wackestone/packstones with increased bioturbation. In the lower portion, the flat clam beds are pristine and lack bioturbation, and the abundance of the clams decreases upward. The rock texture and fabric change as a result of the abundance of clams and the degree of bioturbation.

The next parasequence set is at (10782.8'- 10773.2') (3295.41- 3283.67m) (Figure 13, C-C') and includes thin beds of black flat clam facies, bioclastic packstone, phosphate

pebbles/nodule rudstone, and shell lag deposits approximately .01-.1' thick. This interval contains a greater abundance and variety of bioclasts. Beds are locally bounded by scoured surfaces and display bioturbation, wispy laminations, and/or planar laminations. The abundance of flat clams decreases upwards.

At 10773.2' (3283.67m), a phosphate pebble hard ground is present and marks a change in facies to phosphatic parasequence sets at 10773.2'-10753.5' (3283.67-3277.67) (Figure 13, D-D'). This set is dominated by phosphate parasequences with an overall coarsening upward trend. In the lower portion, the individual package's color grades from to dark brown/black to light grey and 5 repetitive parasequences comprise this interval. The top 0.5' is the organic-rich glauconitic sandstone facies with significant pyritization.

The interval is capped by 0.5' of an organic rich glauconitic sandstone facies (Figure 14A). This facies is also observed in the Phoenix #1 core and may be useful as a marker bed or key surface for mapping the upper contact of the optimal interval regionally. Glauconite has recently been explored as a tool for sequence stratigraphy (Amorosi, 2012). Glauconite is associated with TST's and indicates low sedimentation rates (Amorosi, 2012).

2.7.4 Mechanical Stratigraphy

The Shublik Fm. contains sedimentary features and mechanical stratigraphy properties which include; erosional surfaces, laminations, graded bedding, varied mineralogic composition, textural anisotropy, and isotropy. These features are present at a bedset scale in outcrop (Figure 10A&C) and at a laminae scale in photomicrographs (Figures

5C&B, 6A&C, 8B). The fabric and texture of these properties are directly related to how the rock will respond to hydraulic fracturing. The small-scale brittle-ductile couplets are also recognized at a parasequence scale which can be correlated to well log signature (Slatt and Abousleiman, 2011).

Slatt and Abousleiman (2011) integrate sequence stratigraphy and mechanical stratigraphy as a tool to predict the ideal zone for hydraulic fracturing. They identify brittle and ductile units and classify as first, second, and third order. First order, is at the systems tracts scale; second order, on the parasequence scale; and third order on the scale of brittle-ductile bed couplets. The first and second order units can be correlated and mapped but the third order units are difficult to predict. Pore networks, lithology, fabric, texture, and bedding plane orientation are characteristics at the third order scale which directly impact the orientation of the drill bit for horizontal drilling. (Slatt and Abousleiman, 2011).

2.7.5 Pore Types and Networks

This study documents the different pore types, networks and potential storage capacity identified within the Shublik Fm. Microchannels, microfractures, floccules, intraparticle and moldic porosity were successfully identified (Figures 15; 16; &17). Organic matter pores may be present but they occur at a nanometer scale and in overmature source rocks (Passey et. al., 2010).

The microchannels and floccules are associated with the mudstone portions in both the flat clam facies and the phosphatic facies (Figures 15; 16C; &17A). The clay flakes are individually imaged and pore throats are identified within the muddy areas (Figures 15 & 17A). Microchannels (Figures 15 & 17A) that cross cut bedding planes may create a

network and pathway connecting microfractures and floccule pores and increasing permeability (Slatt and O'Brien, 2011). Microchannels are abundant within the mudstone facies of the Shublik Fm. (Figures 15 & 17A). Microfractures are preferentially aligned with the bedding planes in the flat clam facies (Figures 15; 16C; &17A) and are observed around phosphate nodules.

Pyrite framboids (Figures 15 and 17A&B) contain intraparticle porosity between the individual pyrite crystals. Organic matter also may be contained within the pores of the framboids. The framboids appear to inhibit the compaction of clay flakes (Figures 15 and 17A&B).

The type of pores vary with respect to the type of phosphate grain. The sand sized phosphate grains have a micro-granular texture, revealed in microprobe (Figure 16C) images, with intraparticle porosity (Figure 17B&D). Phosphate nodules that contain a variety of grains (Figures 16B&D, and 17E) may also contain moldic porosity and intraparticle porosity. The interior of a phosphate nodule (Figure 16D) imaged with the FE-SEM contains approximately 12% pore space.

2.7.6 Target Interval Regional Correlation

A regional cross section of sequences 2 and 3 was generated by manually picking the parasequence surfaces from available well log gamma ray profiles (Figure 19; Table 4). The wells included in the cross section were selected if they contained complete Shublik sections and based on their relative proximity to the peak oil thermal maturity zone (Figure 19). The Merak #1 well was used as a correlation point in the attempt to identify the parasequences in the well logs across the region and predict the distribution of

facies. Parasequence sets identified in the well log profiles are identified as P1-4 for sequence 2 and P1-5 for sequence 3(Figure 19).

Sequence 2 correlates farther to the west with a higher level of certainty as compared to sequence 3 (Figure 19). East of Merak to Fire Creek, the parasequences within sequence 2 gradually thicken and are readily correlated. The significant surfaces between the parasequences are mappable. West of Merak to the Peard Test Well (Figure 19 & Table4) sequence 2 is generally thicker as compared to east of Merak with the exception of the E. Teshekpuk well and S. Mead 1 (Figure 19 & Table 4). P1 is relatively thin compared to the other parasequences within sequence 2 and pinches out to the west of the E. Teshekpuk Well. The upper part of P4 in sequence 2 contains flat clam facies that are present across the region. The thickness of P4 increases to the west of the Merak Well.

The parasequence sets in sequence 3 are identified with a higher confidence east of Merak as compared to the west. East of the Merak well all P1-5 remain a consistent thickness. West of the Merak well P5 pinches out at Nechelik 1 and at E. Teshekpuk well and in remaining wells to the west. P4 pinches out at E. Teshekpuk well. West of the E. Simpson Test well the parasequences are not as recognizable (Figure 19 & Table 4).

2.8 Discussion

2.8.1 Organic Richness and Thermal Maturity

The Shublik Fm. is one of the primary source rocks on the North Slope (Peters et al., 2006; Decker, 2011; Houseknecht et al., 2012; Scheirer et al., 2014). The Shublik Fm.

has an average TOC of 2-4% and is oil-prone type I to very oil-prone type II, with an original hydrogen index (HI) of 300-400 mg HC/g TOC (Peters et al., 2006; Decker, 2011; Scheirer et al., 2014). In the Phoenix #1 well, the Shublik Fm. contains hydrocarbons sourced from within the formation and those that migrated from another source (Yurchenko, 2017).

Scheirer et al. (2014) generated a thermal maturity map for the base of the Lower Kingak Shale and the top Shublik Fm. (Figure 18; Table 3). The source rock maturity within this area has a range of >2% R_o in the southern down dip direction to <0.6% R_o in the northern up dip direction. The relative downdip position of the overmature source rocks and the likelihood that any remaining oil will be cracked to gas (Passey et. al., 2010) and expelled are proposed by Scheirer et al., (2014) to be ideal for pushing the peak oil generation updip out of the tight rocks.

The combined thickness of sequence 2 and 3 ranges from zero at the Mikkelsen High to approximately 480' (146.3 m) on the northwest side of the Fish Creek platform (Figure 18). Within the area of peak oil generation, the thickness varies from 80'- 260' (24.4-79.2 m)(Figure 18).

2.8.2 Implications for an Unconventional Resource System

The methods and results covered in this study provide tools to evaluate and explore the Shublik Fm. as an unconventional resource system. The heterogeneity of the Shublik Fm. poses a challenge because it cannot be treated as a single thick package of "shale". The Shublik Fm. should be considered a hybrid shale-oil resource system due

to its lithological characteristics of interbedded fine-grained rocks with coarser-grained carbonate and phosphatic packages.

Hydraulic fracturing success is controlled by the ability to predict how a rock is going to fracture and how to access the prime area within a formation. The results from this study permit the prediction of facies distribution and the unconventional target interval in the Shublik Fm.

The microfacies analysis documents the fine scale heterogeneity from laminae to bedsets and provides direct connection with the facies stacking patterns and the associated parasequences.

The RBis successfully identify a target zone or interval to focus on as an unconventional resource play. The targeted zone includes brittle and organic enriched ductile couplets. These couplets can serve as zones to target for horizontal drilling (Slatt, 2013). Integration of facies stacking patterns and RBis with well logs signatures (Figure 19) provides a regional tool for identifying significant surfaces, correlating the target intervals, and predicting the unconventional resource potential of the Shublik Fm.

The target interval is comprised of flat clam and phosphatic parasequences. The microfacies present within these parasequences were investigated for pore types and networks and mechanical stratigraphy characteristics, including texture, fabric, and isotropy. This can be directly applied to predict how the individual facies will respond to hydraulic fracturing.

Pore types and networks along with mechanical stratigraphy associated with the flat clam and phosphatic parasequences are documented as part of this study. The

coarsening upward flat clam and phosphatic parasequences are juxtaposed and comprise an interconnected pore system including potential storage capacity and migration pathways.

The flat clams are what create the paper-thin laminations, giving the appearance of a papery shale. Laboratory experiment results found that shales will break along lamination when stress is applied parallel to lamination as opposed to perpendicular (Slatt, 2011; Hart et al., 2013; Slatt, 2013). The pristine flat clam facies are anisotropic and contain natural planes of weakness that will fracture more readily.

The flat clam parasequences provide fracture prone intervals and will preferentially fracture along the plane of the clams' orientation. The fracture prone intervals are interbedded with mudstone facies that contain microfracture, microchannel, floccule, and intraparticle porosity.

The phosphatic parasequences also contain a mudstone facies which includes the pores and pore networks associated with the flat clam mudstone facies. In addition to the similar pore types, the phosphatic parasequences also contain moldic and intraparticle porosity observed within the nodular phosphatic limestone facies adding to the potential storage capacity. The most significant difference between the two different parasequences is the isotropy; the flat clam parasequences being anisotropic as compared to the isotropic phosphatic parasequences.

The regional correlation of the parasequences (Figure 19) provides new information of how the parasequences are distributed across the North Slope and the ability to map

the significant surfaces. The pores, network of pores, and mechanical stratigraphy identified as part of this study are predicted both in a lateral and vertical distribution.

Sequence 2 packages are predominantly phosphatic limestone and mudstone with P4 containing flat clam facies towards the top (Figure 19). Therefore, the lower part of sequence 2 contains the greater storage capacity associated with the phosphatic limestone facies, but also contain the network of pores documented within the mudstone facies. The upper part of sequence 2 contains the natural planes of weakness and that will more readily fracture parallel to bedding. These fractures have the potential to provide migration pathways in a lateral direction.

P1 and P2 as part of sequence 3 (Figure 19) are predominately flat clam parasequences. The lower portion of P3 contains flat clam facies and transitions to phosphatic limestone facies upward. P4 and P5 are dominated by nodular phosphatic limestone facies (Figure 19). The transition between sequences 2 and 3 continues to contain the migration pathways and fracture prone intervals associated with the flat clam facies. The upper portion of sequence 3 is another interval that contains the storage potential associated with the phosphatic facies.

The lateral trend of the flat clam and phosphatic parasequences is also predicted with the regional correlation. West of the Merak well, the pore networks associated with the flat clam facies dominate as compared to the pores associated with the nodular phosphatic limestones. East of the Merak well there is more of an equal distribution of the flat clam and phosphatic parasequences.

Chapter 3

Conclusion

- Eighteen Shublik Fm. microfacies were described from outcrop and core locations. The composition of microfacies varies on the bed and laminae levels. The detailed account of the variation of facies can be directly correlated to the sedimentary features and mechanical stratigraphy characteristics; specifically the laminae, erosional features, and isotropy.
- The microfacies associations of these complicated rocks document specific facies stacking patterns that are the building blocks of the flat clam and phosphatic parasequences that make up the target interval.
- A relative brittleness index was used as an approach to identify the target interval for unconventional resource exploration of the Shublik Fm. The targeted zone is composed of sequences 2 and 3 and is dominantly flat clam and phosphatic coarsening upward parasequences. The zone contains both reservoir and source facies that are respectively brittle and ductile, occurring in couplets.
- A detailed log of the Merak core permitted a high-resolution analysis of the parasequences and their associated gamma ray signature. The parasequences were correlated east to west across the North Slope using the gamma ray signature of industry wells.
- A regional isopach and correlation of the targeted interval successfully identifies and allows the mapping and prediction of significant parasequence set surfaces within sequences 2 and 3. The documentation of the pore types and networks associated with the parasequences combined with the regional correlation provides a tool to

predict the regional distribution of potential porosity and expected mechanical stratigraphy characteristics. The new data on the distribution of the pores, pore networks, and mechanical stratigraphy characteristics is important criteria in evaluating the Shublik Fm. as an unconventional resource system.

- Alaska's North Slope is vast, remote and contains limited infrastructure. Commodity prices are in an upward trend, and as technology and recovery methods become more efficient the cost of exploiting unconventional reservoirs will become more cost effective. The results of this study will be beneficial in the future development of unconventional oil and gas production on the North Slope of Alaska. Combining the outcomes of this study provides new insight towards the successful exploration and realization of the Shublik Fm. as an unconventional resource system. The variety of pore types and networks integrated with the ability to identify and map the parasequence set surfaces provides an approach to target intervals that previously were considered too complicated or unrecognizable. This study provides relevant industry tools towards Alaska's future with unconventional resource development.
- Future recommendations
    - The results of this study combined with a comprehensive fracture study of the Shublik Fm. would lead to even better prediction of how the facies would respond to hydraulic fracturing.
    - Utilizing more wells as data points one could build a volumetric model of the target interval by using the thicknesses of the parasequence, significant surfaces to map, and the important characteristics associated with the flat clam and phosphatic parasequences.

- An improved basin model could be generated from the results of this study. The distribution of the microfacies could be refined at a tighter constraint by using the numerous wells that are available and then applied to create a new basin model.

Figures

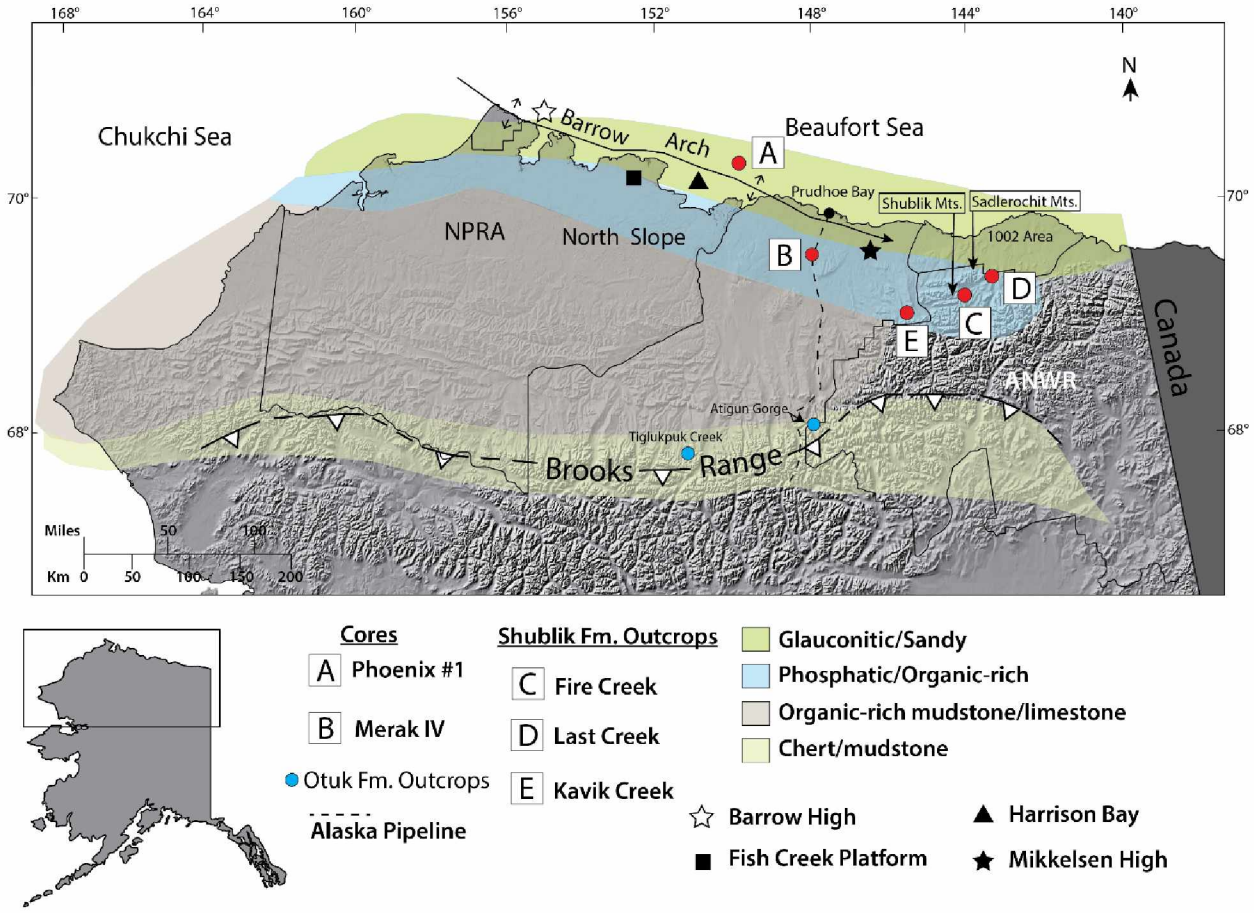

Figure 1. Map of northern Alaska. Lower left shows the location of the map. Cores used as part of this study are labeled A and B. Shublik Fm. outcrop locations that were sampled and measured for this study are labeled C, D, and E. Significant basement features are indicated by symbols. Otuk Fm. outcrop locations are indicated by blue dots. General lithology gradation is illustrated by the translucent colors. (Modified from Kelly et.al., 2007)

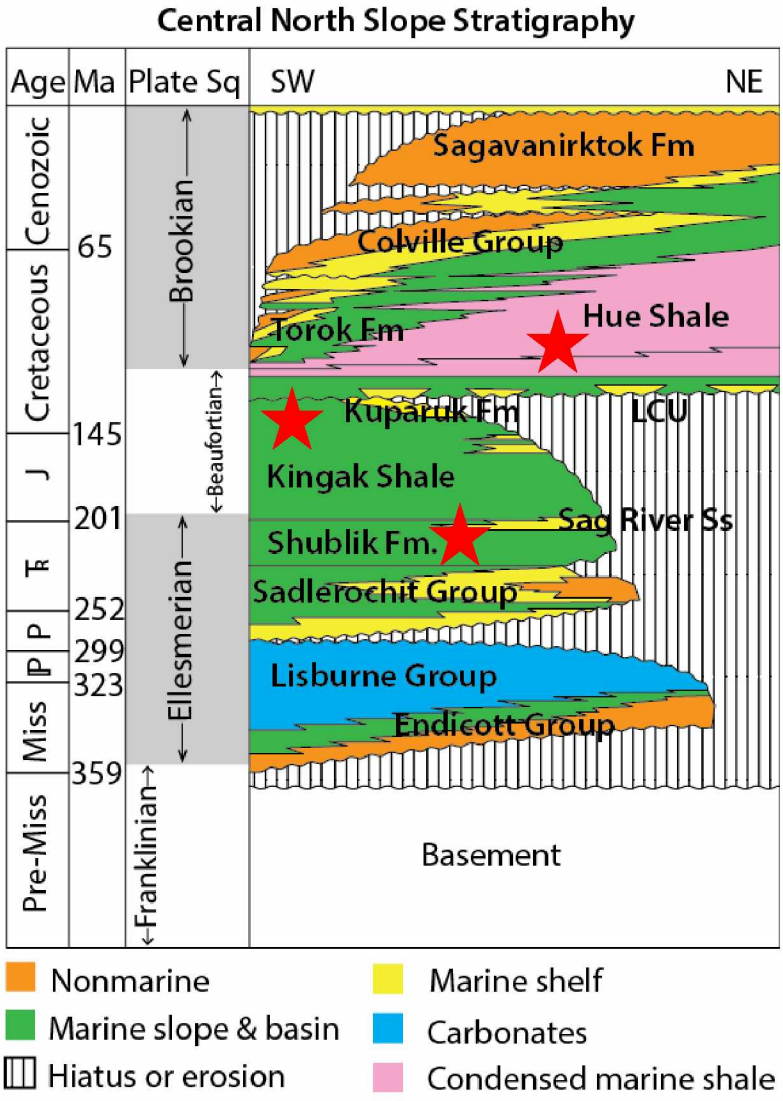

Figure 2. Generalized North Slope stratigraphy. The red stars indicate the primary source rocks; the Shublik Fm., Kingak Shale, Kalubik Fm., and Hue Shale. The Shublik Fm., part of the Upper Ellesmerian plate sequence, is overlain by the Kingak Shale, part of the Beaufortian plate sequence. The Hue Shale was deposited during the Brookian plate sequence (Figure modified from Houseknecht and Bird, 2005).

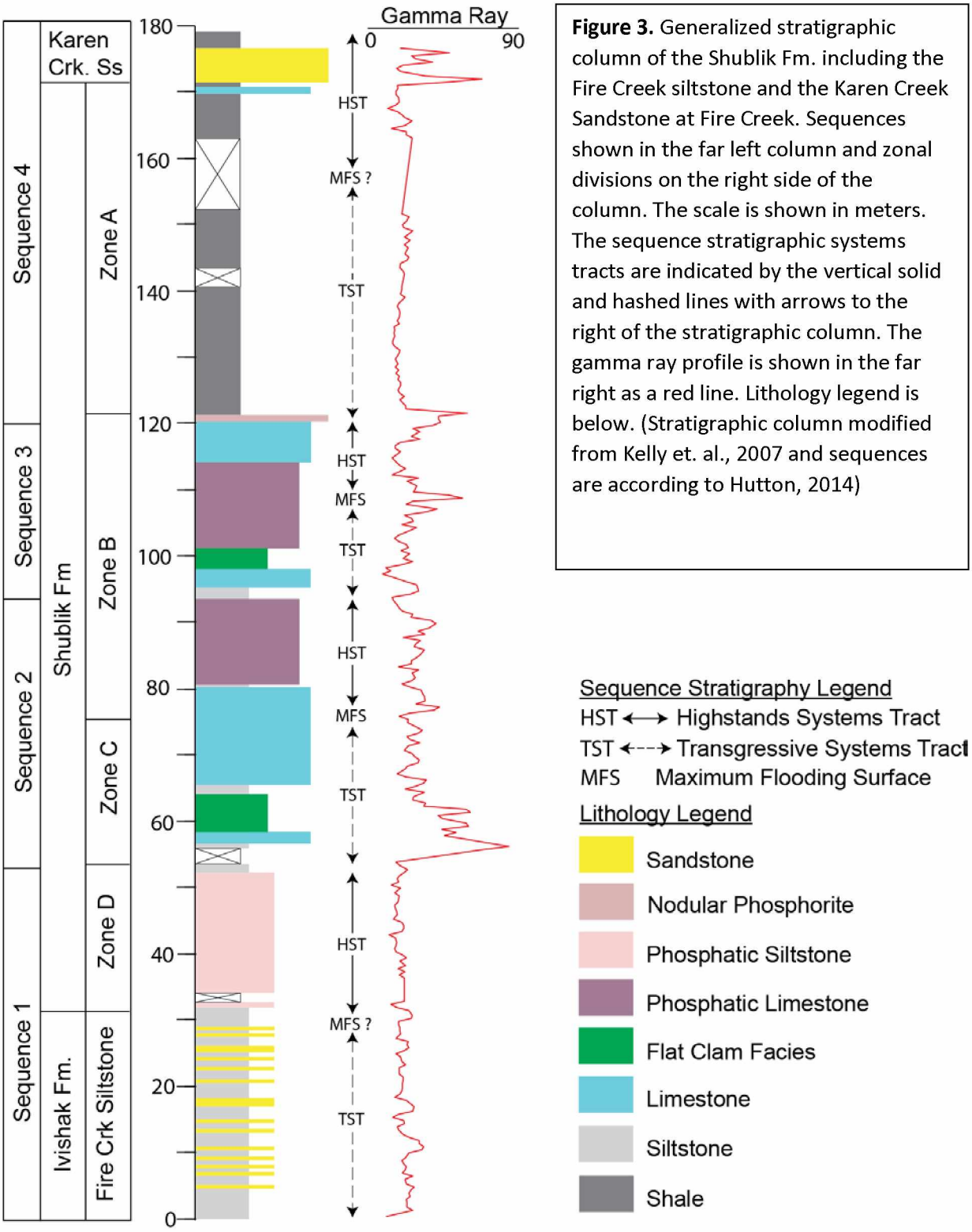

Figure 3. Generalized stratigraphic column of the Shublik Fm. including the Fire Creek siltstone and the Karen Creek Sandstone at Fire Creek. Sequences shown in the far left column and zonal divisions on the right side of the column. The scale is shown in meters. The sequence stratigraphic systems tracts are indicated by the vertical solid and hashed lines with arrows to the right of the stratigraphic column. The gamma ray profile is shown in the far right as a red line. Lithology legend is below. (Stratigraphic column modified from Kelly et. al., 2007 and sequences are according to Hutton, 2014)

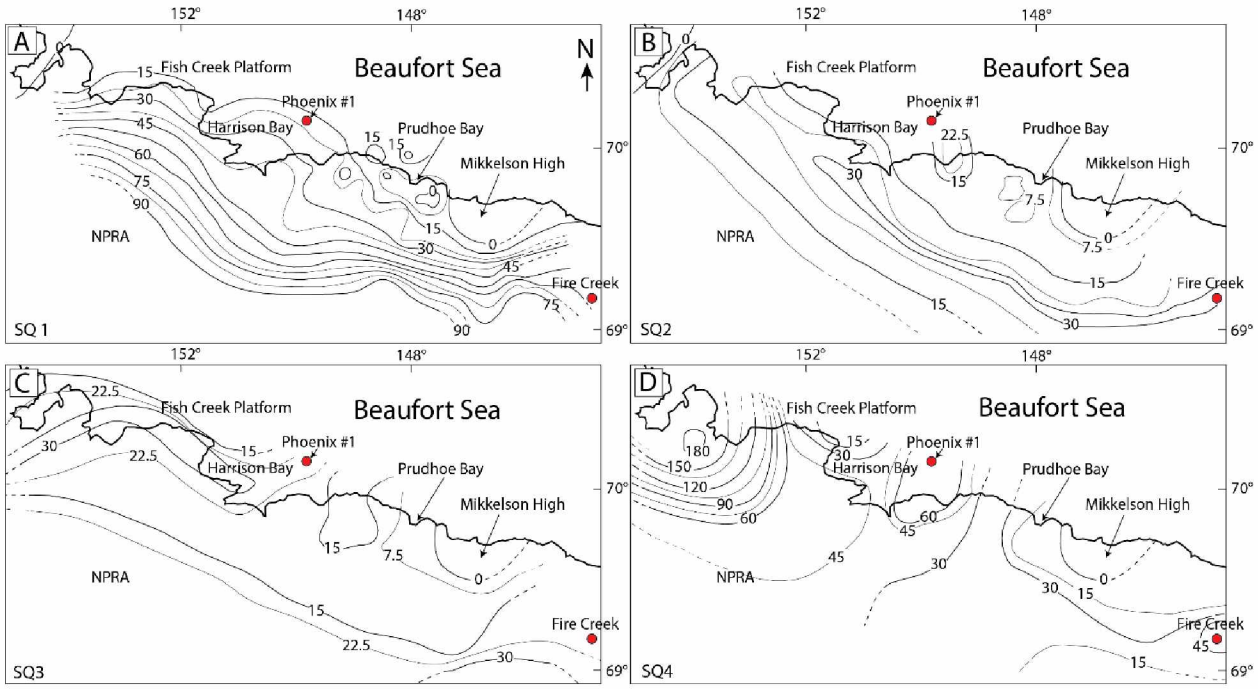

Figure 4. Isopachs of the Shublik Fm. of the individual 4 sequences. Contour intervals are shown in meters. A. Sequence 1 (SQ1); B. Sequence 2 (SQ2); C. Sequence 3 (SQ3); and D. Sequence 4 (SQ4). (Modified from Hutton, 2014)

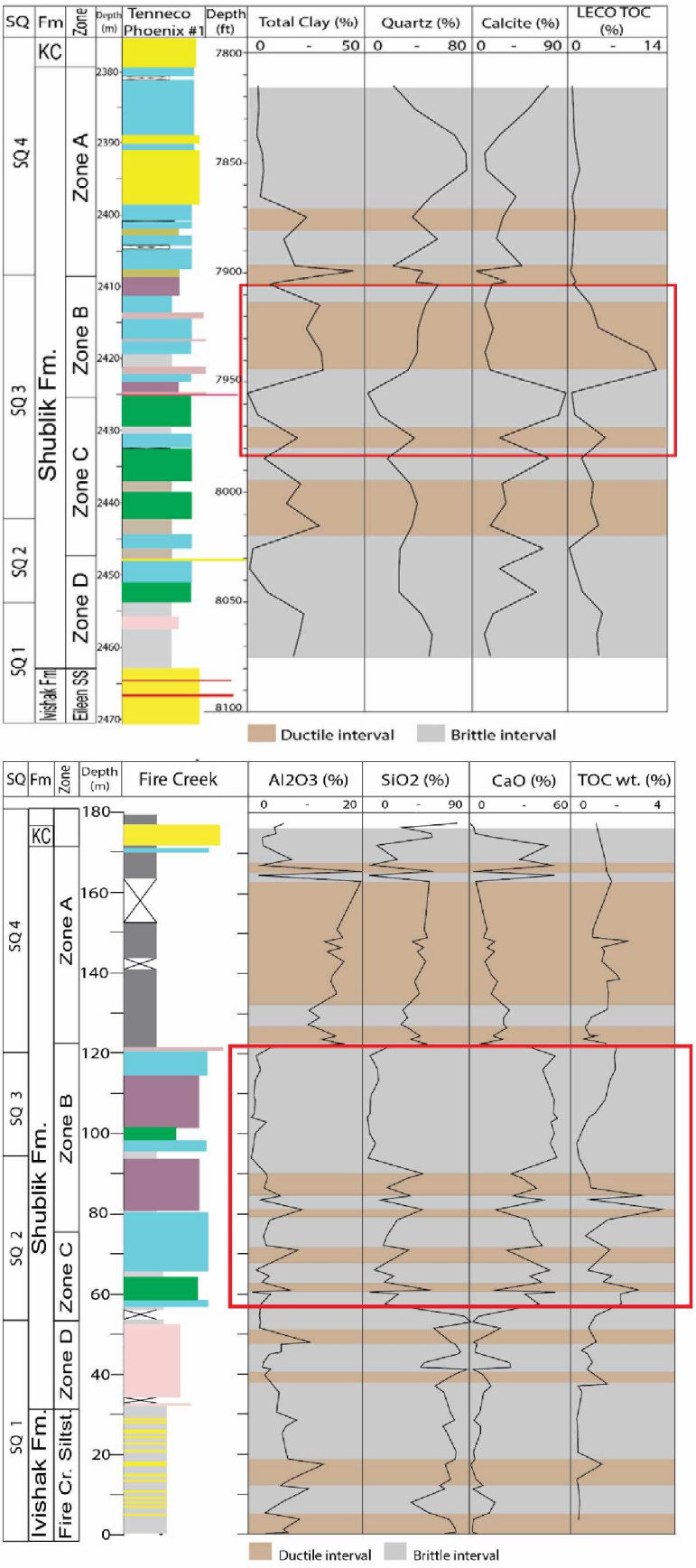

Figure 5. Relative Brittleness Index (RBi). Phoenix well displayed above on the left and Fire Creek outcrop below. Sequences shown in the far left column and zonal divisions on the right side of the column. The Phoenix scale is shown in feet and meters, and generalized stratigraphic column is modified from Hulm (1999). XRD data is plotted as line graphs to the right of the stratigraphic column for total clay, quartz, and calcite percentages. The farthest right side graph is TOC%. For Fire Creek, Kelly's (2004) whole rock geochemistry and TOC are plotted in the columns to the right of the stratigraphy column. Al_2O_3 on the left represents the clay, SiO_2 the quartz, and CaO calcite. The TOC percentage is plotted on the right. The tan colored bands are the ductile intervals and the grey bands are the brittle intervals. The red boxes outline the targeted zone. Refer to Figure 3 for lithology legend.

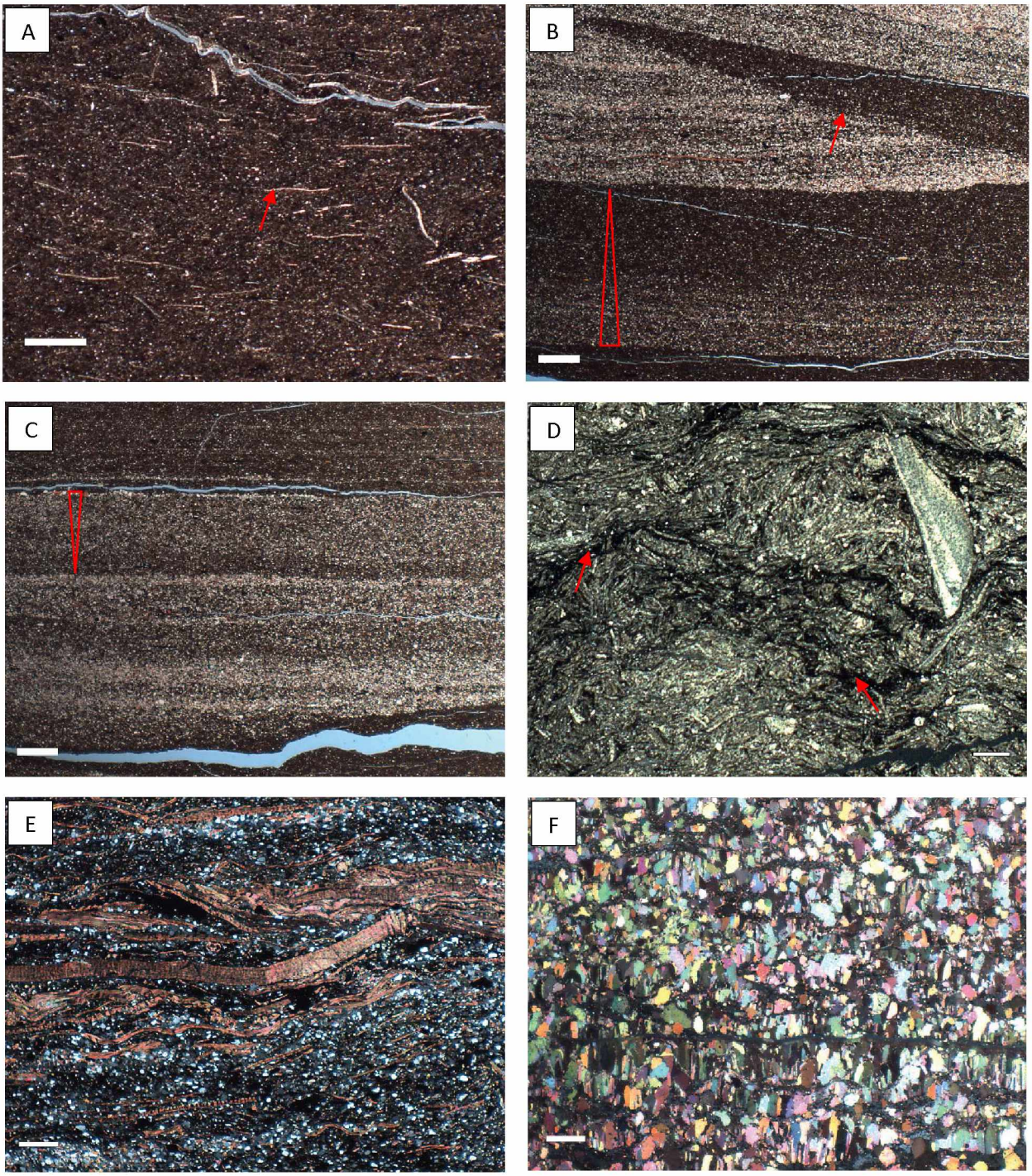

Figure 6. Microfacies photomicrographs (Group 1). A. Organic- rich silty bioclastic mudstone. Fire Creek, 124.4m. 0.5mm scale. Red arrow pointing to bioclast. B. Organic-rich siltstone. Phoenix, 8067.2 ft. (2458.88 m) 1.0mm scale. Normal grading, and red arrow pointing to erosional surface. Eileen Sandstone. C. Organic-rich siltstone. Phoenix, 8071.5 ft. (2460.19 m) 1.0mm scale. Reverse grading. D. Organic-rich bioclastic packstone/grainstone. Merak, 10732.25-10732.42 ft. (3271.19-3271.24 m) 1.0mm scale. Red arrows point to bioturbation. E. Silt-bearing packstone/floatstone; Phoenix, 7879.9 ft. (2401.79 m) 0.5mm scale. F. Organic-rich crystalline limestone; Phoenix 7998.4 ft. (2437.94 m) 1.0mm scale.

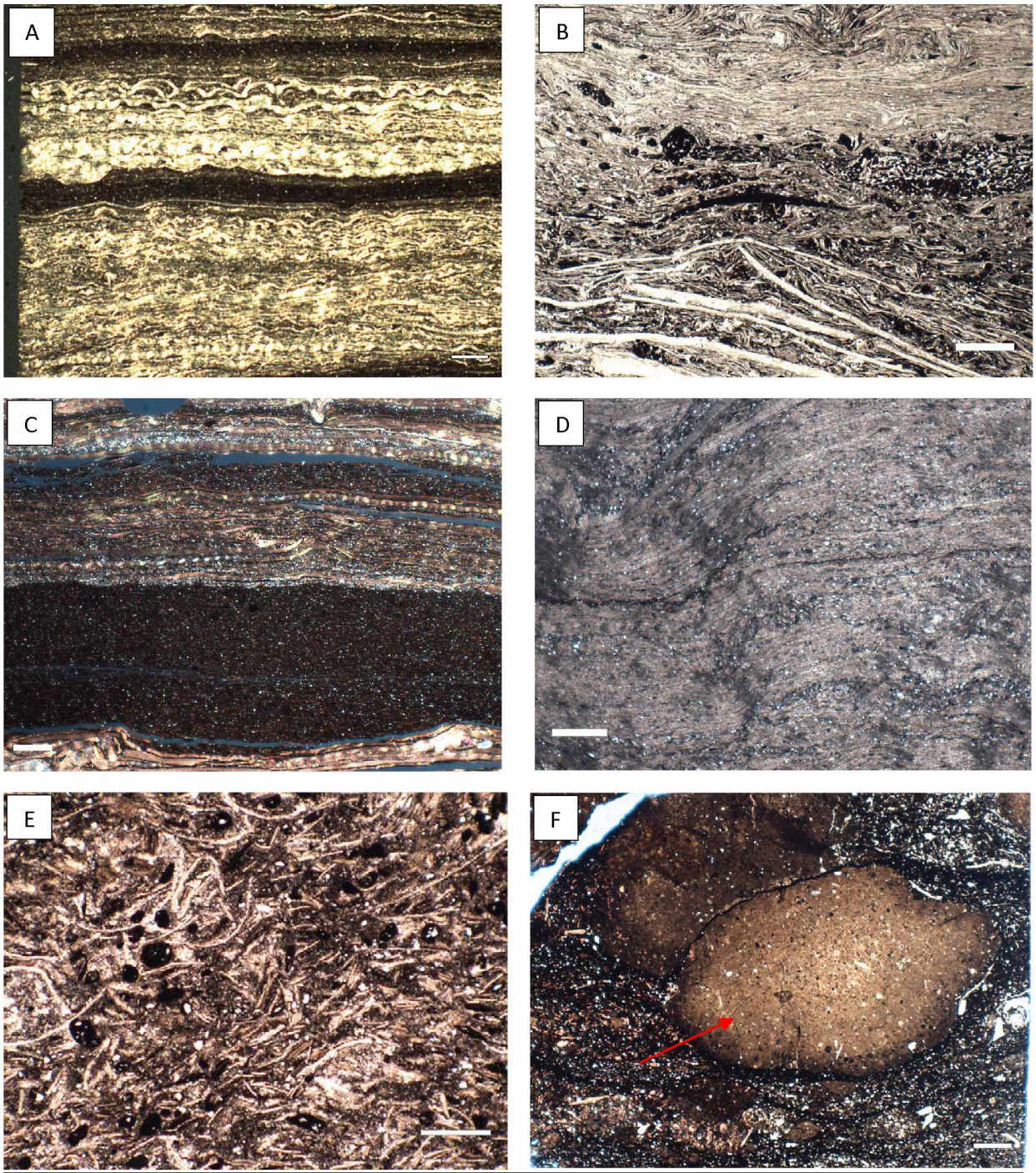

Figure 7. Microfacies photomicrographs (Group 2). A. Organic-rich, flat clam, mudstone/packstone/rudstone; Merak 10810-10810.17 ft. (3294.89-3294.99 m) 1.0mm scale. B. Phosphatic, silt-bearing, flat clam packstone; Merak IV 10783.92-10784 ft. (3286.94-3286.96 m) 1mm scale. C. Organic-rich, silt-bearing, flat clam packstone/rudstone; Phoenix, 7990.2 ft. (2435.41 m) 1.0mm scale. D. Flat clam coquina; Fire Creek 97.5 m. 1.0mm scale. E. Phosphatic coated grain bioclastic packstone; Merak IV 10820.00-10820.15ft. (3297.92-3297.98 m) 0.5mm scale. F. Bioclastic, phosphatic, silt-bearing, organic-rich nodular wackestone; Merak 10764.05-10764.20 ft. (3280.88-3280.93 m) 1.0mm scale. Red arrow pointing to phosphate nodule.

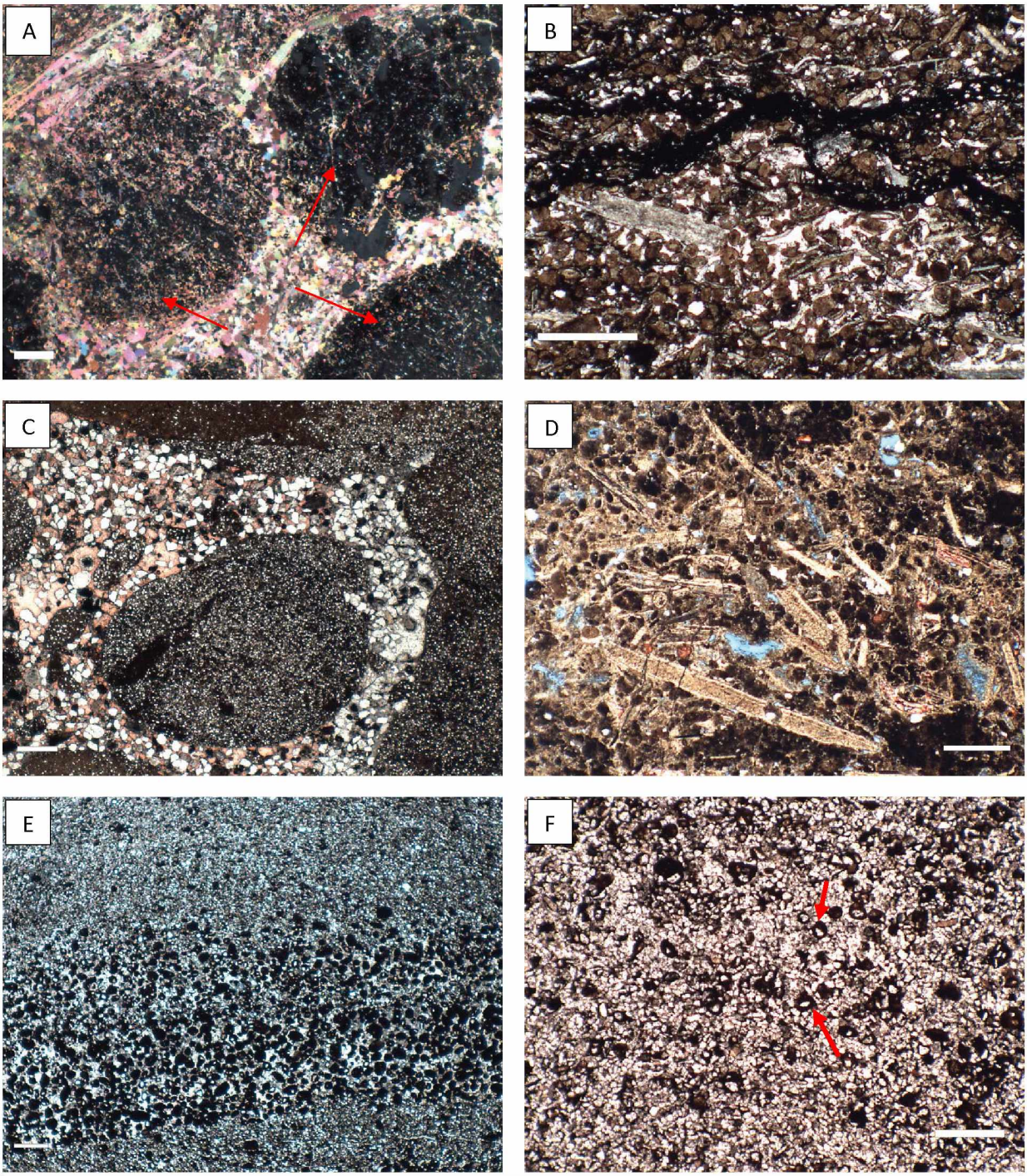

Figure 8. Microfacies photomicrographs (Group 3). A. nodular phosphatic floatstone; Phoenix, 7903.7 ft. (2409.05m) 1.0mm scale. Red arrows point to phosphate nodules. B. Phosphate wackestones/packstone; Merak IV 10771.17-10771.29 ft.(3283.05-3283.09m) .05mm scale. C. Phosphate pebble rudstone; Merak IV 10831.00-10831.15ft. (3301.29-3301.33m) 1.00mm scale. D. Bioclastic phosphatic nodular wackestone; Merak IV 10764.55-10764.75 ft. (3281.03-3281.1m) 0.5mm scale. E. Phosphatic siltstone; Last Creek 50.2m, 0.5mm scale. F. Phosphatic siltstone; Fire Creek 43m. 0.5mm scale. Red arrows point to quartz grains coated in phosphate.

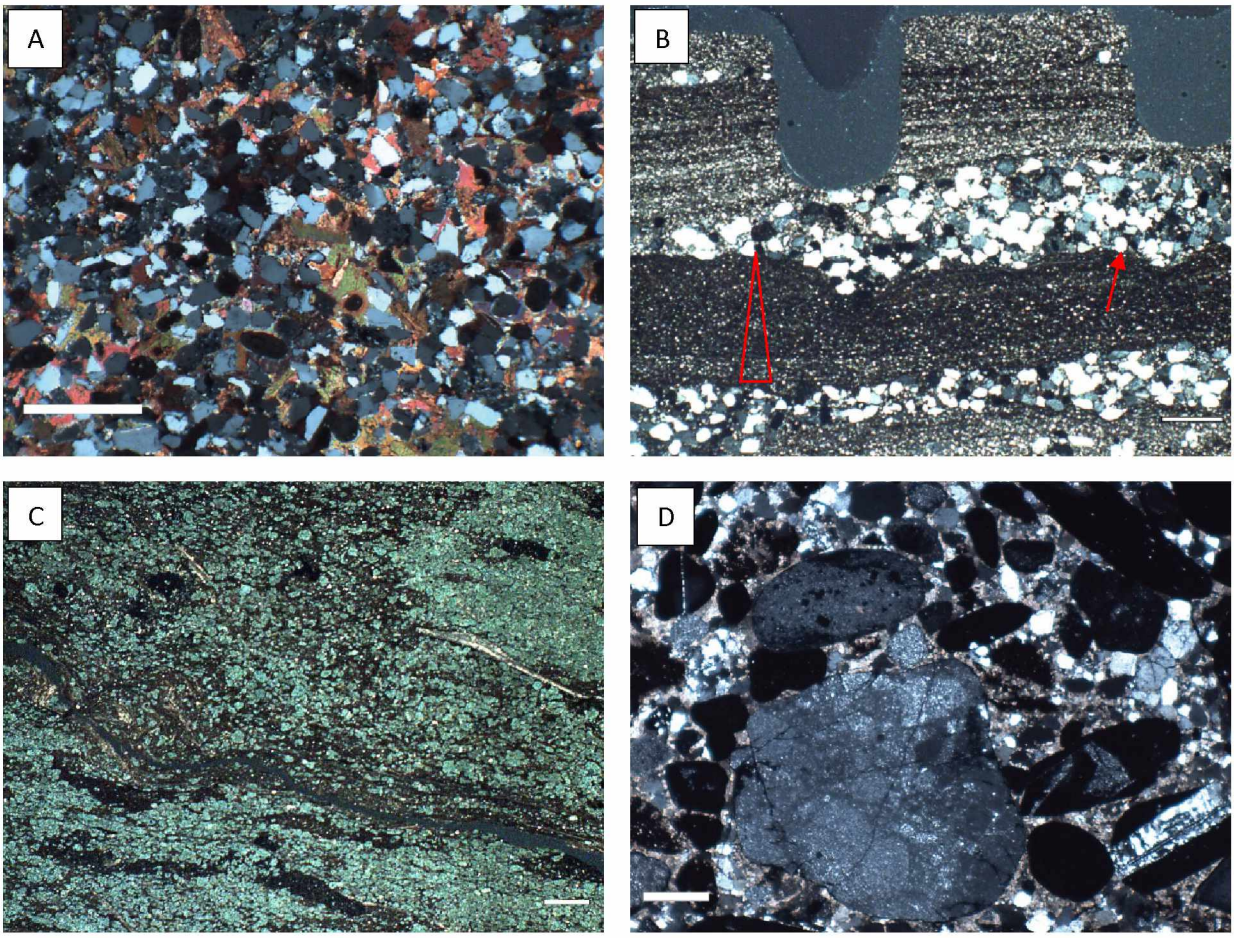

Figure 9. Microfacies photomicrographs (Group 4). A. Calcareous bioclastic sandstone; Phoenix 8034.1 ft. (2248.79m) 0.5mm scale. B. Organic-rich calcareous sandstone/siltstone; Merak IV 10831.15 ft. (3301.33m) 1.0mm scale. Red arrow pointing to erosional surface and red triangle denoting normal grading. C. Organic-rich glauconitic sandstone; Merak IV 10751.05-10751.22 ft. (3276.92-3276.97m) 1.0mm scale. D. Calcareous, silt-bearing, chert pebble conglomerate; Fire Creek 0m, 1.0mm scale.

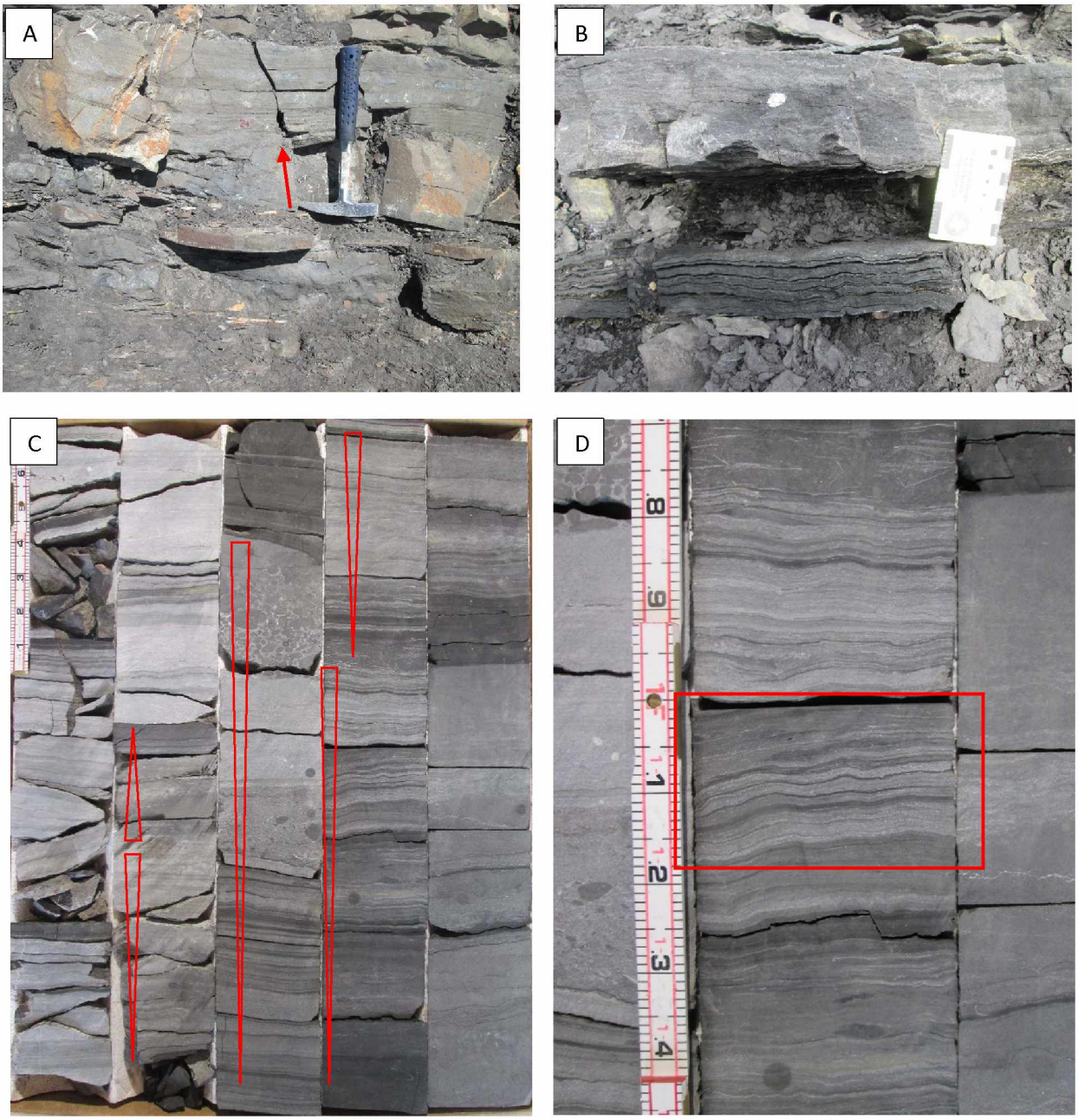

Figure 10. A. Photo from Last Creek Outcrop of the Fire Creek Siltstone red arrow pointing to bed scale Hummocky cross stratification. B. Photo from Kavik Creek outcrop. Cyclical flat clam facies bedding package illustrates bedding scale heterogeneity/anisotropy. Resistant packstone beds coupled with laminated flat clam beds of medium strength and non-competent mudstone. C. Coarsening and fining upward flat clam parasequences. Merak, depths 10803-10813 ft. (3292.75-3295.8m) D. Flat clam mudstone/packstone/rudstone. Preserved laminated beds 2-5mm thick. Merak, 10810-10810.2 ft. (3294.89-3294.95m).

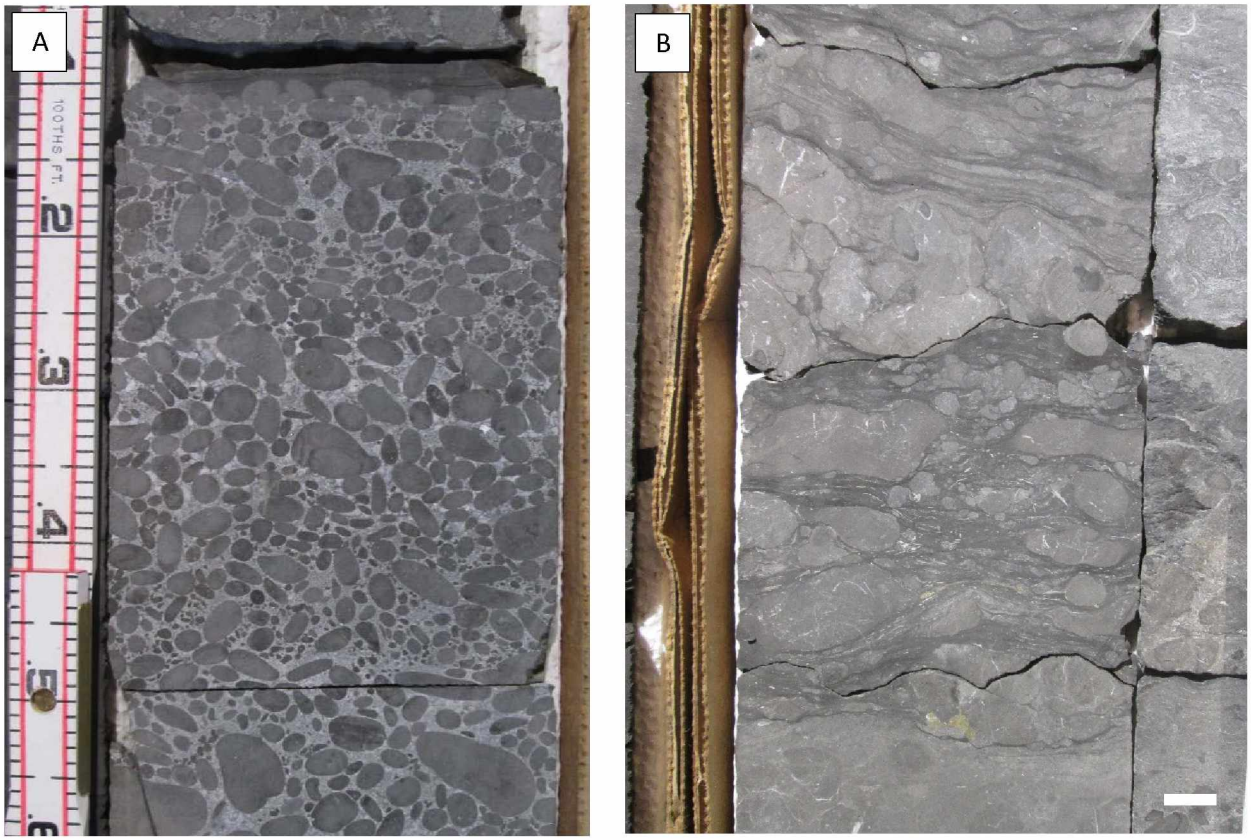

Figure 11. A. Phosphate pebble/nodule rudstone. Merak IV, Depths 10831-10831.6 ft. (3301.29-3301.47m) B. Nodular phosphatic wackestone/floatstone. Merak IV, Depths 10763.8-10764.4 ft. (3280.81-3280.99m) Scale 1 cm. Example of condensed phosphate deposit.

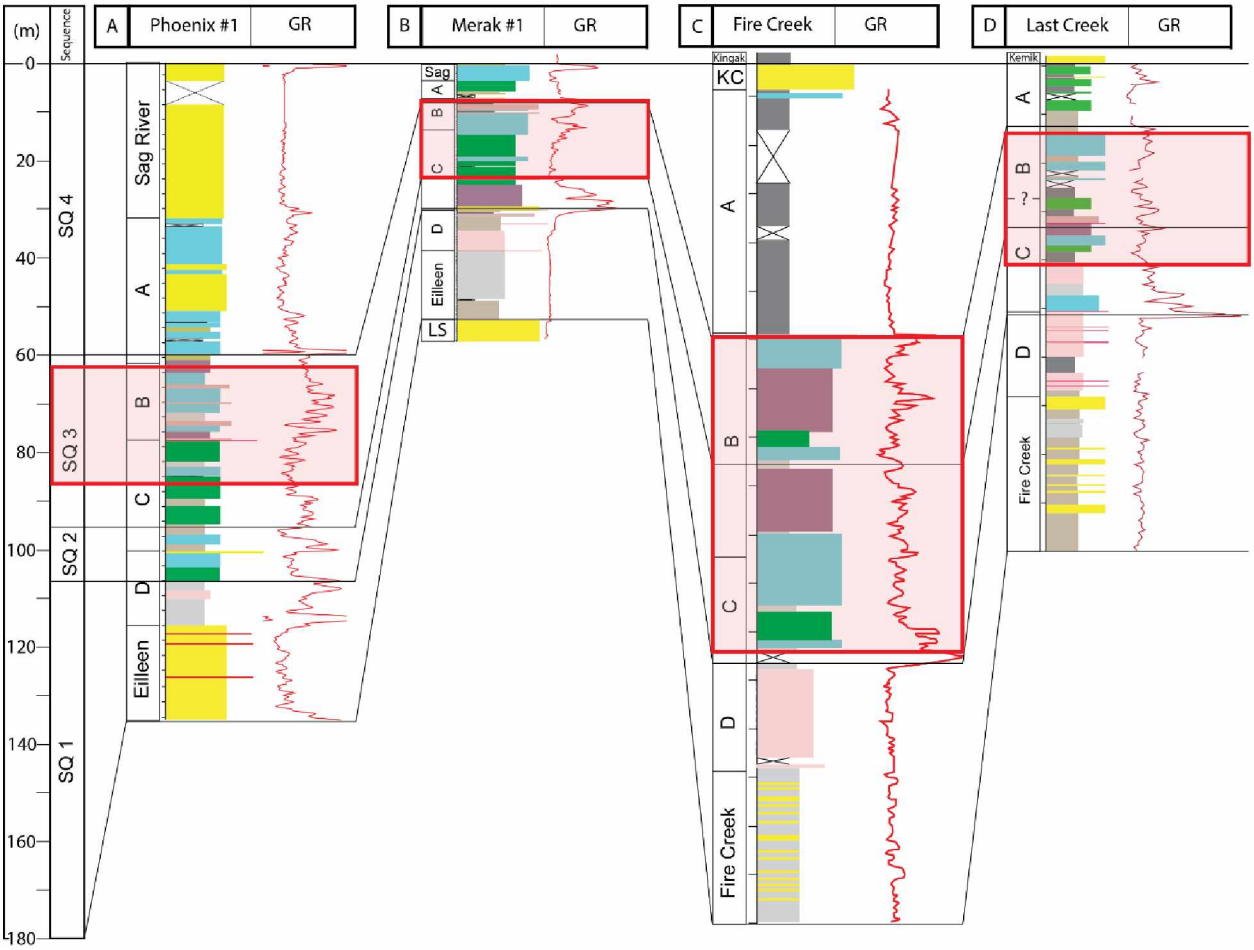

Figure 12. Generalized stratigraphic columns, starting on the left, of Phoenix, Merak, Fire Creek, and Last Creek. Scale is at far left in meters. Hutton's (2014) sequences are in right hand side of column and black lines represent sequence boundaries correlated between sections. Gamma ray is displayed in red to the right of each column. The targeted intervals are highlighted within the red translucent boxes. See Table 2 for descriptions of the target interval. Refer to Figure 3 for lithology legend.

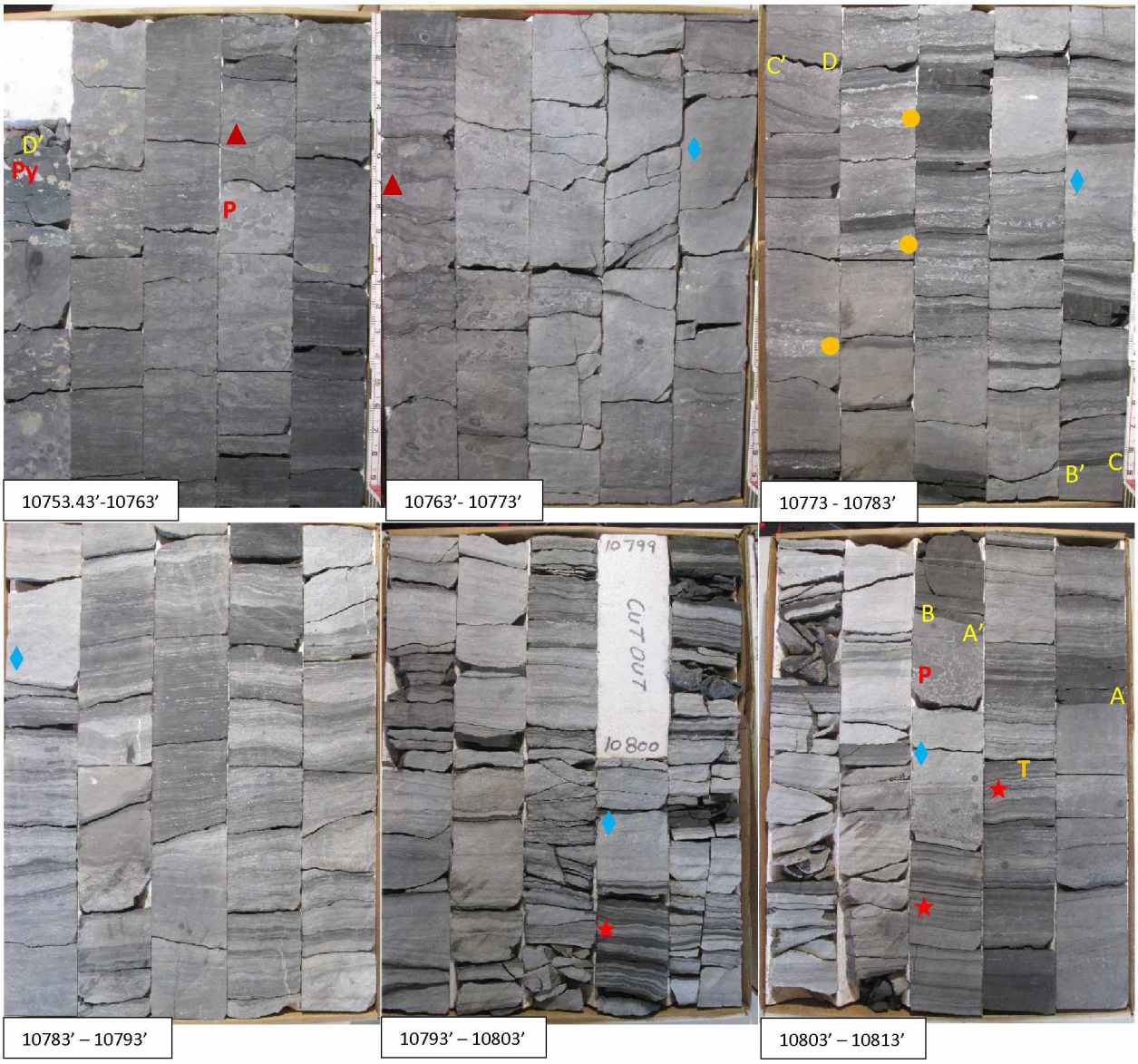

Figure 13. Merak core photo 10753.43' – 10813' (3277.65 - 3295.8m). Sequence 3 upper and lower boundaries at approximately 10753.5' (3277.67m) and 10807.5' (3294.13m) respectively. A-A' (10811.7' – 10807.6')(3295.41- 3294.16m), Cyclic, coarsening upward parasequence. Pristine flat clams (★)create laminations, grading to wackestones and packstones (♦) with bioturbation. Package is topped by phosphate pebble/nodule rudstones (**P**). B-B' (10807.6'-10782.8')(3294.16 - 3286.6m), Cyclic, coarsening upward flat clams parasequence set. The package exhibits a general trend of grading lighter in color with increased bioturbation upwards. The general texture also changes from distinct laminations to mixed/burrowed bioclastic packstones. C-C' (10782.8'- 10773.2')(3286.6 – 3283.67m) contains thin beds of black flat clam facies, flat clam mudstone, bioturbated wacke/packstone, phosphate pebble/nodule rudstones, and multiple shell lag deposits (●) approximately .01-0.1' thick, and first occurrences of condensed/winnowed phosphate pebble beds. Not clearly coarsening or fining upward more consistent repeated beds.

Figure 13 cont. D-D' (10773.2'-10753.5')(3283.67 – 32777.67m), Coarsening upward phosphate parasequence set, approximately 7 parasequences. Grade from black organic-rich to condensed (▲) and phosphate pebbles/nodule rudstone facies. Bioturbation and reworking present. Approximately 5 winnowed phosphate pebble beds are present. Glauconitc facies with abundant pyrite (**Py**) present at the uphole .5' contact. Thin sections (**T**)

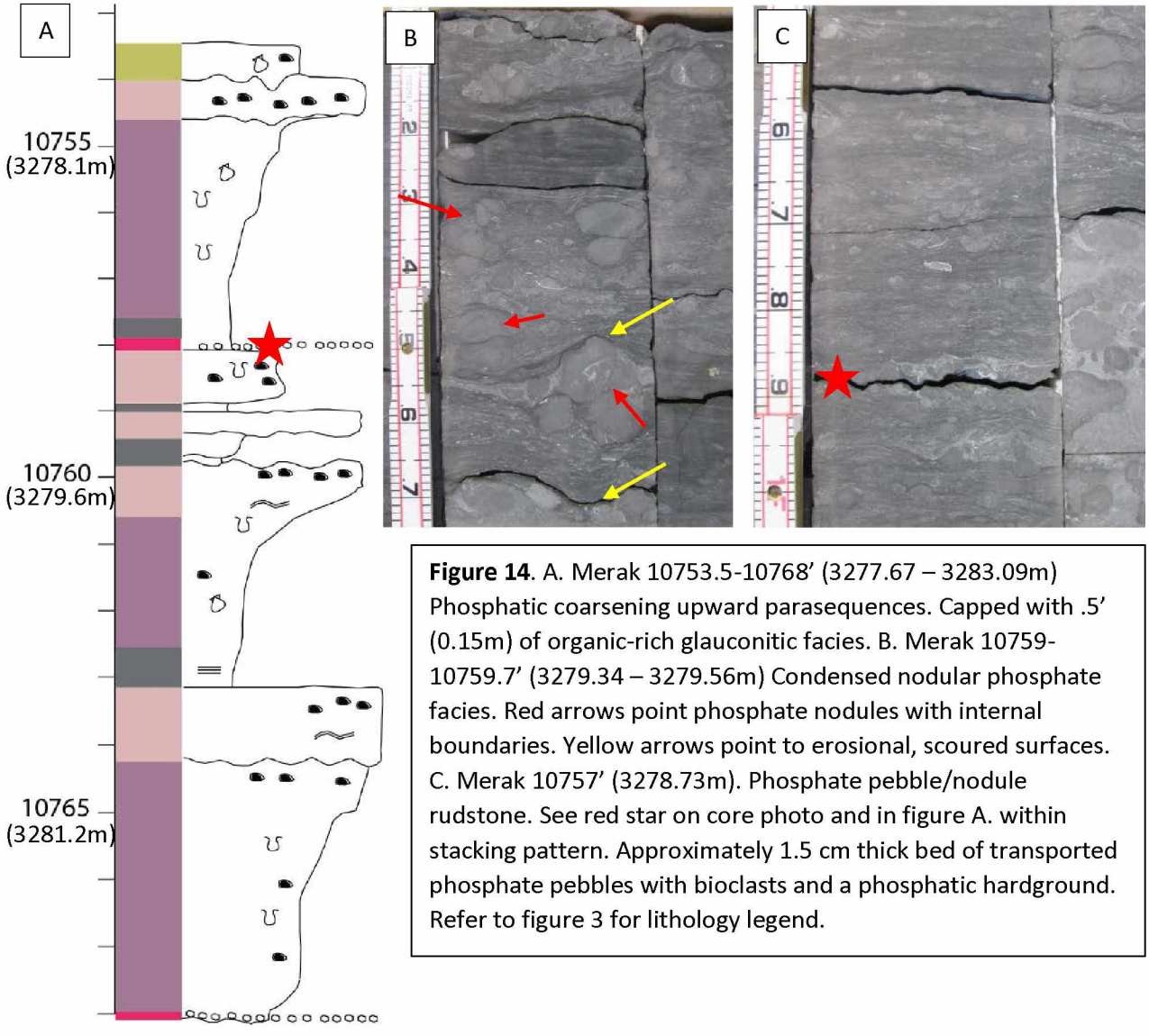

Figure 14. A. Merak 10753.5-10768' (3277.67 – 3283.09m) Phosphatic coarsening upward parasequences. Capped with .5' (0.15m) of organic-rich glauconitic facies. B. Merak 10759-10759.7' (3279.34 – 3279.56m) Condensed nodular phosphate facies. Red arrows point phosphate nodules with internal boundaries. Yellow arrows point to erosional, scoured surfaces. C. Merak 10757' (3278.73m). Phosphate pebble/nodule rudstone. See red star on core photo and in figure A. within stacking pattern. Approximately 1.5 cm thick bed of transported phosphate pebbles with bioclasts and a phosphatic hardground. Refer to figure 3 for lithology legend.

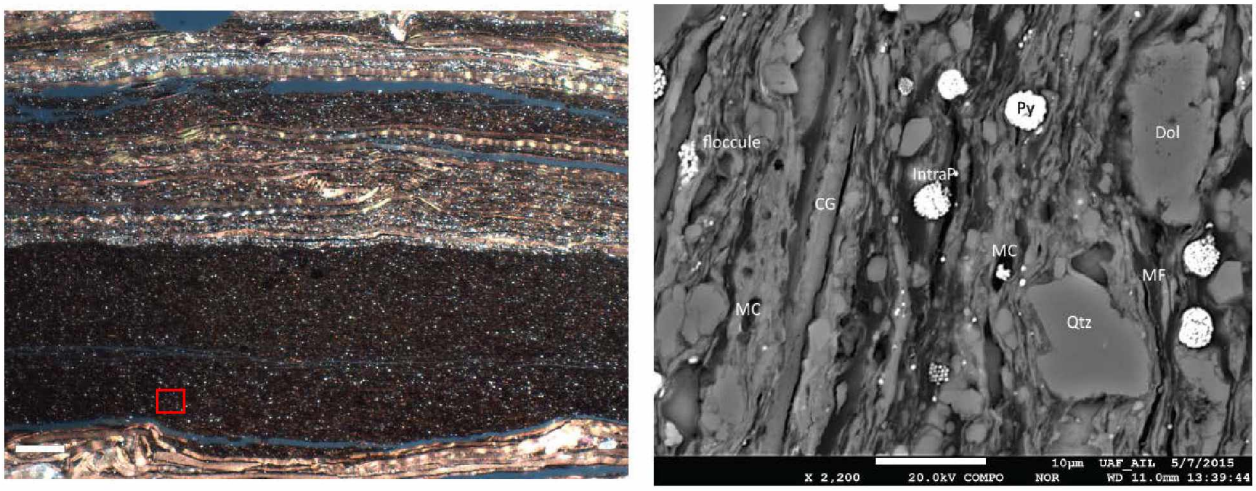

Figure 15. A Photomicrograph of 0rganic-rich silt-bearing flat clam packstone/rudstone interbedded with flat clam mudstone; Phoenix, 7990.2 ft. (2435.41m) 1.0mm scale. On the right is a BSE image within red outline of the mudstone portion between the flat clams. Stratigraphic up direction on the BSE is to the left. 10µm scale. Microchannels (MC) are abundant, note the black irregular to oval shaped voids, Microfractures (MF) are located mostly parallel with respect to bedding, individual clay flakes are distributed throughout compaction of the flakes is reduced by the pyrite framboids (Py) and intraparticle porosity (IntraP) is present within the framboids, floccules are present creating another pore type. Grains present include quartz (Qtz), dolomite (Dol), thin (approx. 2 um) flat clam carbonate grains (CG).

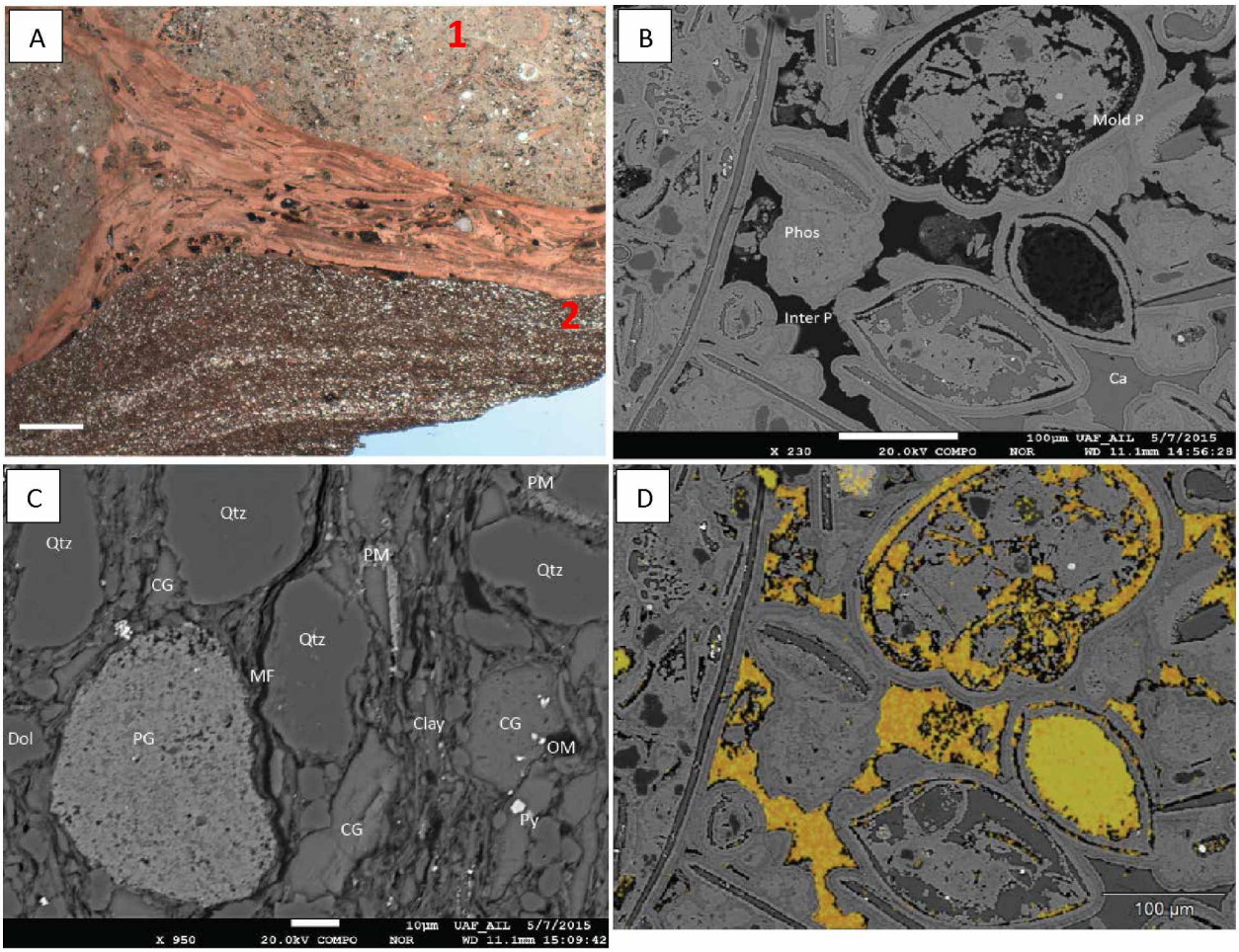

Figure 16. A. Photomicrograph of a flat clam nodular phosphate packstone/grainstone containing an erosional contact with an organic-rich siltstone. Phoenix, 7955.9 ft. (2424.96m) 1.0mm scale. B. BSE image is from interior of phosphate nodule located at the red 1 on the photomicrograph. The primary porosity present within the phosphate nodules is interparticle (InterP) and moldic porosity. Directly below the BSE labeled with a D. is the estimated porosity highlighted in yellow within the nodule totaling approximately 12%. C. BSE image of the muddy area of the photomicrograph located at the red 2. Clay, quartz, and phosphate are the primary components. Carbonate grains (CG) and Dolomite (Dol) are also present. The types of pores present in this area are microfractures (MF), and microchannels. The phosphate grain (PG) has a granular texture exhibiting intraparticle porosity. Phosphate is also present as matrix (PM).

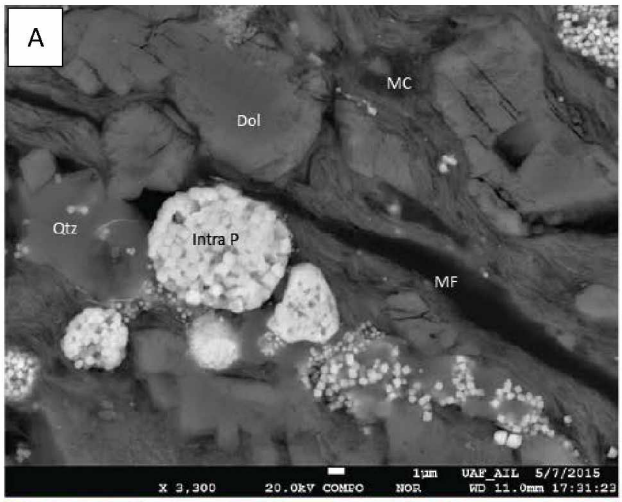

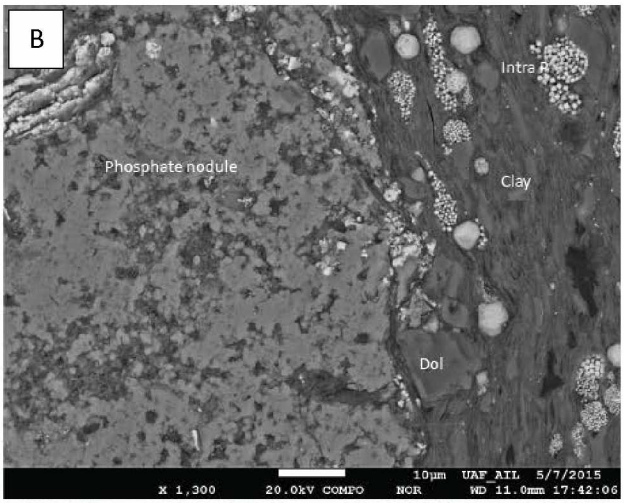

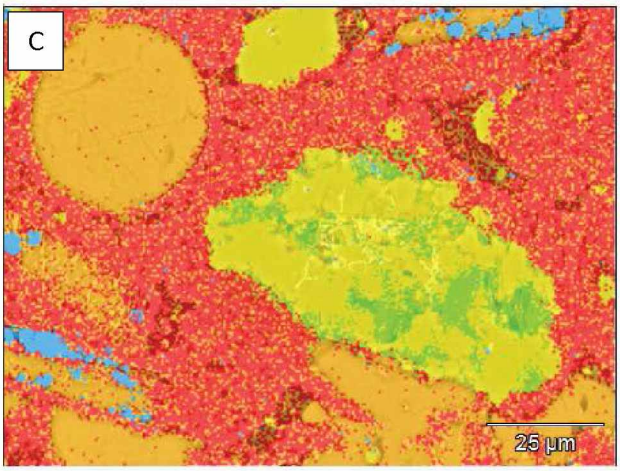

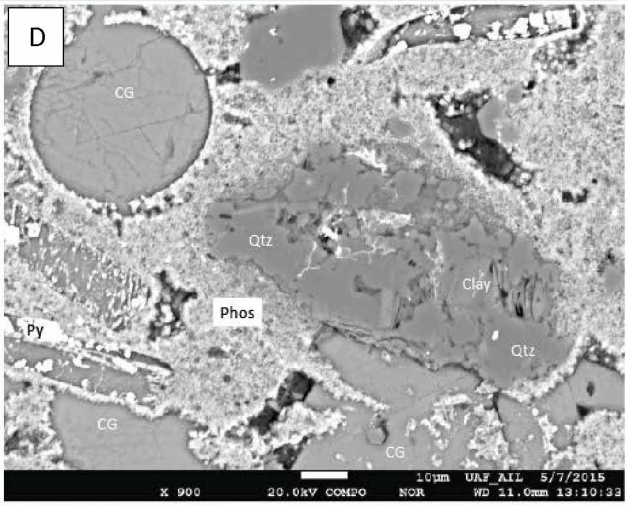

Figure 17. A & B are BSE images of a nodular phosphatic bioclastic, silt-bearing, organic-rich wackestone/floatstone; Merak 10764.05-10764.20 ft. (3280.88-3280.93m) A. Images the muddy area; microfracture (MF), microchannel (MC), and Intraparticle porosity are present. B. images the boundary of phosphate nodule and muddy matrix. The nodule contains intraparticle porosity and the muddy area has abundant framboids and microfractures between the clay flakes. C is an elemental phase map & D is a BSE image and is a nodular phosphorite floatstone; Phoenix, 7903.7 ft. (2409.05m) imaging an interior of a nodule. C. elemental phase map documenting the minerals present. D. Contains inter and intraparticle porosity within the phosphate and between the clay flakes.

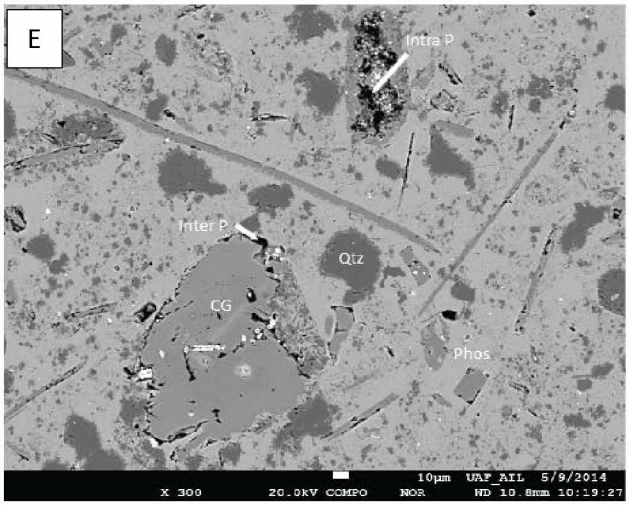

Figure 17 cont. E. BSE image from Fire Creek within a phosphate nodule. Intraparticle porosity is present within a peloid and interparticle porosity is present in and around carbonate grains (CG).

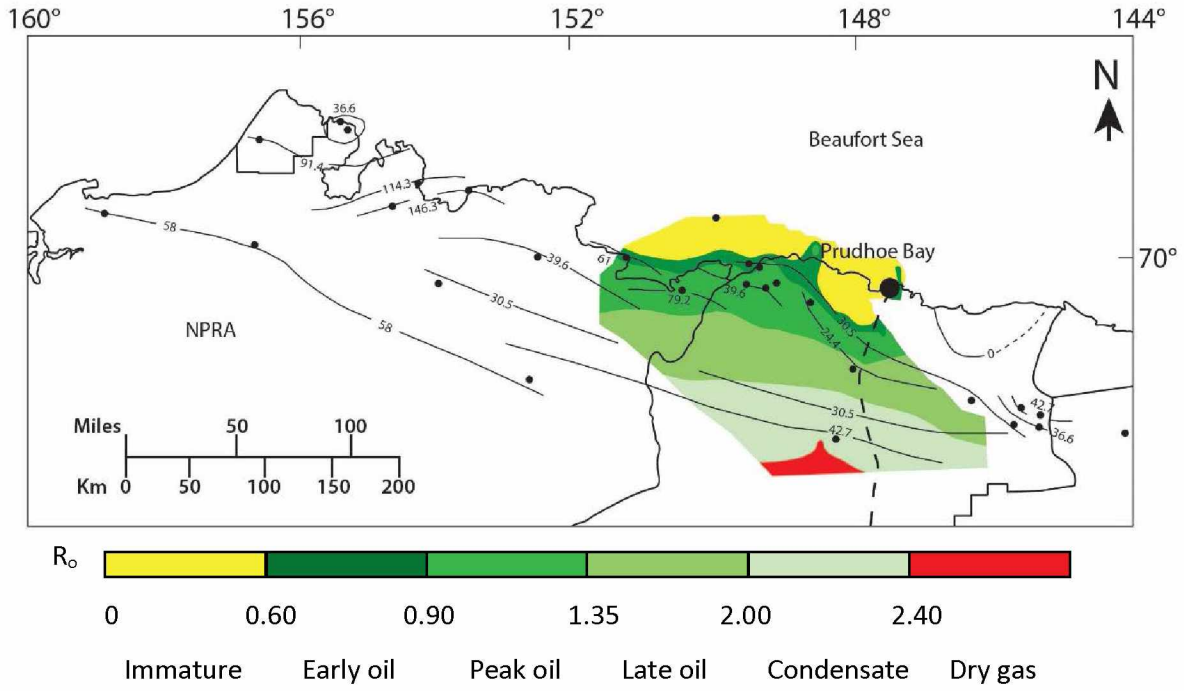

Figure 18. Regional isopach of sequences 2 and 3 of the Shublik Fm. The black points are the locations of the wells used to generate the thicknesses. The thickness is displayed in meters. The colored area of the map is the thermal maturity of the base of Kingak Shale and top of Shublik Fm. modified from Scheirer et al., (2014). The color bar represents the percent R_o. List of wells and locations in Table 2.

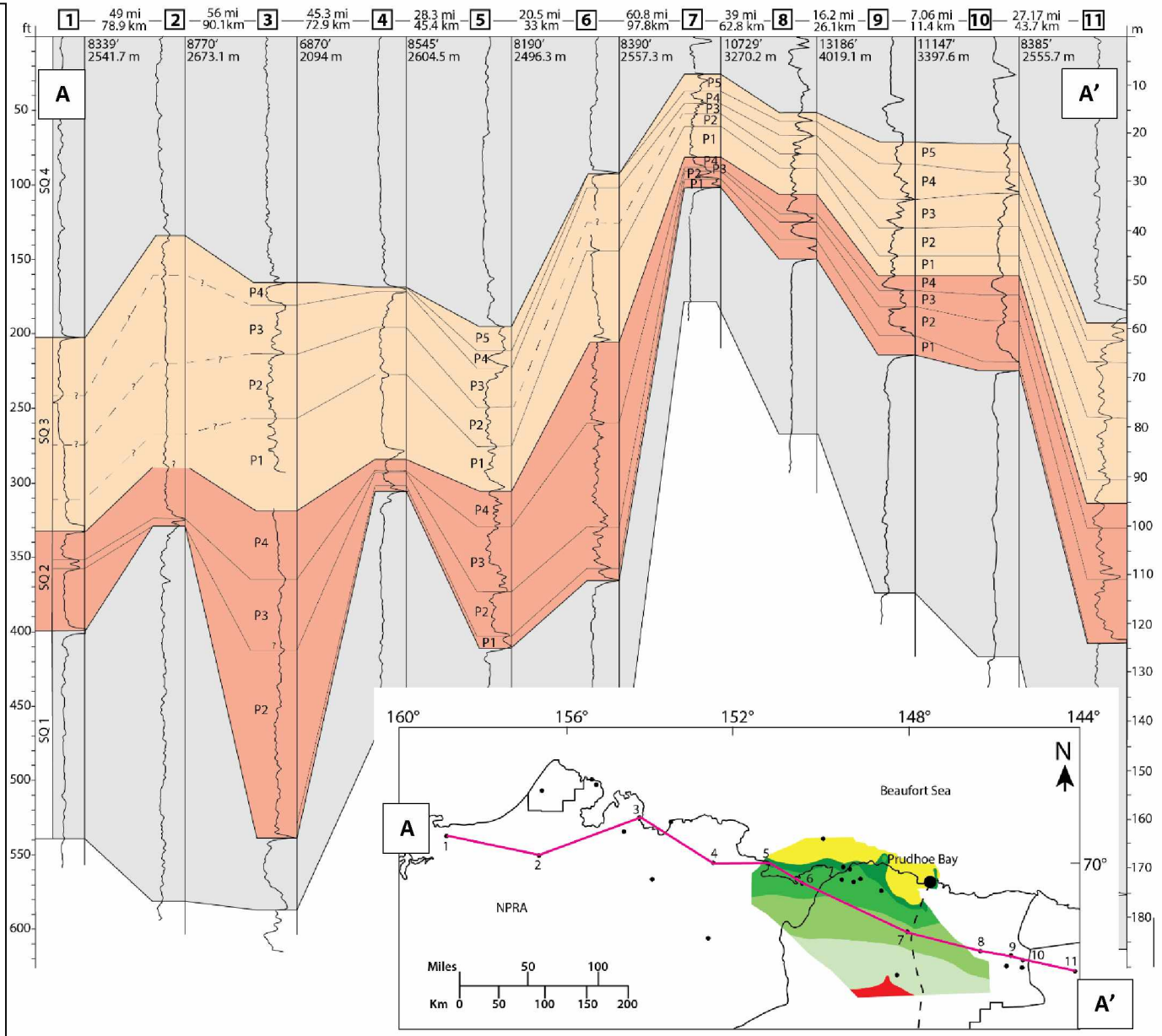

Figure 19. Cross section of Shublik Fm. generated from West to East well correlation of well locations indicated on map on the left of A-A'. The well names are located in Table 1 and correspond to the number above the well logs. Well logs are gamma ray profiles. Sequences 1-4 are shown. The base of sequence one is the top of the Ledge Sandstone. The wells are hung from the top of sequence 4 (Sag River Sandstone). The depth scale thickness is on the left in feet and on the right in meters. Sequences 1 and 4 are shaded grey and sequence 2 is dark orange and 3 is light orange. The heavy black line indicates sequences boundaries. Individual parasequences within sequences 2 are labeled P1-P4 and sequence 3 P1-P5 and are correlated by a lighter-weighted lines.

Tables

Table 1. Location of Shublik Fm. outcrop and cores shown on map in Figure 1.

Outcrops	**Location**
Fire Creek	N69°/W145°
Last Creek	69°37'48.2"N/144°26'11.58"W
Kavik Creek	69°21'25.00"N/146°31'40.00"W
Core	
Merak IV	69°58'5.077"N/148°43'1.3188"W
Phoenix 1	70.71722/-150.07166

Table 2. Target zone description of the four Shublik Fm. sections.

Section	**Phoenix core**	**Merak #1 core**	**Fire Creek**	**Last Creek**
Sequences the target interval is present	Sequence 3	Sequence 3 and part of sequence 2	Sequences 2 and 3	Sequences 2 and 3
Thickness of target interval	20.1 meters	17.22 meters	65 meters	36.5 meters
Lithofacies present (in order of abundance)	limestone (TOC%: 3.31- 11.20) flat clam facies (TOC%: 1.06 - 1.99) phosphatic limestone (TOC%: 0.62 -12.5) siltstone	flat clam facies non-phosphatic limestone phosphatic limestone (TOC%: 1.42-2.52) siltstone sandstone	limestone (TOC% 0.23 – 0.26) phosphatic limestone (TOC% 0.6 – 3.53) flat clam facies (TOC%: 0.2 – 1.43) siltstone (TOC%: 2.58)	Phosphatic limestone non-phosphatic limestone siltstone flat clam facies

Table 3. List of wells with location and API number used to generate isopach in Figure 17

Well Name	API	Location
ATIGARU PT #1	50103200080000	70.55612/-151.71718
BELI UNIT #1	50179200020000	69.71077/-146.53551
BURGLIN #33-1	50029211060000	70.17314/-148.57830
BUSH FED #1	50223200040000	69.65856/-149.03332
CANNING RIV U BLK A #1	50179200050000	69.60616/-146.33538
CANNING RIV UNIT #B-1	50179200060000	69.66385/-146.27537
DREW PT #1	50279200020000	70.87976/-153.89999
E HARRISON BAY ST #1	50703200010000	70.49447/-150.03020
E SIMPSON TEST WELL #1	50279200050000	70.91779/-154.61799
E TESHEKPUK #1	50103200060000	70.56992/-152.94359
E UGNU #1	50029200520000	70.39929/-149.67122
HEMI SPRINGS ST #1	50029210560000	70.23185/-149.21928
HEMI SPRINGS UNIT #3	50029212850000	70.13637/-148.71677
HIGHLAND ST #1	50029201990000	70.29189/-149.21833
IKPIKPUK #1	50279200040000	70.45547/-154.33133
INIGOK #1	50279200030000	70.00485/-153.09917
KALUBIK CK #1	50103201650000	70.49396/-150.27502
KAVIK UNIT #2	50179200030000	69.63244/-146.65597
KAVIK UNIT #3	50179200040000	69.63228/-146.53230
NECHELIK #1	50103200200000	70.39330/-150.97913
OCS Y-0338 PHOENIX	55231000050000	70.71722/-150.07166
OLIKTOK PT #1	50029207010000	70.48119/-149.87141
PEARD TEST WELL #1	50301200020000	70.71565/-159.00070
S MEADE #1	50163200010000	70.61498/-156.88986
S SIMPSON #1	50279200010000	70.80687/-154.98184
SIMPSON TEST #1	50279100320000	70.95333/-155.36444
TULAGEAK #1	50023200180000	71.18933/-155.73356
UGNU #1	50029200090000	70.38162/-149.82603
W DEASE #1	50023200140000	71.15907/-155.62922
W KAVIK UNIT #1	50223200020000	69.77024/-147.18560
WALAKPA #01	50023200130000	71.09934/-156.88439
KALUBIK CK #1	50103200010000	70.40497/-150.07025

Table 4. List of wells for cross section in Figure 18.

1	Peard Test Well
2	S Meade 1
3	E Simpson Test
4	E Teshekpuk
5	Atigaru Pt
6	Nechelik 1
7	Merak 1
8	W Kavik
9	Beli Unit
10	Canning River B-1
11	Fire Creek outcrop

Appendix A. Kelly (2004) data set of trace, elemental, and TOC% from Fire Creek at measured stratigraphic intervals.

Sample ID	Meters Fire Cr	U (ppm)	Mo (ppm)	V (ppm)	Ni (ppm)	Co (ppm)	Th (ppm)	Cr ppm	Ni (ppm)	Cu (ppm)	P (%)	Ba (ppm)
1FC177.5	177.50	4.70	6.00	203.00	33.00	4.00	7.40	75.00	33.00	30.00	0.04	559.00
1FC176.5	176.50	2.80	8.00	215.00	42.00	9.00	3.90	91.00	42.00	27.00	0.04	205.00
1FC175	175.00	5.60	4.00	899.00	43.00	8.00	15.60	2360.00	43.00	11.00	0.57	59.00
1FC174	174.00	24.90	0.00	289.00	25.00	7.00	6.40	621.00	25.00	13.00	3.66	84.00
1FC172	172.00	1.50	0.00	35.00	9.00	<2	1.80	15.00	9.00	18.00	0.02	155.00
1FC168.5	168.50	15.10	4.00	115.00	40.00	4.00	3.80	53.00	40.00	29.00	0.34	670.00
1FC167	167.00	1.10	0.00	30.00	7.00	<2	1.20	29.00	7.00	17.00	0.07	130.00
1FC165.5	165.50	4.00	18.00	330.00	69.00	16.00	12.00	116.00	69.00	56.00	0.04	1190.00
1FC164.5	164.50	0.70	0.00	19.00	6.00	<2	1.00	10.00	6.00	17.00	0.06	100.00
1FC163	163.00	5.40	27.00	454.00	77.00	15.00	13.20	124.00	77.00	58.00	0.03	1080.00
1FC151	151.00	3.90	0.00	232.00	46.00	9.00	9.80	164.00	46.00	35.00	0.06	1130.00
1FC149	149.00	3.80	0.00	207.00	37.00	8.00	11.20	96.00	37.00	40.00	0.08	1980.00
1FC148	148.00	9.00	80.00	185.00	79.00	15.00	9.00	91.00	79.00	64.00	0.07	1120.00
1FC146.5	146.50	4.20	0.00	262.00	42.00	8.00	11.20	228.00	42.00	37.00	0.07	1160.00
1FC145.5	145.50	4.70	0.00	286.00	48.00	9.00	9.30	174.00	48.00	41.00	0.08	1020.00
1FC143	143.00	4.10	0.00	297.00	56.00	10.00	10.60	243.00	56.00	44.00	0.07	1220.00
1FC139.5	139.50	4.30	0.00	238.00	67.00	11.00	9.30	269.00	67.00	48.00	0.10	1130.00
1FC138.5	138.50											
1FC138	138.00	3.70	0.00	250.00	48.00	8.00	8.70	248.00	48.00	39.00	0.09	1130.00
1FC135	135.00	4.00	0.00	244.00	64.00	11.00	10.20	279.00	64.00	46.00	0.10	1250.00
1FC130.9	130.90	4.50	4.00	220.00	61.00	8.00	7.20	254.00	61.00	52.00	0.09	1070.00
1FC129	129.00	4.20	0.00	179.00	33.00	7.00	8.40	88.00	33.00	39.00	0.10	1110.00
1FC127.3	127.30	4.60	5.00	128.00	120.00	19.00	5.90	103.00	120.00	55.00	0.23	54.00
1FC126.5	126.50	4.30	0.00	168.00	24.00	6.00	7.50	144.00	24.00	33.00	0.12	1190.00
1FC124.5	124.50											
1FC124.4	124.40	4.40	0.00	191.00	49.00	11.00	9.10	210.00	49.00	51.00	0.07	1690.00
1FC123.6	123.60	4.50	0.00	167.00	38.00	8.00	8.10	69.00	38.00	30.00	0.06	1430.00
1FC122.5	122.50	6.20	0.00	203.00	42.00	10.00	11.60	221.00	42.00	38.00	0.13	1730.00
1FC122	122.00											
1FC121.5	121.50	108.00	9.00	71.00	35.00	5.00	2.60	58.00	35.00	26.00	6.99	111.00
1FC119.5	119.50	30.70	17.00	39.00	33.00	<2	1.60	62.00	33.00	34.00	4.65	437.00

Appendix A cont.

Sample ID	Meters Fire Cr	U (ppm)	Mo (ppm)	V (ppm)	Ni (ppm)	Co (ppm)	Th (ppm)	Cr ppm	Ni (ppm)	Cu (ppm)	P (%)	Ba (ppm)
1FC116	116.00	10.50	3.00	33.00	37.00	2.00	1.90	104.00	37.00	37.00	1.50	834.00
1FC113.3	113.30	14.00	2.00	26.00	27.00	<2	1.40	39.00	27.00	31.00	2.86	822.00
1FC109.5	109.50	12.90	3.00	43.00	15.00	<2	1.80	43.00	15.00	22.00	1.60	519.00
1FC108.5	108.50	34.60	8.00	61.00	15.00	<2	3.40	49.00	15.00	23.00	6.63	607.00
1FC105.2	105.20	1.90	20.00	185.00	32.00	<2	0.90	9.00	32.00	34.00	0.01	215.00
1FC104.1	104.10	3.70	11.00	103.00	33.00	<2	0.70	<2	33.00	0.00	0.02	133.00
1FC103	103.00	1.00	12.00	178.00	16.00	3.00	0.90	9.00	16.00	21.00	0.01	295.00
1FC100.1	100.10	3.70	16.00	111.00	31.00	<2	0.70	<2	31.00	0.00	0.02	121.00
1FC97.5	97.50	5.50	3.00	11.00	11.00	<2	1.40	4.00	11.00	0.00	0.05	137.00
1FC94	94.00	4.50	2.00	49.00	7.00	<2	1.10	5.00	7.00	0.00	0.16	89.00
1FC90	90.00	18.80	6.00	63.00	25.00	2.00	6.10	29.00	25.00	7.00	1.44	222.00
1FC89	89.00	14.50	5.00	47.00	15.00	3.00	4.60	20.00	15.00	7.00	2.30	207.00
F37	86.50	7.20	4.00	33.00	22.00	2.00	3.10	61.00	22.00	5.00	0.66	195.00
F36	84.50	10.50	9.00	83.00	37.00	4.00	5.40	98.00	37.00	25.00	2.01	677.00
F35	83.50	5.10	6.00	26.00	16.00	2.00	2.30	36.00	16.00	0.00	0.51	130.00
1FC81.1	81.10	14.90	13.00	157.00	80.00	8.00	8.00	103.00	80.00	73.00	1.63	488.00
1FC78.5	78.50	15.10	7.00	65.00	42.00	3.00	4.70	55.00	42.00	28.00	2.71	303.00
1FC74.5	74.50	4.10	29.00	32.00	22.00	<2	4.00	47.00	22.00	6.00	0.37	221.00
IFC72.1	72.10	6.00	4.00	38.00	21.00	3.00	3.30	49.00	21.00	6.00	1.74	276.00
IFC71	71.00	11.00	16.00	119.00	60.00	7.00	8.50	55.00	60.00	43.00	1.01	551.00
F34	66.00	6.80	4.00	37.00	15.00	<2	2.10	14.00	15.00	0.00	1.30	112.00
F33	64.50	22.10	7.00	46.00	32.00	2.00	5.80	71.00	32.00	24.00	4.94	219.00
F32	63.00	15.00	7.00	54.00	27.00	<2	3.70	28.00	27.00	12.00	3.74	240.00
F31	61.00	43.10	45.00	582.00	103.00	5.00	11.50	60.00	103.00	66.00	2.79	371.00
F30	60.50	4.60	4.00	34.00	7.00	<2	1.00	16.00	7.00	0.00	0.73	48.00
F29	60.00	67.40	11.00	288.00	39.00	2.00	6.90	115.00	39.00	41.00	7.29	321.00
1FC57.6	57.50	41.20	4.00	176.00	26.00	<2	3.80	64.00	26.00	21.00	8.31	230.00
F28	54.50	5.20	3.00	43.00	13.00	2.00	6.70	10.00	13.00	7.00	1.42	115.00
1FC53	53.00	2.10	2.00	46.00	8.00	<2	5.30	7.00	8.00	8.00	0.25	120.00
F27	51.50	13.90	3.00	36.00	10.00	<2	4.50	15.00	10.00	7.00	4.29	204.00
F26	48.00	5.30	5.00	175.00	31.00	6.00	10.10	62.00	31.00	25.00	0.43	414.00
F25	47.50	3.40	3.00	79.00	19.00	3.00	6.30	44.00	19.00	11.00	0.89	289.00

Appendix A cont.

Sample ID	Meters Fire Cr	U (ppm)	Mo (ppm)	V (ppm)	Ni (ppm)	Co (ppm)	Th (ppm)	Cr ppm	Ni (ppm)	Cu (ppm)	P (%)	Ba (ppm)
F24	46.00											
F23	45.50	5.30	3.00	109.00	19.00	3.00	7.10	29.00	19.00	11.00	0.69	219.00
1FC45	45.00	5.60	2.00	62.00	14.00	<2	4.30	20.00	14.00	10.00	1.63	184.00
1FC42.9	42.90	11.90	0.00	37.00	14.00	2.00	2.80	18.00	14.00	12.00	7.03	204.00
F22	41.75	13.10	0.00	41.00	14.00	<2	2.60	29.00	14.00	14.00	7.40	406.00
F21	41.25	3.50	3.00	86.00	17.00	3.00	6.00	38.00	17.00	12.00	0.31	177.00
F20	40.00	7.10	0.00	50.00	10.00	<2	5.00	39.00	10.00	9.00	2.00	216.00
F19	37.50											
F18	37.00	4.90	0.00	59.00	12.00	2.00	4.80	41.00	12.00	13.00	2.75	301.00
F17	35.50	2.30	0.00	55.00	14.00	3.00	4.50	30.00	14.00	13.00	0.82	242.00
F16	30.50	3.40	0.00	59.00	14.00	3.00	10.60	32.00	14.00	8.00	0.36	255.00
1FC28.5	28.50	2.30	0.00	64.00	21.00	8.00	7.90	14.00	21.00	13.00	0.18	310.00
1FC27	27.00	2.30	0.00	41.00	21.00	6.00	7.20	15.00	21.00	10.00	0.21	236.00
1FC25.3	25.30	4.20	0.00	63.00	41.00	12.00	8.70	37.00	41.00	15.00	1.27	261.00
F15	20.50	2.80	0.00	57.00	29.00	9.00	7.40	27.00	29.00	18.00	0.29	208.00
1FC18.8	18.80	2.90	0.00	61.00	26.00	7.00	8.00	16.00	26.00	12.00	0.19	414.00
F14	17.50	3.60	0.00	126.00	44.00	9.00	11.10	68.00	44.00	24.00	0.18	440.00
F13	13.70	2.50	0.10	48.00	27.00	8.00	7.90	29.00	27.00	10.00	0.17	241.00
F12	12.20	2.00	0.10	40.00	16.00	4.00	5.90	32.00	16.00	12.00	0.14	172.00
F11	11.40	3.10	0.10	83.00	43.00	11.00	9.40	43.00	43.00	17.00	0.20	343.00
F10	8.00	2.00	2.00	58.00	23.00	5.00	5.80	33.00	23.00	14.00	0.19	199.00
F9	5.40	1.60	4.00	28.00	32.00	5.00	3.80	17.00	32.00	11.00	0.27	99.00
F8	3.80	3.00	1.00	78.00	24.00	8.00	8.90	47.00	24.00	14.00	0.20	258.00
F5	1.25	3.10	9.00	52.00	106.00	9.00	5.60	37.00	106.00	23.00	0.33	164.00
F4	0.50	2.60	3.00	62.00	25.00	6.00	7.30	29.00	25.00	12.00	0.25	181.00
F2	0.20	2.60	12.00	39.00	35.00	4.00	2.90	15.00	35.00	16.00	0.59	180.00

Appendix A cont.

Sample ID	Meters Fire Cr	Zn (ppm)	Mo (ppm)	TOC (wt%)	Al (%)	SiO2 (%)	Si (%)calc	K (%)	Ti %ICP40	Cr2O3 % XRF	Cr (%)calc	Co (ppm)	Cr ppm
1FC177.5	177.50	90.00	6.00	0.98	4.72	79.70	37.25	1.42	0.28	0.02	0.01	4.00	75.00
1FC176.5	176.50	70.00	8.00		2.39	33.20	15.52	0.30	0.12	0.02	0.01	9.00	91.00
1FC175	175.00	472.00	4.00		2.49	57.80	27.02	0.03	0.12	0.62	0.42	8.00	2360.00
1FC174	174.00	219.00	0.00		1.32	58.90	27.53	0.06	0.08	0.17	0.12	7.00	621.00
1FC172	172.00	21.00	0.00		1.32	11.60	5.42	0.31	0.06	0.00	0.00	<2	15.00
1FC168.5	168.50	74.00	4.00	1.32	4.22	29.10	13.60	0.96	0.19	0.02	0.01	4.00	53.00
1FC167	167.00	15.00	0.00		1.04	5.76	2.69	0.23	0.04	0.00	0.00	<2	29.00
1FC165.5	165.50	126.00	18.00	1.38	10.20	59.60	27.86	2.29	0.46	0.02	0.01	16.00	116.00
1FC164.5	164.50	13.00	0.00		0.87	5.45	2.55	0.19	0.03	0.00	0.00	<2	10.00
1FC163	163.00	123.00	27.00	1.57	10.20	56.20	26.27	2.13	0.44	0.02	0.01	15.00	124.00
1FC151	151.00	111.00	0.00	0.86	8.68	51.90	24.26	1.89	0.34	0.03	0.02	9.00	164.00
1FC149	149.00	94.00	0.00	0.83	8.94	54.70	25.57	1.88	0.37	0.02	0.01	8.00	96.00
1FC148	148.00	98.00	80.00	2.22	7.40	42.00	19.63	1.57	0.31	0.01	0.01	15.00	91.00
1FC146.5	146.50	106.00	0.00	1.19	8.63	51.70	24.17	1.85	0.31	0.04	0.03	8.00	228.00
1FC145.5	145.50	121.00	0.00	1.29	7.74	46.20	21.60	1.77	0.31	0.04	0.03	9.00	174.00
1FC143	143.00	133.00	0.00	1.20	8.77	53.20	24.87	2.04	0.34	0.04	0.03	10.00	243.00
1FC139.5	139.50	143.00	0.00	1.79	7.85	46.60	21.78	1.84	0.31	0.04	0.03	11.00	269.00
1FC138.5	138.50			1.87			0.00				0.00		
1FC138	138.00	121.00	0.00	1.39	7.67	43.80	20.47	1.79	0.30	0.04	0.03	8.00	248.00
1FC135	135.00	128.00	0.00	1.45	8.56	47.80	22.34	1.97	0.32	0.04	0.03	11.00	279.00
1FC130.9	130.90	121.00	4.00	1.42	5.76	33.80	15.80	1.44	0.21	0.04	0.03	8.00	254.00
1FC129	129.00	91.00	0.00	0.80	6.56	37.90	17.72	1.56	0.26	0.03	0.02	7.00	88.00
1FC127.3	127.30	82.00	5.00	0.64	4.67	32.10	15.00	1.14	0.18	0.02	0.01	19.00	103.00
1FC126.5	126.50	82.00	0.00	0.54	6.41	37.70	17.62	1.62	0.25	0.02	0.01	6.00	144.00
1FC124.5	124.50			0.73			0.00				0.00		
1FC124.4	124.40	91.00	0.00	1.01	8.05	48.60	22.72	2.07	0.31	0.03	0.02	11.00	210.00
1FC123.6	123.60	113.00	0.00	0.51	6.91	40.90	19.12	1.77	0.26	0.02	0.01	8.00	69.00
1FC122.5	122.50	114.00	0.00	1.34	8.81	53.20	24.87	2.34	0.32	0.03	0.02	10.00	221.00
1FC122	122.00			1.40							0.00		
1FC121.5	121.50	123.00	9.00	1.77	2.12	20.30	9.49	0.31	0.05	0.01	0.01	5.00	58.00
1FC119.5	119.50	89.00	17.00	1.68	0.70	6.16	2.88	0.11	0.02	0.00	0.00	<2	62.00

Appendix A cont.

Sample ID	Meters Fire Cr	Zn (ppm)	Mo (ppm)	TOC (wt%)	Al (%)	SiO2 (%)	Si (%)calc	K (%)	Ti %ICP40	Cr2O3 % XRF	Cr (%)calc	Co (ppm)	Cr ppm
1FC116	116.00	87.00	3.00	1.72	1.14	12.70	5.94	0.34	0.04	0.01	0.01	2.00	104.00
1FC113.3	113.30	84.00	2.00	1.51	0.63	13.20	6.17	0.19	0.03	0.01	0.01	<2	39.00
1FC109.5	109.50	44.00	3.00		0.50	6.84	3.20	0.16	0.02	0.00	0.00	<2	43.00
1FC108.5	108.50	58.00	8.00	1.33	0.51	6.50	3.04	0.14	0.02	0.00	0.00	<2	49.00
1FC105.2	105.20	196.00	20.00	0.95	0.53	6.24	2.92	0.18	0.02	0.00	0.00	<2	9.00
1FC104.1	104.10	27.00	11.00	0.71	0.27	3.74	1.75	0.08	0.02	0.00	0.00	<2	<2
1FC103	103.00	39.00	12.00	0.60	1.65	4.38	2.05	0.37	0.11	0.00	0.00	3.00	9.00
1FC100.1	100.10	35.00	16.00		0.60	5.79	2.71	0.19	0.03	0.00	0.00	<2	<2
1FC97.5	97.50	12.00	3.00	0.23	0.47	10.70	5.00	0.13	0.03	0.00	0.00	<2	4.00
1FC94	94.00	18.00	2.00	0.32	0.25	4.36	2.04	0.08	0.02	0.00	0.00	<2	5.00
1FC90	90.00	40.00	6.00		1.60	50.90	23.79	0.46	0.10	0.00	0.00	2.00	29.00
1FC89	89.00	99.00	5.00	0.71	1.74	38.40	17.95	0.54	0.10	0.00	0.00	3.00	20.00
F37	86.50	39.00	4.00	0.78	1.36	21.10	9.86	0.48	0.08	0.00	0.00	2.00	61.00
F36	84.50	75.00	9.00	2.74	2.84	40.00	18.70	1.02	0.14	0.01	0.01	4.00	98.00
F35	83.50	29.00	6.00	0.73	1.00	14.50	6.78	0.33	0.06	0.00	0.00	2.00	36.00
1FC81.1	81.10	147.00	13.00	3.53	4.82	50.50	23.60	1.83	0.25	0.03	0.02	8.00	103.00
1FC78.5	78.50	72.00	7.00	1.43	1.92	29.10	13.60	0.68	0.10	0.02	0.01	3.00	55.00
1FC74.5	74.50	26.00	29.00	0.56	1.33	20.40	9.54	0.46	0.08	0.00	0.00	<2	47.00
IFC72.1	72.10	38.00	4.00		1.60	17.20	8.04	0.60	0.08	0.00	0.00	3.00	49.00
IFC71	71.00	82.00	16.00	1.51	4.47	39.00	18.23	1.73	0.21	0.02	0.01	7.00	55.00
F34	66.00	36.00	4.00	0.68	0.67	9.54	4.46	0.23	0.04	0.00	0.00	<2	14.00
F33	64.50	70.00	7.00	1.60	1.89	26.30	12.29	0.65	0.09	0.00	0.00	2.00	71.00
F32	63.00	45.00	7.00	1.25	1.20	18.10	8.46	0.42	0.06	0.00	0.00	<2	28.00
F31	61.00	166.00	45.00	2.58	3.74	55.80	26.08	1.41	0.20	0.02	0.01	5.00	60.00
F30	60.50	52.00	4.00		0.34	5.83	2.73	0.10	0.02	0.00	0.00	<2	16.00
F29	60.00	118.00	11.00	1.91	2.07	30.00	14.02	0.76	0.07	0.02	0.01	2.00	115.00
1FC57.6	57.50	71.00	4.00	1.94	1.16	18.80	8.79	0.42	0.05	0.00	0.00	<2	64.00
F28	54.50	39.00	3.00	0.95	0.98	85.80	40.11	0.30	0.06	0.00	0.00	2.00	10.00
1FC53	53.00	20.00	2.00		1.07	91.70	42.86	0.34	0.06	0.00	0.00	<2	7.00
F27	51.50	38.00	3.00	0.69	1.01	60.10	28.09	0.26	0.05	0.00	0.00	<2	15.00
F26	48.00	98.00	5.00	0.98	5.43	74.60	34.87	1.92	0.39	0.01	0.01	6.00	62.00
F25	47.50	63.00	3.00		3.10	78.20	36.55	1.06	0.15	0.00	0.00	3.00	44.00

Appendix A cont.

Sample ID	Meters Fire Cr	Zn (ppm)	Mo (ppm)	TOC (wt%)	Al (%)	SiO2 (%)	Si (%)calc	K (%)	Ti %ICP40	Cr2O3 % XRF	Cr (%)calc	Co (ppm)	Cr ppm
F24	46.00			0.42						0.00	0.00		
F23	45.50	77.00	3.00		2.87	82.90	38.75	0.95	0.13	0.00	0.00	3.00	29.00
1FC45	45.00	48.00	2.00	0.65	1.94	80.10	37.44	0.61	0.10	0.00	0.00	<2	20.00
1FC42.9	42.90	65.00	0.00	0.84	1.49	52.20	24.40	0.44	0.04	0.00	0.00	2.00	18.00
F22	41.75	41.00	0.00		1.39	48.90	22.86	0.41	0.03	0.00	0.00	<2	29.00
F21	41.25	51.00	3.00	0.63	2.03	88.60	41.41	0.71	0.09	0.00	0.00	3.00	38.00
F20	40.00	43.00	0.00		1.52	77.70	36.32	0.50	0.07	0.00	0.00	<2	39.00
F19	37.50			1.41						0.00	0.00		
F18	37.00	106.00	0.00	0.28	2.46	61.00	28.51	0.81	0.10	0.00	0.00	2.00	41.00
F17	35.50	72.00	0.00	0.44	2.86	68.60	32.07	0.99	0.13	0.00	0.00	3.00	30.00
F16	30.50	50.00	0.00	0.29	2.60	74.00	34.59	0.94	0.12	0.00	0.00	3.00	32.00
1FC28.5	28.50	69.00	0.00	0.23	4.44	77.60	36.27	1.42	0.21	0.00	0.00	8.00	14.00
1FC27	27.00	45.00	0.00	0.26	3.42	67.90	31.74	1.02	0.17	0.00	0.00	6.00	15.00
1FC25.3	25.30	91.00	0.00		3.28	71.50	33.42	0.98	0.16	0.00	0.00	12.00	37.00
F15	20.50	187.00	0.00	0.27	3.55	78.70	36.79	1.04	0.15	0.00	0.00	9.00	27.00
1FC18.8	18.80	144.00	0.00		3.63	78.20	36.55	1.09	0.18	0.00	0.00	7.00	16.00
F14	17.50	452.00	0.00	1.20	6.80	69.80	32.63	2.23	0.32	0.01	0.01	9.00	68.00
F13	13.70	155.00	0.10	0.22	3.83	74.30	34.73	1.08	0.17	0.00	0.00	8.00	29.00
F12	12.20	66.00	0.10	0.29	3.06	65.10	30.43	0.91	0.15	0.00	0.00	4.00	32.00
F11	11.40	147.00	0.10		5.54	69.60	32.53	1.74	0.27	0.00	0.00	11.00	43.00
F10	8.00	47.00	2.00	0.33	3.19	40.90	19.12	1.00	0.13	0.00	0.00	5.00	33.00
F9	5.40	45.00	4.00		1.62	55.70	26.04	0.44	0.08	0.00	0.00	5.00	17.00
F8	3.80	86.00	1.00	0.31	4.75	73.10	34.17	1.41	0.21	0.00	0.00	8.00	47.00
F5	1.25	337.00	9.00		3.15	77.80	36.37	0.73	0.12	0.00	0.00	9.00	37.00
F4	0.50	118.00	3.00		3.74	79.10	36.97	1.01	0.18	0.00	0.00	6.00	29.00
F2	0.20	41.00	12.00		1.54	68.80	32.16	0.42	0.05	0.00	0.00	4.00	15.00

Appendix B. Fire Creek major oxide from Kelly (2004)

Meters Fire Cr	Sample ID	Al2O3 % XRF	CaO % XRF	Fe2O3 % XRF	K2O % XRF	Na2O % XRF	P2O5 % XRF	SiO2 % XRF	TiO2 % XRF
0.2	F2	2.88	4.57	11.1	0.47	0.07	1.26	68.80	0.192
0.5	F4	6.89	1.81	4.18	1.12	0.14	0.5	79.10	0.549
1.25	F5	6.11	1.50	6.51	0.86	0.09	0.72	77.80	0.354
3.8	F8	8.94	2.18	5.15	1.6	0.18	0.41	73.10	0.724
5.4	F9	2.91	11.70	8.17	0.47	0.14	0.57	55.70	0.255
8	F10	5.81	15.00	8.19	1.13	0.24	0.42	40.90	0.438
11.4	F11	10.50	1.91	5.91	2.01	0.37	0.43	69.60	0.742
12.2	F12	5.61	7.89	5.24	0.97	0.31	0.29	65.10	0.525
13.7	F13	7.27	3.73	3.99	1.22	0.35	0.36	74.30	0.577
17.5	F14	13.20	0.60	5.16	2.65	0.44	0.38	69.80	0.88
18.8	1FC18.8	6.90	3.03	3.44	1.23	0.43	0.41	78.20	0.589
20.5	F15	6.59	2.10	4.25	1.18	0.37	0.58	78.70	0.502
25.3	1FC25.3	5.87	6.07	4.45	1.11	0.40	2.64	71.50	0.441
27	1FC27	6.59	6.31	4.6	1.19	0.64	0.46	67.90	0.556
28.5	1FC28.5	8.39	2.54	2.91	1.58	0.63	0.38	77.60	0.676
30.5	F16	4.92	5.89	3.35	1.08	0.17	0.77	74.00	0.363
35.5	F17	5.33	8.22	2.53	1.11	0.35	1.77	68.60	0.391
37	F18	4.42	12.70	2.39	0.91	0.44	5.65	61.00	0.315
37.5	F19								
40	F20	2.80	7.58	1.5	0.58	0.29	4.25	77.70	0.217
41.25	F21	3.87	1.80	0.98	0.84	0.22	0.65	88.60	0.271
41.75	F22	2.40	24.40	1.2	0.46	0.35	16.6	48.90	0.174
42.9	1FC42.9	2.59	23.80	0.97	0.46	0.38	14	52.20	0.194
45	1FC45	3.67	6.51	1.38	0.69	0.43	3.48	80.10	0.317
45.5	F23	5.67	3.04	0.93	1.12	0.54	1.48	82.90	0.469
46	F24								
47.5	F25	5.75	4.49	1.57	1.22	0.44	1.83	78.20	0.475
48	F26	10.70	2.31	2.02	2.37	0.50	1.05	74.60	0.797
51.5	F27	1.90	18.30	1.4	0.33	0.43	9.99	60.10	0.186
53	1FC53	2.12	1.58	0.58	0.45	0.23	0.59	91.70	0.159
54.5	F28	1.93	5.26	0.7	0.39	0.27	3.35	85.80	0.176
57.5	1FC57.6	2.16	41.20	0.48	0.52	0.22	20	18.80	0.156
60	F29	3.82	32.70	0.87	0.93	0.31	18.7	30.00	0.265
60.5	F30	0.65	50.90	0.28	0.14	0.16	1.89	5.83	0.052
61	F31	7.23	15.00	1.66	1.73	0.43	6.98	55.80	0.522
63	F32	2.32	43.20	0.98	0.54	0.31	8.75	18.10	0.182
64.5	F33	3.66	35.60	1.53	0.81	0.47	11.5	26.30	0.274
66	F34	1.26	47.70	0.62	0.28	0.22	3.39	9.54	0.1
71	IFC71	8.68	21.90	2.76	2.22	0.41	2.63	39.00	0.552
72.1	IFC72.1	3.08	43.20	1.35	0.74	0.31	4.01	17.20	0.209
74.5	1FC74.5	2.59	38.10	2.61	0.6	0.36	0.97	20.40	0.222
78.5	1FC78.5	3.70	34.90	1.5	0.83	0.45	6.48	29.10	0.288
81.1	1FC81.1	9.37	15.40	2.82	2.22	0.63	3.93	50.50	0.653
83.5	F35	2.02	44.10	1.16	0.46	0.35	1.34	14.50	0.17
84.5	F36	5.55	25.90	1.78	1.34	0.57	4.68	40.00	0.404

Appendix B cont.

Meters Fire Cr	Sample ID	Al2O3 % XRF	CaO % XRF	Fe2O3 % XRF	K2O % XRF	Na2O % XRF	P2O5 % XRF	SiO2 % XRF	TiO2 % XRF
86.5	F37	2.71	39.70	1.02	0.64	0.36	1.75	21.10	0.223
89	1FC89	3.33	30.90	1.39	0.69	0.58	5.38	38.40	0.294
90	1FC90	3.09	24.60	0.67	0.58	0.69	3.33	50.90	0.3
94	1FC94	0.45	52.20	0.14	0.11	0.13	0.56	4.36	0.044
97.5	1FC97.5	0.88	47.80	0.48	0.18	0.24	0.11	10.70	0.085
100.1	1FC100.1	1.15	50.40	0.51	0.23	0.14	0.07	5.79	0.067
103	1FC103	3.10	48.40	2.05	0.44	0.15	0.02	4.38	0.21
104.1	1FC104.1	0.48	52.20	0.25	0.12	0.11	0.05	3.74	0.037
105.2	1FC105.2	0.99	49.80	0.4	0.2	0.12	0.02	6.24	0.063
108.5	1FC108.5	1.11	50.30	0.34	0.16	0.12	15.3	6.50	0.046
109.5	1FC109.5	0.91	49.40	0.32	0.12	0.07	4.2	6.84	0.063
113.3	1FC113.3	1.14	45.80	0.49	0.21	0.09	6.87	13.20	0.063
116	1FC116	2.12	43.40	0.74	0.4	0.09	3.94	12.70	0.113
119.5	1FC119.5	1.28	50.90	0.38	0.12	0.09	11.1	6.16	0.067
121.5	1FC121.5	3.85	36.50	3.46	0.43	0.11	16.8	20.30	0.147
122	1FC122								
122.5	1FC122.5	16.40	7.01	5.31	2.79	0.45	0.29	53.20	0.79
123.6	1FC123.6	12.90	19.40	2.99	2.12	0.40	0.16	40.90	0.632
124.4	1FC124.4	15.30	13.90	1.84	2.55	0.45	0.19	48.60	0.735
124.5	1FC124.5								
126.5	1FC126.5	11.90	22.00	2.96	1.99	0.39	0.31	37.70	0.607
127.3	1FC127.3	10.40	20.10	8.25	1.64	0.33	0.31	32.10	0.522
129	1FC129	12.40	20.40	5.28	1.93	0.36	0.25	37.90	0.612
130.9	1FC130.9	10.60	23.50	4.73	1.78	0.32	0.21	33.80	0.533
135	1FC135	15.50	12.70	4.28	2.35	0.46	0.27	47.80	0.746
138	1FC138	14.40	16.50	3.88	2.17	0.44	0.23	43.80	0.7
138.5	1FC138.5								
139.5	1FC139.5	14.80	13.10	5.01	2.26	0.48	0.29	46.60	0.736
143	1FC143	16.70	9.02	3.88	2.46	0.50	0.17	53.20	0.842
145.5	1FC145.5	13.80	14.70	4.8	2	0.42	0.16	46.20	0.721
146.5	1FC146.5	16.30	10.10	5.01	2.12	0.48	0.18	51.70	0.83
148	1FC148	13.30	14.90	8.64	1.69	0.42	0.16	42.00	0.702
149	1FC149	16.50	8.14	4.39	2.21	0.53	0.18	54.70	0.886
151	1FC151	15.50	10.20	4.39	2.23	0.50	0.13	51.90	0.812
163	1FC163	19.70	3.63	4.63	2.65	0.74	0.06	56.20	0.949
164.5	1FC164.5	1.70	50.50	0.59	0.22	0.12	0.15	5.45	0.091
165.5	1FC165.5	19.90	1.97	4.99	2.8	0.69	0.09	59.60	0.948
167	1FC167	1.98	49.70	0.7	0.28	0.12	0.18	5.76	0.103
168.5	1FC168.5	7.49	29.90	3.39	1.08	0.30	1.05	29.10	0.414
172	1FC172	2.50	46.60	0.85	0.38	0.13	0.04	11.60	0.166
174	1FC174	2.37	14.30	6.27	0.08	0.03	9.11	58.90	0.389
175	1FC175	4.81	3.10	19.5	0.04	<0.01	1.44	57.80	0.913
176.5	1FC176.5	4.51	2.38	35.7	0.39	0.06	0.1	33.20	0.355
177.5	1FC177.5	9.17	0.15	2.92	1.75	0.23	0.11	79.70	0.682

Appendix C. Last Creek major oxide, trace, and elemental data.

Sample ID	Meters	SiO2 (%)	Al2O3 (%)	FeO (%)	MnO (%)	CaO (%)	K2O (%)	TiO2 (%)	P2O5 (%)	Sr (ppm)	Rb (ppm)
14LC2-44.1	95.30	9.28	3.82	1.49	0.00	66.83	0.00	0.16	1.07	934.00	0.00
14LC2-43	94.20	10.19	3.84	1.41	0.00	66.23	0.50	0.22	0.67	1536.33	0.00
14LC2-38	89.20	10.13	1.90	0.53	0.00	71.55	0.00	0.11	0.22	2251.33	0.00
14LC2-33.1	84.30	21.35	3.08	0.64	0.00	59.96	0.55	0.23	0.61	1495.33	56.00
14LC2-30.4	81.60	21.23	2.17	0.42	0.00	62.00	0.00	0.15	0.72	1829.67	0.00
14LC2-26	77.20	32.17	3.31	0.70	0.00	50.21	0.66	0.30	1.27	1338.67	0.00
14LC2-23	74.20	25.58	3.85	1.15	0.00	53.75	0.77	0.32	0.98	1384.00	63.00
14LC-74	74.00	44.94	8.61	1.74	0.00	29.91	1.79	0.69	3.48	1153.67	115.00
14LC-72.2	72.20	25.15	4.04	1.35	0.00	49.63	0.81	0.35	7.13	2187.00	54.00
14LC-70.7	70.70	42.02	10.94	2.03	0.00	28.18	2.09	0.77	2.65	1101.67	112.00
14LC-66.3	66.30	20.61	3.73	1.53	0.00	47.62	0.59	0.17	20.07	2032.00	0.00
14LC-65.7	65.70	28.02	5.03	2.20	0.00	46.71	1.07	0.40	8.61	1672.67	82.33
14LC-63.9	63.90	38.78	12.54	4.11	0.00	27.66	2.70	0.91	1.24	1198.00	175.00
14LC-61.8	61.80	17.22	2.67	0.94	0.00	61.24	0.63	0.18	7.22	2186.33	63.00
14LC-61.5	61.50	25.89	8.98	2.01	0.00	45.05	1.59	0.46	2.49	1644.00	123.00
14LC-56.8	56.80	38.47	11.76	1.91	0.00	27.42	2.21	0.66	14.06	1414.33	138.67
14LC-55.8	55.80	45.53	15.36	3.52	0.03	19.53	3.18	0.88	1.73	721.00	242.00
14LC-55	55.00	18.62	3.60	1.10	0.00	55.81	0.73	0.23	11.64	1811.17	61.33
14LC-52.3	52.30	28.81	4.22	1.30	0.00	47.90	0.77	0.34	1.42	908.67	58.50
14LC-50.2	50.20	41.34	4.58	1.34	0.00	34.35	0.85	0.36	16.58	1584.67	71.33
14LC-49.1	49.10	25.30	3.16	0.84	0.03	44.23	0.63	0.20	32.54	2988.33	72.33
14LC-48.1	48.10	89.30	3.48	0.81	0.00	2.73	0.57	0.17	0.94	144.00	38.00
14LC-46	46.00	38.68	3.92	3.08	0.00	28.39	0.63	0.28	22.29	1761.33	54.00
14LC45.3	45.30	63.62	12.87	3.62	0.00	7.19	2.71	1.32	3.00	441.33	117.00
14LC-43.0	43.00	38.57	5.01	8.21	0.00	24.19	0.70	0.23	19.46	1379.33	53.00
14LC-42.8	42.80	60.35	18.46	2.99	0.03	4.48	3.95	1.08	1.01	316.67	290.33
14LC-37.3	37.30	65.43	21.37	1.12	0.00	0.87	4.07	1.11	0.00	253.00	288.33
14LC-34.7	34.70	83.75	4.65	2.25	0.00	2.80	0.74	0.22	1.01	218.00	57.33
14LC-33.1	33.10	63.04	1.70	5.72	0.06	13.79	0.00	0.10	5.89	990.00	67.33
14LC-32.95	32.95	70.13	18.42	1.03	0.00	0.35	3.43	1.14	0.29	310.67	211.33
14LC-32.7	32.70	78.62	6.14	7.44	0.06	1.07	0.81	0.44	0.37	143.67	53.00
14LC-21.1	21.10	78.90	4.82	3.72	0.04	6.01	0.67	0.43	1.06	315.67	57.67

Appendix C cont.

Sample ID	Meters	SiO2 (%)	Al2O3 (%)	FeO (%)	MnO (%)	CaO (%)	K2O (%)	TiO2 (%)	P2O5 (%)	Sr (ppm)	Rb (ppm)
14LC-18.2	18.20	66.06	18.93	2.74	0.04	1.20	3.23	1.12	0.25	241.00	190.00
14LC-14.3	14.30	81.08	2.73	7.72	0.08	2.35	0.00	0.16	1.10	212.67	0.00
14LC-10.5	10.50	79.34	5.84	3.43	0.04	5.13	0.80	0.36	0.31	223.00	52.67
14LC-4.7	4.70	72.95	9.60	5.78	0.05	2.79	1.42	0.53	0.35	187.67	89.67
14LC-1.2	1.20	85.39	4.54	3.89	0.04	1.72	0.52	0.36	0.24	136.67	31.00
14LC-0.1	0.10	78.46	5.46	7.15	0.06	1.72	0.66	0.26	0.57	225.00	54.33

Appendix C cont.

Sample ID2	Meters 2	Nb (ppm)	Zr (ppm)	Pb (ppm)	Zn (ppm)	Mo (ppm)	Sn (ppm)	S (ppm)
14LC2-44.1	95.30	0.00	0.00	0.00	0.00	0.00	0.00	3573.67
14LC2-43	94.20	0.00	89.33	0.00	0.00	0.00	0.00	6628.00
14LC2-38	89.20	0.00	134.80	0.00	0.00	0.00	0.00	3161.67
14LC2-33.1	84.30	0.00	161.33	0.00	0.00	0.00	464.00	2209.00
14LC2-30.4	81.60	0.00	112.00	0.00	0.00	0.00	0.00	1177.33
14LC2-26	77.20	0.00	256.27	0.00	42.50	0.00	0.00	1617.67
14LC2-23	74.20	0.00	171.20	0.00	0.00	0.00	0.00	2664.67
14LC-74	74.00	75.00	386.13	0.00	276.67	0.00	340.00	15067.33
14LC-72.2	72.20	83.00	199.73	0.00	55.00	0.00	0.00	12439.00
14LC-70.7	70.70	69.00	295.73	0.00	143.33	0.00	0.00	12962.33
14LC-66.3	66.30	0.00	107.73	0.00	0.00	0.00	0.00	13503.33
14LC-65.7	65.70	0.00	234.93	0.00	42.00	0.00	0.00	10830.33
14LC-63.9	63.90	81.00	359.73	0.00	85.33	0.00	0.00	25443.00
14LC-61.8	61.80	0.00	122.40	0.00	0.00	0.00	0.00	6492.33
14LC-61.5	61.50	0.00	117.33	0.00	61.00	0.00	0.00	15251.33
14LC-56.8	56.80	52.00	274.13	0.00	130.67	0.00	328.00	6170.00
14LC-55.8	55.80	0.00	372.00	0.00	212.67	116.00	350.50	23149.00
14LC-55	55.00	64.67	116.67	0.00	46.67	0.00	0.00	8375.67
14LC-52.3	52.30	0.00	193.07	0.00	0.00	0.00	0.00	4720.00
14LC-50.2	50.20	54.00	219.20	0.00	216.67	0.00	0.00	8165.33
14LC-49.1	49.10	0.00	123.20	0.00	181.33	0.00	0.00	3122.33
14LC-48.1	48.10	32.00	93.60	0.00	0.00	0.00	0.00	2801.00
14LC-46	46.00	0.00	157.60	0.00	162.00	0.00	0.00	40882.33
14LC45.3	45.30	59.00	373.60	0.00	57.00	0.00	389.00	12020.33
14LC-43.0	43.00	0.00	125.60	0.00	35.67	0.00	0.00	49407.00
14LC-42.8	42.80	50.00	229.07	0.00	104.33	0.00	0.00	19178.67
14LC-37.3	37.30	53.33	229.07	58.00	0.00	0.00	225.00	6086.00
14LC-34.7	34.70	39.00	214.40	47.50	212.67	0.00	0.00	19136.33
14LC-33.1	33.10	0.00	132.40	0.00	108.67	0.00	0.00	70258.00
14LC-32.95	32.95	44.00	436.53	0.00	0.00	0.00	203.00	4168.00
14LC-32.7	32.70	36.00	279.20	0.00	37.00	0.00	0.00	909.33
14LC-21.1	21.10	0.00	739.47	0.00	21.50	0.00	0.00	589.00

Appendix C cont.

Sample ID	Meters	Nb (ppm)	Zr (ppm)	Pb (ppm)	Zn (ppm)	Mo (ppm)	Sn (ppm)	S (ppm)
14LC-18.2	18.20	61.33	481.07	0.00	38.00	47.00	261.00	7807.67
14LC-14.3	14.30	41.00	260.80	0.00	188.33	0.00	445.00	707.00
14LC-10.5	10.50	37.00	273.07	0.00	56.33	0.00	238.00	1991.67
14LC-4.7	4.70	40.33	264.27	0.00	71.67	0.00	0.00	12969.00
14LC-1.2	1.20	33.00	265.87	0.00	0.00	0.00	223.00	928.50
14LC-0.1	0.10	52.00	240.00	0.00	209.33	0.00	0.00	1340.67

Appendix D. Kavik Creek outcrop major oxide, trace, and elemental data.

Sample ID	Strat Interval	SiO2 (%)	Al2O3 (%)	FeO(%)	MnO(%)	CaO(%)	K2O(%)	TiO2(%)
14KC3-20.4	187.3	26.58	4.43	1.43	0.00	48.42	0.78	0.34
14KC3-16.3	183.2	42.33	7.28	2.00	0.00	31.86	1.52	0.62
14KC3-15.3	182.2	35.06	3.65	1.26	0.00	44.13	0.67	0.35
14KC3-14.7	181.6	44.59	4.72	1.96	0.00	35.49	0.90	0.45
14KC3-12.9	179.8	58.77	5.64	1.68	0.00	20.91	1.02	0.45
14KC3-12.5	179.4	66.16	7.13	1.81	0.00	14.46	1.36	0.65
14KC3-11	177.9	18.25	2.20	1.02	0.00	54.55	0.00	0.16
14KC3-9.7	176.6	45.67	18.44	9.43	0.00	5.44	4.20	1.18
14KC3-9.0	175.9	19.57	2.36	8.03	0.00	39.17	0.00	0.06
14KC3-8.6	175.5	86.48	3.71	1.51	0.00	3.74	0.54	0.29
14KC3-7.8	174.7	76.79	7.34	1.64	0.00	4.90	1.69	0.47
14KC3-7.0	173.9	70.80	1.96	1.97	0.00	10.04	0.78	0.32
14KC3-6.0	172.9	30.97	6.26	2.28	0.00	33.02	1.38	0.53
14KC3-5.5	172.4	77.81	2.52	2.20	0.04	11.40	0.00	0.34
14KC3-3.6	170.5	55.06	21.82	2.99	0.00	4.87	4.27	1.56
14KC3-3.0	169.9	86.50	3.95	2.36	0.00	1.16	0.72	0.46
14KC3-2.6	169.5	77.19	6.63	1.77	0.00	7.25	1.11	0.88
14KC3-1.3	168.2	16.05	4.35	9.01	0.04	51.16	0.80	0.29
14KC3-0.8	167.7	10.35	2.83	7.40	0.00	59.44	0.00	0.23
14KC2-22.3	90.6	22.67	4.40	1.34	0.00	55.07	0.69	0.20
14KC2-22	90.3	13.58	3.22	1.11	0.00	66.36	0.51	0.15
14KC2-20.5	88.8	17.98	4.04	1.31	0.00	60.06	0.67	0.21
14KC2-19.8	88.1	8.57	2.45	0.69	0.00	70.61	0.00	0.09
14KC2-19.5	87.8	6.61	2.41	0.46	0.00	71.15	0.00	0.07
14KC2-18.8	87.1	40.37	9.18	4.45	0.00	32.17	1.62	0.66
14KC2-18.2	86.5	8.20	2.16	0.64	0.00	72.82	0.00	0.08
14KC2-17.2	85.5	8.34	2.21	0.47	0.00	71.40	0.00	0.05
14KC2-16.7	85	46.99	10.10	2.63	0.00	27.66	1.66	0.63
14KC2-15.4	83.7	7.97	1.99	0.38	0.00	72.45	0.00	0.06
14KC2-14.1	82.4	49.87	1.71	0.22	0.00	38.82	0.00	0.03
14KC2-14	82.3	12.61	1.60	0.07	0.00	68.34	0.00	0.00
14KC2-12.4	80.7	12.33	3.02	0.70	0.00	66.40	0.00	0.10
14KC2-12.3	80.6	7.52	1.77	0.43	0.00	74.18	0.00	0.05

Appendix D cont.

Sample ID	Strat Interval	SiO2 (%)	Al2O3 (%)	FeO(%)	MnO(%)	CaO(%)	K2O(%)	TiO2(%)
14KC2-11.5	79.8	3.87	1.50	0.24	0.00	76.23	0.00	0.00
14KC2-10.5	78.8	2.97	1.60	0.10	0.00	77.61	0.00	0.00
14KC2-10.3	78.6	13.15	1.95	0.48	0.00	68.93	0.00	0.10
14KC2-9.7	78	6.59	1.94	0.62	0.00	74.15	0.00	0.11
14KC2-9.3	77.6	4.72	1.83	0.50	0.00	76.01	0.00	0.09
14KC2-8.3	76.6	32.85	3.56	2.35	0.00	40.91	0.97	0.37
14KC2-7.6	75.9	23.17	2.66	0.76	0.00	52.18	0.00	0.11
14KC2-6.6	74.9	55.79	4.52	1.57	0.00	27.84	0.82	0.55
14KC2-5.6	73.9	32.59	4.05	0.84	0.00	41.86	0.00	0.26
14KC2-4.8	73.1	40.25	4.38	1.96	0.00	34.58	0.75	0.43
14KC2-4.2	72.5	34.85	6.55	2.89	0.00	34.28	1.08	0.50
14KC2-3.5	71.8	15.54	2.71	1.93	0.00	61.98	0.52	0.19
14KC2-2.5	70.8	32.49	6.69	1.54	0.00	36.80	1.19	0.56
14KC2-1.5	69.8	14.62	2.65	0.95	0.00	65.05	0.50	0.19
14KC2-0.8	69.1	28.48	4.28	2.45	0.00	48.22	0.82	0.37
14KC2-0.1	68.4	26.08	4.05	4.89	0.00	47.48	0.68	0.36
14KC1-64	64	11.99	3.09	0.98	0.00	66.58	0.62	0.19
14KC1-54.6	54.6	10.07	3.49	1.07	0.00	65.87	0.64	0.16
14KC1-46	46	10.78	3.33	0.69	0.00	63.31	0.54	0.14
14KC1-38.6	38.6	18.91	4.33	1.19	0.00	58.07	0.75	0.28
14KC1-20	20	24.86	3.17	1.98	0.03	53.90	0.55	0.29
14KC1-17.4	17.4	35.43	5.22	1.02	0.00	41.64	0.77	0.35
14KC1-12.9	12.9	15.22	2.69	0.78	0.00	56.53	0.50	0.16
14KC1-3.9	3.9	86.65	2.94	1.13	0.02	5.31	0.50	0.24
14KC1-2.5	2.5	88.78	3.95	2.38	0.00	0.78	0.00	0.24
14KC1-1.5	1.5	86.35	4.29	2.15	0.02	2.25	0.65	0.31
14KC1-1.0	1	25.18	5.13	2.47	0.00	39.37	1.03	0.37
14KC1-.05	0.05	29.75	3.54	1.34	0.00	39.04	0.50	0.17

Appendix D cont.

Sample ID2	Strat Interval3	P2O5(%)	Sr ppm	Rb ppm	Nb ppm	Zr ppm	Co ppm
14KC3-20.4	187.3	12.80	1345.67	68.67	0.00	166.67	0.00
14KC3-16.3	183.2	8.61	1100.00	106.33	78.00	254.93	0.00
14KC3-15.3	182.2	7.19	923.00	59.33	0.00	167.73	0.00
14KC3-14.7	181.6	3.62	744.67	72.00	96.00	212.53	0.00
14KC3-12.9	179.8	3.93	607.33	77.67	65.00	257.87	0.00
14KC3-12.5	179.4	3.64	431.00	97.33	58.50	341.60	0.00
14KC3-11	177.9	27.65	1761.67	0.00	80.00	84.00	0.00
14KC3-9.7	176.6	2.80	281.67	523.33	105.00	539.73	0.00
14KC3-9.0	175.9	31.69	1193.33	0.00	69.00	64.80	0.00
14KC3-8.6	175.5	0.37	72.33	29.00	40.00	199.47	0.00
14KC3-7.8	174.7	4.76	188.33	98.33	48.67	298.40	0.00
14KC3-7.0	173.9	11.00	331.00	62.33	57.00	216.00	155.00
14KC3-6.0	172.9	22.85	1376.00	115.33	97.67	190.93	0.00
14KC3-5.5	172.4	1.93	230.67	0.00	44.00	565.60	0.00
14KC3-3.6	170.5	1.62	154.67	326.00	67.67	297.60	0.00
14KC3-3.0	169.9	0.00	58.00	62.33	46.67	249.07	0.00
14KC3-2.6	169.5	0.25	213.00	86.33	57.33	284.53	0.00
14KC3-1.3	168.2	0.26	1601.00	67.00	0.00	109.07	0.00
14KC3-0.8	167.7	0.29	1717.00	0.00	105.00	91.20	0.00
14KC2-22.3	90.6	1.27	1897.33	0.00	0.00	67.20	0.00
14KC2-22	90.3	0.32	966.50	54.00	0.00	66.40	0.00
14KC2-20.5	88.8	2.16	2126.33	73.67	0.00	108.53	0.00
14KC2-19.8	88.1	0.38	926.67	0.00	0.00	63.20	0.00
14KC2-19.5	87.8	0.40	1028.33	0.00	0.00	63.20	0.00
14KC2-18.8	87.1	0.28	1230.67	65.00	0.00	168.00	0.00
14KC2-18.2	86.5	0.23	1280.00	0.00	0.00	58.40	0.00
14KC2-17.2	85.5	0.33	1177.33	0.00	0.00	52.80	0.00
14KC2-16.7	85	1.28	1005.33	75.33	58.00	158.40	0.00
14KC2-15.4	83.7	0.26	1279.67	0.00	0.00	57.60	0.00
14KC2-14.1	82.4	0.28	1425.67	0.00	0.00	110.40	0.00
14KC2-14	82.3	0.20	755.33	0.00	0.00	0.00	0.00
14KC2-12.4	80.7	0.34	974.00	0.00	0.00	84.40	0.00
14KC2-12.3	80.6	0.16	1130.00	0.00	0.00	70.40	0.00

Appendix D cont.

Sample ID	Strat Interval	P2O5(%)	Sr ppm	Rb ppm	Nb ppm	Zr ppm	Co ppm
14KC2-11.5	79.8	0.29	1192.67	0.00	0.00	0.00	0.00
14KC2-10.5	78.8	0.25	870.33	0.00	90.00	0.00	0.00
14KC2-10.3	78.6	0.25	2269.33	0.00	0.00	89.60	0.00
14KC2-9.7	78	0.48	1815.00	0.00	0.00	82.40	0.00
14KC2-9.3	77.6	0.30	1873.33	0.00	0.00	63.20	0.00
14KC2-8.3	76.6	15.88	1543.33	77.33	59.00	265.33	258.00
14KC2-7.6	75.9	16.78	1669.33	0.00	63.50	95.47	0.00
14KC2-6.6	74.9	1.00	802.00	66.67	79.00	351.73	0.00
14KC2-5.6	73.9	12.27	1320.00	0.00	0.00	160.80	0.00
14KC2-4.8	73.1	11.95	1327.67	59.00	62.00	237.33	0.00
14KC2-4.2	72.5	7.44	1310.00	81.00	56.50	258.40	0.00
14KC2-3.5	71.8	5.89	1414.00	52.00	0.00	110.93	0.00
14KC2-2.5	70.8	9.26	1341.33	85.67	76.00	279.73	171.00
14KC2-1.5	69.8	3.90	1464.33	0.00	0.00	131.20	0.00
14KC2-0.8	69.1	3.67	1575.67	73.33	0.00	222.93	0.00
14KC2-0.1	68.4	1.36	980.00	57.00	0.00	226.00	0.00
14KC1-64	64	0.88	1123.67	69.00	0.00	109.60	0.00
14KC1-54.6	54.6	3.17	1374.33	0.00	0.00	56.80	0.00
14KC1-46	46	4.92	1038.67	0.00	0.00	81.33	0.00
14KC1-38.6	38.6	5.47	1324.33	78.00	0.00	118.13	0.00
14KC1-20	20	3.92	973.33	0.00	87.00	177.33	0.00
14KC1-17.4	17.4	4.27	752.50	56.50	0.00	148.40	0.00
14KC1-12.9	12.9	22.92	1961.00	55.00	0.00	79.00	0.00
14KC1-3.9	3.9	0.36	90.00	37.00	0.00	233.00	0.00
14KC1-2.5	2.5	0.32	37.00	28.00	0.00	166.00	0.00
14KC1-1.5	1.5	0.99	93.00	45.00	40.00	239.00	0.00
14KC1-1.0	1	31.99	1411.00	98.00	56.00	137.00	0.00
14KC1-.05	0.05	31.23	1899.00	51.00	54.00	146.00	0.00

Appendix D cont.

Sample ID3	Strat Interval2	Ni ppm	Cr ppm	Cu ppm	Pb ppm	Zn ppm	Mo ppm	Sn ppm	S ppm
14KC3-20.4	187.3	0.00	0.00	0.00	0.00	48.33	0.00	0.00	3536.67
14KC3-16.3	183.2	0.00	0.00	113.00	0.00	204.00	0.00	0.00	14186.67
14KC3-15.3	182.2	0.00	0.00	7822.00	0.00	242.33	0.00	497.00	3417.00
14KC3-14.7	181.6	0.00	0.00	0.00	0.00	56.33	0.00	0.00	7018.67
14KC3-12.9	179.8	0.00	0.00	0.00	0.00	62.00	0.00	0.00	21294.33
14KC3-12.5	179.4	0.00	0.00	4481.00	0.00	315.00	53.00	323.00	3110.00
14KC3-11	177.9	0.00	0.00	0.00	0.00	53.33	0.00	0.00	4295.00
14KC3-9.7	176.6	758.67	0.00	759.33	0.00	2140.67	314.00	496.00	39143.33
14KC3-9.0	175.9	0.00	0.00	532.00	0.00	373.00	0.00	0.00	51122.00
14KC3-8.6	175.5	0.00	0.00	35.00	0.00	33.67	0.00	0.00	10503.33
14KC3-7.8	174.7	0.00	0.00	980.50	55.50	103.67	0.00	287.00	10898.67
14KC3-7.0	173.9	0.00	0.00	0.00	0.00	98.00	0.00	307.00	71948.00
14KC3-6.0	172.9	0.00	0.00	655.00	105.00	82.50	0.00	0.00	62606.00
14KC3-5.5	172.4	0.00	0.00	0.00	0.00	0.00	0.00	0.00	2922.00
14KC3-3.6	170.5	75.33	0.00	66.00	0.00	146.00	0.00	0.00	18297.33
14KC3-3.0	169.9	0.00	675.67	4299.00	0.00	246.33	36.00	0.00	15981.33
14KC3-2.6	169.5	0.00	1803.67	133.00	0.00	156.67	0.00	0.00	1283.00
14KC3-1.3	168.2	0.00	0.00	0.00	0.00	0.00	0.00	0.00	3900.33
14KC3-0.8	167.7	0.00	0.00	0.00	0.00	0.00	0.00	0.00	4220.33
14KC2-22.3	90.6	128.33	0.00	0.00	0.00	327.00	106.00	412.00	21597.33
14KC2-22	90.3	0.00	0.00	0.00	0.00	85.75	116.00	0.00	4543.50
14KC2-20.5	88.8	180.33	0.00	0.00	0.00	506.67	91.00	0.00	3192.33
14KC2-19.8	88.1	0.00	0.00	301.00	0.00	50.33	100.00	0.00	3147.00
14KC2-19.5	87.8	0.00	0.00	2195.00	0.00	114.00	0.00	0.00	2248.67
14KC2-18.8	87.1	531.33	0.00	134.00	0.00	673.00	186.00	396.00	5256.33
14KC2-18.2	86.5	0.00	0.00	0.00	0.00	0.00	78.00	428.00	2834.67
14KC2-17.2	85.5	112.00	0.00	823.00	0.00	66.33	0.00	0.00	2766.00
14KC2-16.7	85	335.00	0.00	142.33	0.00	218.33	173.67	0.00	5540.33
14KC2-15.4	83.7	0.00	0.00	0.00	0.00	0.00	0.00	0.00	2154.67
14KC2-14.1	82.4	0.00	0.00	0.00	0.00	0.00	0.00	349.00	5590.67
14KC2-14	82.3	0.00	0.00	0.00	0.00	0.00	0.00	0.00	1644.00
14KC2-12.4	80.7	0.00	0.00	0.00	0.00	0.00	0.00	0.00	2148.33
14KC2-12.3	80.6	0.00	0.00	0.00	0.00	0.00	0.00	481.00	3078.67

Appendix D cont.

Sample ID	Strat Interval	Ni ppm	Cr ppm	Cu ppm	Pb ppm	Zn ppm	Mo ppm	Sn ppm	S ppm
14KC2-11.5	79.8	0.00	0.00	836.50	0.00	59.00	0.00	387.00	2261.33
14KC2-10.5	78.8	0.00	0.00	3983.00	0.00	230.00	0.00	556.00	1443.67
14KC2-10.3	78.6	0.00	0.00	0.00	0.00	0.00	0.00	0.00	2428.00
14KC2-9.7	78	0.00	0.00	0.00	0.00	0.00	0.00	0.00	8055.00
14KC2-9.3	77.6	0.00	0.00	5420.00	0.00	335.00	0.00	447.00	5969.67
14KC2-8.3	76.6	0.00	0.00	22135.00	0.00	1946.00	0.00	0.00	18870.00
14KC2-7.6	75.9	0.00	0.00	0.00	0.00	66.00	0.00	485.00	7746.67
14KC2-6.6	74.9	0.00	0.00	0.00	0.00	53.50	0.00	0.00	7210.00
14KC2-5.6	73.9	0.00	0.00	0.00	0.00	46.00	0.00	0.00	3201.00
14KC2-4.8	73.1	0.00	0.00	231.00	0.00	42.00	0.00	0.00	19700.00
14KC2-4.2	72.5	0.00	0.00	2185.00	0.00	94.33	0.00	0.00	52872.33
14KC2-3.5	71.8	0.00	0.00	1572.00	0.00	140.00	0.00	0.00	9804.33
14KC2-2.5	70.8	0.00	0.00	1599.67	0.00	197.33	0.00	0.00	21393.67
14KC2-1.5	69.8	0.00	0.00	0.00	0.00	46.00	0.00	0.00	4486.33
14KC2-0.8	69.1	0.00	0.00	0.00	0.00	68.67	0.00	0.00	18256.00
14KC2-0.1	68.4	0.00	0.00	0.00	0.00	0.00	0.00	0.00	32049.00
14KC1-64	64	0.00	0.00	0.00	0.00	0.00	0.00	0.00	6575.33
14KC1-54.6	54.6	0.00	0.00	0.00	0.00	61.50	0.00	0.00	2796.33
14KC1-46	46	0.00	0.00	0.00	0.00	0.00	0.00	0.00	4161.00
14KC1-38.6	38.6	0.00	0.00	0.00	0.00	95.33	0.00	0.00	2882.00
14KC1-20	20	0.00	0.00	0.00	0.00	0.00	0.00	0.00	5662.67
14KC1-17.4	17.4	0.00	0.00	0.00	0.00	35.00	0.00	0.00	3142.50
14KC1-12.9	12.9	0.00	0.00	0.00	0.00	76.00	0.00	0.00	2982.00
14KC1-3.9	3.9	0.00	0.00	0.00	0.00	25.00	0.00	288.00	5229.00
14KC1-2.5	2.5	0.00	0.00	24.00	47.00	0.00	0.00	240.00	14899.00
14KC1-1.5	1.5	0.00	0.00	231.00	0.00	57.00	0.00	233.00	3591.00
14KC1-1.0	1	0.00	0.00	0.00	0.00	46.00	0.00	0.00	5826.00
14KC1-.05	0.05	0.00	0.00	0.00	0.00	42.00	0.00	0.00	9262.00

Appendix E. Phoenix #1 mineralogy and TOC provided by Hutton (2014) unpublished.

Well	Phoenix-1	Phoenix-1	Phoenix-1	Phoenix-1	Phoenix-1	Phoenix-1
Depth	7815.00	7825.50	7837.50	7845.60	7853.40	7865.30
LECO TOC	0.69	0.86	0.98	1.35	1.71	0.71
Weight % Mineralogy						
(Without TOC)						
Quartz	21.2	37.2	66.9	75.2	75.7	49.2
K-Feldspar	0.0	0.0	0.7	0.7	0.5	0.6
Plagioclase	0.0	0.0	0.5	0.5	0.5	0.4
Jarosite	0.0	0.0	0.0	0.0	0.0	0.0
Calcite	72.2	53.8	26.1	12.0	13.7	41.6
Dolomite & Fe-Dolomite	0.7	2.9	1.1	3.9	0.7	1.7
Fluorapatite	0.0	0.0	0.0	0.0	0.0	0.0
Siderite	0.0	0.0	0.0	0.0	0.0	0.0
Pyrite	1.5	1.5	0.8	1.5	2.1	1.3
Marcasite	0.0	0.0	0.0	0.0	0.0	0.0
Total Clay	4.4	4.7	3.9	6.2	6.8	5.4
%Gypsum Removed	0.0	0.0	0.0	0.0	0.0	0.0
%Barite Removed	0.0	0.0	0.0	0.0	0.0	0.0
Relative Clay %						
Illite/Smectite	52.1	50.0	43.4	38.4	34.8	46.2
Illite & Mica	41.8	40.4	50.8	23.3	33.6	28.1
Kaolinite	6.1	9.7	5.8	23.5	21.4	17.8
Chlorite	0.0	0.0	0.0	14.8	10.3	8.0
%S in I/S*	20-30	20-30	20-30	20-30	20-30	20-30
Sum Bulk	100.0	100.1	100.0	100.0	100.0	100.2
Sum Clay	100.0	100.1	100.0	100.0	100.1	100.1
Volume % Composition						
(Includes TOC)						
Quartz	21.4	37.3	66.1	73.9	73.8	49.2
K-Feldspar	0.0	0.0	0.7	0.7	0.5	0.6
Plagioclase	0.0	0.0	0.5	0.5	0.5	0.4
Jarosite	0.0	0.0	0.0	0.0	0.0	0.0
Calcite	71.2	52.7	25.2	11.6	13.0	40.7
Dolomite & Fe-Dolomite	0.7	2.6	1.0	3.6	0.7	1.5
Fluorapatite	0.0	0.0	0.0	0.0	0.0	0.0
Siderite	0.0	0.0	0.0	0.0	0.0	0.0
Pyrite	0.8	0.8	0.4	0.8	1.1	0.7
Marcasite	0.0	0.0	0.0	0.0	0.0	0.0
Illite/Smectite	2.3	2.4	1.7	2.4	2.3	2.5
Illite & Mica	1.8	1.9	1.9	1.4	2.2	1.5
Kaolinite	0.3	0.5	0.2	1.5	1.4	1.0
Chlorite	0.0	0.0	0.0	0.8	0.6	0.4
Kerogen	1.6	1.9	2.2	3.0	3.8	1.6
Total	100.1	100.1	99.9	100.2	99.9	100.1
vClay	4.4	4.8	3.8	6.1	6.5	5.4
Calc. G.D. (g/cc)	2.692	2.679	2.648	2.643	2.634	2.672

Appendix E cont.

Well	Phoenix-1	Phoenix-1	Phoenix-1	Phoenix-1	Phoenix-1	Phoenix-1
Depth	7874.70	7884.70	7896.80	7899.20	7904.30	7905.30
LECO TOC	1.07	0.87	0.64	0.45	1.21	0.82
Weight % Mineralogy						
(Without TOC)						
Quartz	35.3	54.1	21.0	43.0	37.8	54.5
K-Feldspar	0.5	0.0	0.9	0.0	0.6	0.7
Plagioclase	0.5	0.4	1.0	1.6	0.5	0.8
Jarosite	0.0	0.0	0.0	0.0	0.0	0.0
Calcite	29.3	23.1	47.3	3.8	32.8	19.0
Dolomite & Fe-Dolomite	5.0	4.6	7.5	0.8	6.7	11.2
Fluorapatite	0.0	0.0	0.0	0.0	0.0	0.0
Siderite	0.4	0.0	0.0	0.9	0.0	0.0
Pyrite	3.8	2.4	1.5	2.2	8.2	4.0
Marcasite	0.0	0.0	0.6	2.5	0.0	0.4
Total Clay	25.3	15.4	20.2	45.2	13.4	9.4
%Gypsum Removed	0.0	0.0	0.0	0.0	0.7	0.0
%Barite Removed	0.0	0.0	0.0	0.0	0.0	0.0
Relative Clay %						
Illite/Smectite	36.6	48.0	49.2	72.0	43.1	42.1
Illite & Mica	33.0	35.7	38.4	24.8	36.5	29.6
Kaolinite	20.8	11.7	8.5	3.2	13.3	23.0
Chlorite	9.6	4.7	3.8	0.0	7.1	5.2
%S in I/S*	20-30	20-30	20-30	20-30	20-30	20-30
Sum Bulk	100.1	100.0	100.0	100.0	100.0	100.0
Sum Clay	100.0	100.1	99.9	100.0	100.0	99.9
Volume % Composition						
(Includes TOC)						
Quartz	35.5	54.1	21.3	43.6	38.8	55.3
K-Feldspar	0.5	0.0	0.9	0.0	0.6	0.7
Plagioclase	0.5	0.4	1.0	1.6	0.5	0.8
Jarosite	0.0	0.0	0.0	0.0	0.0	0.0
Calcite	28.9	22.6	46.8	3.8	32.8	18.9
Dolomite & Fe-Dolomite	4.6	4.2	7.0	0.8	6.4	10.5
Fluorapatite	0.0	0.0	0.0	0.0	0.0	0.0
Siderite	0.2	0.0	0.0	0.6	0.0	0.0
Pyrite	2.0	1.3	0.8	1.2	4.5	2.1
Marcasite	0.0	0.0	0.4	1.4	0.0	0.2
Illite/Smectite	9.4	7.5	10.1	33.2	5.9	4.0
Illite & Mica	8.3	5.5	7.8	11.3	5.0	2.8
Kaolinite	5.4	1.8	1.8	1.5	1.9	2.2
Chlorite	2.2	0.7	0.7	0.0	0.9	0.5
Kerogen	2.4	2.0	1.5	1.0	2.8	1.9
Total	99.9	100.1	100.1	100.0	100.1	99.9
vClay	25.3	15.5	20.4	46.0	13.7	9.5
Calc. G.D. (g/cc)	2.699	2.676	2.700	2.701	2.752	2.714

Appendix E cont.

Well	Phoenix-1	Phoenix-1	Phoenix-1	Phoenix-1	Phoenix-1	Phoenix-1
Depth	7914.70	7925.60	7936.60	7944.50	7954.90	7964.90
LECO TOC	3.31	4.36	11.20	12.50	0.62	1.06
Weight % Mineralogy						
(Without TOC)						
Quartz	45.0	39.4	38.9	32.1	2.0	11.0
K-Feldspar	0.9	0.7	1.1	1.6	0.0	0.0
Plagioclase	1.0	0.8	1.7	2.6	0.0	0.0
Jarosite	0.0	0.0	0.0	0.0	0.0	0.0
Calcite	12.1	20.0	12.2	17.1	89.2	82.5
Dolomite & Fe-Dolomite	1.2	2.9	3.3	4.4	0.0	1.0
Fluorapatite	0.0	1.5	2.1	1.2	8.7	0.0
Siderite	0.0	0.0	0.0	0.0	0.0	0.0
Pyrite	8.9	9.7	9.1	8.9	0.0	1.1
Marcasite	0.0	0.0	0.0	0.0	0.0	0.0
Total Clay	30.9	25.1	31.5	32.3	0.0	4.3
%Gypsum Removed	0.0	0.0	0.0	0.0	0.0	0.0
%Barite Removed	0.0	0.0	0.0	0.0	0.0	0.0
Relative Clay %						
Illite/Smectite	40.8	40.1	35.9	41.3	0.0	54.9
Illite & Mica	37.3	38.1	43.9	41.9	0.0	35.2
Kaolinite	15.1	16.9	14.7	12.0	0.0	10.0
Chlorite	6.8	5.0	5.5	4.8	0.0	0.0
%S in I/S*	20-30	20-30	20-30	20-30	0.0	20-30
Sum Bulk	100.0	100.1	99.9	100.2	99.9	99.9
Sum Clay	100.0	100.1	100.0	100.0	0.0	100.1
Volume % Composition						
(Includes TOC)						
Quartz	43.6	37.6	31.5	25.2	2.1	11.0
K-Feldspar	0.9	0.7	0.9	1.3	0.0	0.0
Plagioclase	1.0	0.7	1.4	2.0	0.0	0.0
Jarosite	0.0	0.0	0.0	0.0	0.0	0.0
Calcite	11.5	18.7	9.7	13.1	89.0	80.7
Dolomite & Fe-Dolomite	1.0	2.5	2.4	3.2	0.0	0.9
Fluorapatite	0.0	1.2	1.4	0.8	7.5	0.0
Siderite	0.0	0.0	0.0	0.0	0.0	0.0
Pyrite	4.6	4.9	3.9	3.7	0.0	0.6
Marcasite	0.0	0.0	0.0	0.0	0.0	0.0
Illite/Smectite	12.3	9.7	9.2	10.6	0.0	2.4
Illite & Mica	11.1	9.0	11.1	10.5	0.0	1.5
Kaolinite	4.6	4.1	3.8	3.1	0.0	0.4
Chlorite	1.9	1.1	1.3	1.1	0.0	0.0
Kerogen	7.5	9.8	23.2	25.5	1.4	2.4
Total	100.0	100.0	99.8	100.1	100.0	99.9
vClay	29.9	23.9	25.4	25.3	0.0	4.3
Calc. G.D. (g/cc)	2.669	2.656	2.449	2.412	2.722	2.682

Appendix E cont.

Well	Phoenix-1	Phoenix-1	Phoenix-1	Phoenix-1	Phoenix-1	Phoenix-1
Depth	7975.30	7984.70	7996.20	8005.20	8015.30	8025.60
LECO TOC	5.30	1.99	3.64	3.32	4.39	0.26
Weight % Mineralogy						
(Without TOC)						
Quartz	36.9	16.6	33.8	39.0	35.0	26.0
K-Feldspar	0.4	0.0	0.5	0.3	0.9	0.0
Plagioclase	1.3	0.7	1.7	2.2	1.5	2.3
Jarosite	0.0	0.0	0.0	0.0	0.0	0.0
Calcite	26.2	72.8	28.6	32.1	17.1	67.5
Dolomite & Fe-Dolomite	4.7	0.4	4.7	4.8	1.9	0.9
Fluorapatite	2.6	0.0	0.0	0.0	0.0	0.0
Siderite	0.0	0.0	0.0	0.0	0.0	0.0
Pyrite	6.6	2.5	8.1	5.0	12.8	1.1
Marcasite	0.0	0.0	0.0	0.0	0.0	0.0
Total Clay	21.3	7.0	22.6	16.6	30.7	2.2
%Gypsum Removed	0.0	0.0	0.0	0.0	1.1	0.0
%Barite Removed	0.0	0.0	0.0	0.0	0.0	0.0
Relative Clay %						
Illite/Smectite	40.1	59.1	48.3	41.5	36.4	0.0
Illite & Mica	52.1	32.8	40.6	44.9	37.7	63.0
Kaolinite	7.8	8.0	8.5	8.9	18.6	37.0
Chlorite	0.0	0.0	2.6	4.8	7.2	0.0
%S in I/S*	20-30	20-30	20-30	20-30	20-30	0.0
Sum Bulk	100.0	100.0	100.0	100.0	99.9	100.0
Sum Clay	100.0	99.9	100.0	100.1	99.9	100.0
Volume % Composition						
(Includes TOC)						
Quartz	34.1	16.3	32.6	37.4	33.8	26.4
K-Feldspar	0.4	0.0	0.5	0.3	0.9	0.0
Plagioclase	1.2	0.7	1.7	2.1	1.5	2.4
Jarosite	0.0	0.0	0.0	0.0	0.0	0.0
Calcite	23.7	70.0	27.0	30.1	16.1	67.0
Dolomite & Fe-Dolomite	4.0	0.4	4.2	4.3	1.7	0.9
Fluorapatite	2.0	0.0	0.0	0.0	0.0	0.0
Siderite	0.0	0.0	0.0	0.0	0.0	0.0
Pyrite	3.2	1.3	4.1	2.5	6.5	0.6
Marcasite	0.0	0.0	0.0	0.0	0.0	0.0
Illite/Smectite	8.0	4.1	10.6	6.7	10.8	0.0
Illite & Mica	10.2	2.2	8.8	7.1	11.1	1.4
Kaolinite	1.6	0.6	1.9	1.4	5.6	0.8
Chlorite	0.0	0.0	0.5	0.7	1.9	0.0
Kerogen	11.7	4.5	8.2	7.4	10.0	0.6
Total	100.1	100.1	100.1	100.0	99.9	100.1
vClay	19.8	6.9	21.8	15.9	29.4	2.2
Calc. G.D. (g/cc)	2.601	2.663	2.661	2.638	2.685	2.697

Appendix E cont.

Well	Phoenix-1	Phoenix-1	Phoenix-1	Phoenix-1	Phoenix-1
Depth	8034.80	8045.50	8055.20	8064.70	8074.60
LECO TOC	1.06	2.12	4.91	4.13	4.40
Weight % Mineralogy					
(Without TOC)					
Quartz	25.4	25.4	41.8	50.1	47.8
K-Feldspar	0.0	0.0	0.0	0.0	0.5
Plagioclase	0.8	0.6	1.5	2.6	3.4
Jarosite	0.0	0.0	0.0	0.0	0.0
Calcite	26.1	60.9	20.2	11.5	17.3
Dolomite & Fe-Dolomite	0.5	2.1	4.7	6.3	6.0
Fluorapatite	44.0	0.0	0.0	0.0	1.0
Siderite	0.0	0.0	0.0	0.0	0.0
Pyrite	2.5	2.5	7.8	7.3	4.3
Marcasite	0.0	0.0	0.0	0.0	0.0
Total Clay	0.8	8.5	23.9	22.1	19.6
%Gypsum Removed	0.0	0.0	1.0	0.0	0.0
%Barite Removed	0.0	0.0	0.0	0.0	0.0
Relative Clay %					
Illite/Smectite	0.0	40.5	40.7	40.6	38.4
Illite & Mica	0.0	38.4	40.1	38.8	39.2
Kaolinite	100.0	15.4	15.4	15.5	17.8
Chlorite	0.0	5.7	3.8	5.1	4.6
%S in I/S*	0.0	20-30	20-30	20-30	20-30
Sum Bulk	100.1	100.0	99.9	99.9	99.9
Sum Clay	100.0	100.0	100.0	100.0	100.0
Volume % Composition					
(Includes TOC)					
Quartz	27.2	24.9	39.0	47.5	44.5
K-Feldspar	0.0	0.0	0.0	0.0	0.5
Plagioclase	0.9	0.6	1.5	2.5	3.2
Jarosite	0.0	0.0	0.0	0.0	0.0
Calcite	27.2	58.3	18.5	10.7	15.8
Dolomite & Fe-Dolomite	0.5	1.9	4.1	5.6	5.2
Fluorapatite	39.5	0.0	0.0	0.0	0.8
Siderite	0.0	0.0	0.0	0.0	0.0
Pyrite	1.4	1.3	3.8	3.6	2.1
Marcasite	0.0	0.0	0.0	0.0	0.0
Illite/Smectite	0.0	3.4	9.2	8.6	7.1
Illite & Mica	0.0	3.2	8.9	8.1	7.1
Kaolinite	0.9	1.3	3.5	3.3	3.3
Chlorite	0.0	0.4	0.8	1.0	0.8
Kerogen	2.6	4.8	10.9	9.2	9.7
Total	100.2	100.1	100.2	100.1	100.1
vClay	0.9	8.3	22.4	21.0	18.3
Calc. G.D. (g/cc)	2.863	2.656	2.614	2.631	2.594

Appendix F. Phoenix #1 Rock Eval provided by Hutton (2014) unpublished.

Sample Type	Top Measured Depth [m]	Bottom Measured Depth [m]	Rock Unit	S3 [mgCO2/gTOC]	Tmax [deg C]	OI [mgCO2/gTOC]	
CT	7470	7480	none	1.58	428	40	0.05
CT	7560	7570	none	6.65	428	559	0.2
CO	7592	0	none	0.96	0	20	0
CO	7596	0	none	0.3	0	5	0
CO	7597	0	none	26.76	0	603	0
CO	7599	0	none	0.84	0	12	0
CO	7603	0	none	1.92	0	40	0
CO	7606	0	none	0.68	0	15	0
CO	7611	0	none	2.73	0	60	0
CO	7620	0	none	0.77	0	13	0
CO	7620	0	none	1.27	0	23	0
CO	7621	0	none	1.09	0	27	0
CO	7628	0	none	3.38	0	85	0
CO	7633	0	none	0.41	0	7	0
CO	7636	0	none	0.97	0	23	0
CO	7638	0	none	0.79	0	14	0
CO	7643	0	none	0.35	0	10	0
CO	7645	0	none	0.39	0	18	0
CO	7646	0	none	0.33	0	16	0
CO	7650	0	none	10.14	0	476	0
CO	7650	0	none	1.47	0	108	0
CO	7655	0	none	0.65	0	30	0
CO	7663	0	none	0.37	0	13	0
CO	7663	0	none	0.7	0	50	0
CO	7668	0	none	0.33	0	22	0
CO	7671	0	none	0.88	0	48	0
CO	7683	0	none	0.53	0	29	0
CO	7693	0	none	0.51	0	25	0
CO	7813.3	0	none	0.54	445	25	0.2
CO	7818.7	0	none	0.67	438	19	0.15
CO	7825.9	0	none	0.55	438	36	0.34

Appendix F cont.

Sample Type	Top Measured Depth [m]	Bottom Measured Depth [m]	Rock Unit	S3 [mgCO2/gTOC]	Tmax [deg C]	OI [mgCO2/gTOC]	
CO	7833.6	0	none	0.63	438	27	0.12
CO	7839.8	0	none	0.54	437	22	0.18
CO	7847.4	0	none	0.63	436	37	0.25
CO	7849.5	0	none	0.58	440	30	0.29
CO	7855.1	0	none	0.76	435	48	0.39
CO	7857.7	0	none	0.68	446	25	0.32
CO	7864.6	0	none	0.67	447	48	0.28
CO	7870.2	0	none	0.59	446	43	0.36
CO	7876.2	0	none	0.69	434	16	0.12
CO	7881.2	0	none	0.26	459	21	0.17
CT	7890	7900	none	9.81	429	104	0.06
CO	7893.7	0	none	0.65	0	41	0.15
CO	7897.2	0	none	0.82	448	51	0.12
CO	7901.9	0	none	0.98	453	61	0.2
CO	7912.8	0	none	1.52	439	23	0.07
CO	7918.2	0	none	1.25	447	22	0.05
CO	7924.6	0	none	0.54	438	7	0.06
CO	7930.4	0	none	0.37	434	26	0.27
CO	7931.7	0	none	0.59	434	14	0.06
CO	7932.7	0	none	0.27	439	4	0.05
CO	7941.3	0	none	0.56	438	6	0.05
RCO	7941.6	7946.4	none	0.69	430	8	0.03
RSO	7941.6	7946.4	none	0.99	445	17	0.27
CO	7946.4	0	none	0.37	441	4	0.04
CO	7946.8	0	none	0.55	434	13	0.12
CO	7949.9	0	none	0.53	436	19	0.12
CT	7950	7960	none	1.79	430	45	0.03
CO	7953	0	none	0.4	438	32	0.16
CO	7957.5	0	none	0.42	441	6	0.03
CO	7966.3	0	none	0.51	443	8	0.03
CO	7972.3	0	none	0.63	442	11	0.03

Appendix F cont.

Sample Type	Top Measured Depth [m]	Bottom Measured Depth [m]	Rock Unit	S3 [mgCO2/gTOC]	Tmax [deg C]	OI [mgCO2/gTOC]	
CO	7974.6	0	none	0.42	439	29	0.08
CO	7975	0	none	0.37	440	18	0.04
CO	7976.4	0	none	0.62	440	8	0.03
CO	7984.1	0	none	0.74	431	39	0.04
CO	7992.3	0	none	0.57	438	19	0.03
CO	7995.4	0	none	0.8	432	25	0.04
CO	8001.3	0	none	1.17	433	18	0.04
CO	8006.3	0	none	0.88	436	17	0.05
CO	8012.2	0	none	1.04	439	15	0.04
CO	8013.7	0	none	1.14	442	22	0.05
CO	8020.5	0	none	1.07	431	102	0.16
CO	8023.2	0	none	0.98	0	34	0.39
CO	8026.7	0	none	0.19	438	6	0.06
CO	8029.3	0	none	0.23	0	46	0.21
CO	8034.9	0	none	0.43	432	26	0.27
CO	8037.5	0	none	0.58	435	17	0.07
CO	8039.7	0	none	0.59	435	59	0.15
CO	8039.8	0	none	0.51	438	19	0.09
CT	8040	8050	none	4.91	428	104	0.08
CO	8049.3	0	none	0.59	435	20	0.08
CO	8054.6	0	none	0.51	444	13	0.08
CO	8060.9	0	none	0.63	451	7	0.05
CO	8063.6	0	none	0.26	444	8	0.08
CO	8066.4	0	none	0.42	445	4	0.06
CO	8069.9	0	none	0.62	442	7	0.06
CT	8070	8080	none	5.71	427	89	0.07
CO	8074.8	0	none	0.44	444	6	0.09
CO	8078.1	0	none	0.34	442	3	0.07
CO	8079.1	0	none	0.39	442	15	0.17
CO	8082.8	0	none	0.82	444	6	0.07

Appendix F cont.

Sample Type	Top Measured Depth [m]	Bottom Measured Depth [m]	TOC [wt-%]	S1 [mgHC/gRock]	S2 [mgHC/gRock]	HI [mgHC/gTOC]	Assumed HIO [mgHC/gTOC]	Assumed PIO [%]
CT	7470	7480	3.93	0.74	13.68	348	0	0
CT	7560	7570	1.19	0.37	1.48	124	0	0
CO	7592	0	4.76	0	2.8	59	0	0
CO	7596	0	6.05	0	1.33	22	0	0
CO	7597	0	4.44	0	0.35	8	0	0
CO	7599	0	6.76	0	2.42	36	0	0
CO	7603	0	4.82	0	2.11	44	0	0
CO	7606	0	4.63	0	2.7	58	0	0
CO	7611	0	4.56	0	2.74	60	0	0
CO	7620	0	6	0	1.71	29	0	0
CO	7620	0	5.42	0	0.27	5	0	0
CO	7621	0	3.98	0	1.95	49	0	0
CO	7628	0	3.98	0	1.49	37	0	0
CO	7633	0	5.53	0	1.2	22	0	0
CO	7636	0	4.24	0	1.63	38	0	0
CO	7638	0	5.5	0	1.33	24	0	0
CO	7643	0	3.68	0	1.42	39	0	0
CO	7645	0	2.21	0	1.36	62	0	0
CO	7646	0	2.05	0	0.82	40	0	0
CO	7650	0	2.13	0	0.24	11	0	0
CO	7650	0	1.36	0	0.35	26	0	0
CO	7655	0	2.19	0	1.42	65	0	0
CO	7663	0	2.87	0	1.81	63	0	0
CO	7663	0	1.4	0	2.02	144	0	0
CO	7668	0	1.49	0	0.48	32	0	0
CO	7671	0	1.82	0	3.38	185	0	0
CO	7683	0	1.81	0	2.98	164	0	0
CO	7693	0	2.05	0	2.59	126	0	0
CO	7813.3	0	2.18	2.24	8.88	407	0	0
CO	7818.7	0	3.56	2.2	12.27	345	0	0
CO	7825.9	0	1.53	1.19	2.3	151	0	0

Appendix F cont.

Sample Type	Top Measured Depth [m]	Bottom Measured Depth [m]	TOC [wt-%]	S1 [mgHC/gRock]	S2 [mgHC/gRock]	HI [mgHC/gTOC]	Assumed HIO [mgHC/gTOC]	Assumed PIO [%]
CO	7833.6	0	2.34	1.54	11.14	476	0	0
CO	7839.8	0	2.46	2	9.01	366	0	0
CO	7847.4	0	1.69	1.67	4.98	294	0	0
CO	7849.5	0	1.91	2.22	5.49	287	0	0
CO	7855.1	0	1.58	1.47	2.29	145	0	0
CO	7857.7	0	2.77	3.27	6.8	245	0	0
CO	7864.6	0	1.39	0.85	2.16	155	0	0
CO	7870.2	0	1.36	2	3.57	262	0	0
CO	7876.2	0	4.19	2.4	17.31	413	0	0
CO	7881.2	0	1.26	0.33	1.66	132	0	0
CT	7890	7900	9.43	0.49	7.81	83	0	0
CO	7893.7	0	1.58	0.24	1.34	85	0	0
CO	7897.2	0	1.61	0.27	2.06	128	0	0
CO	7901.9	0	1.61	0.54	2.11	131	0	0
CO	7912.8	0	6.5	3.14	38.93	599	0	0
CO	7918.2	0	5.77	2.39	48.5	840	0	0
CO	7924.6	0	7.43	3.47	59.31	798	0	0
CO	7930.4	0	1.41	4.93	13.6	965	0	0
CO	7931.7	0	4.25	1.92	32.48	764	0	0
CO	7932.7	0	6.63	2.99	58.59	884	0	0
CO	7941.3	0	8.94	3.92	75.15	841	0	0
RCO	7941.6	7946.4	7.99	1.41	50.31	629	0	0
RSO	7941.6	7946.4	5.59	2.09	5.64	100	0	0
CO	7946.4	0	8.97	3.25	73.58	820	0	0
CO	7946.8	0	4.25	5	36.77	865	0	0
CO	7949.9	0	2.77	2.26	16.06	580	0	0
CT	7950	7960	3.95	0.56	18.45	467	0	0
CO	7953	0	1.25	0.47	2.45	196	0	0
CO	7957.5	0	7.44	1.6	49.87	670	0	0
CO	7966.3	0	6.21	1.27	35.97	579	0	0
CO	7972.3	0	5.58	1.3	43.01	771	0	0

Appendix F cont.

Sample Type	Top Measured Depth [m]	Bottom Measured Depth [m]	TOC [wt-%]	S1 [mgHC/gRock]	S2 [mgHC/gRock]	HI [mgHC/gTOC]	Assumed HIO [mgHC/gTOC]	Assumed PIO [%]
CO	7974.6	0	1.43	0.29	3.28	229	0	0
CO	7975	0	2.08	0.39	10.58	508	0	0
CO	7976.4	0	7.44	1.53	55.36	744	0	0
CO	7984.1	0	1.87	0.39	9.78	523	0	0
CO	7992.3	0	3.07	0.59	18.11	590	0	0
CO	7995.4	0	3.16	0.74	16.8	532	0	0
CO	8001.3	0	6.48	1.78	38.54	595	0	0
CO	8006.3	0	5.03	1.29	26.72	531	0	0
CO	8012.2	0	6.84	1.86	45.31	662	0	0
CO	8013.7	0	5.28	1.8	34.67	657	0	0
CO	8020.5	0	1.05	0.34	1.74	166	0	0
CO	8023.2	0	2.85	0.52	0.82	29	0	0
CO	8026.7	0	3.06	1.42	21.09	689	0	0
CO	8029.3	0	0.5	0.21	0.77	154	0	0
CO	8034.9	0	1.62	2.33	6.19	382	0	0
CO	8037.5	0	3.42	1.9	26.18	765	0	0
CO	8039.7	0	0.99	0.64	3.73	377	0	0
CO	8039.8	0	2.66	1.33	12.91	485	0	0
CT	8040	8050	4.72	0.5	5.6	119	0	0
CO	8049.3	0	2.88	1.52	18.3	636	0	0
CO	8054.6	0	3.93	1.98	23.81	606	0	0
CO	8060.9	0	8.57	3.51	61.34	716	0	0
CO	8063.6	0	3.26	1.6	18.46	566	0	0
CO	8066.4	0	10.04	1.97	28.77	287	0	0
CO	8069.9	0	9.07	3.85	62.56	690	0	0
CT	8070	8080	6.45	0.61	8.27	128	0	0
CO	8074.8	0	6.78	4.68	48.27	712	0	0
CO	8078.1	0	10.2	4.91	67.47	661	0	0
CO	8079.1	0	2.6	2.76	13.44	517	0	0
CO	8082.8	0	13.05	6.26	84.7	649	0	0

References

Amorosi, A., 2012, The occurrence of glaucony in the stratigraphic record: distribution patterns and sequence-stratigraphic significance. In: Morad, S., Ketzer, J.M., De Ros, L.F. (Eds.), Linking Diagenesis to Sequence Special Publication of the International Association of Sedimentology 45. Wiley-Blackwell, p. 37-54.

Baccelle, L. and Bosellini, A., 1965, Diagrammi per Ia stima visiva della composizione percentuale nelle rocche sedimentaie.- Annali deii' Universita di Ferrara (Nuova Serie), Sezione 9, Scienze geologiche e paleontologiche, v. 1, n. 3, p. 59-62.

Berndmeyer, C., Birgel, D., Brunner, B., Wehrmann, L. M., Jöns, N., Bach, W., Arning, E. T., Föllmi, K. B., and Peckmann, J., 2012, The influence of bacterial activity on phosphorite formation in the Miocene Monterey Formation, California: Palaelogeography, Palaeoclimatology, Palaoecology, v. 317-318, p. 171-181.

Bird, K. J., and Molenaar, C. M., 1987, Petroleum Geology of the Northern Part of the Arctic National Wildlife Refuge, Northeastern Alaska: U.S. Geological Survey Bulletin 1778, p. 37-59.

Bohacs, K. M., Grabowski Jr. G J., Carroll, A. R., Mankiewicz, P. J., Miskell-Gerhardt, K. J., Schwalbach, J. R., Wegner, M. B., and Simo, J. A., 2005, Production, destruction, and dilution-- the many paths to source-rock development: Society for Sedimentary Geology Special Pudblication, n. 82, p. 61-101.

Burchette, T. P., and Wright, V. P. 1992, Carbonate ramp depositional systems: Sedimentary Geology, n. 79, p. 3-57.

Campbell, Charles V., 1967, Lamina, laminaset, bed, and bedset: Sedimentology, v. 8, p. 7-26.

Decker, P.L., 2011, Source-reservoired Oil Resources, Alaskan North Slope: Newsletter of the Alaska Geological Society, September.

Detterman, R. L., 1989, Triassic phosphate deposits, north-eastern Alaska, *in* Notholt, A. J. G., Sheldon, R. P., and Davidson, D. F., eds., Phosphate deposits of the world: Cambridge University Press, v. 2, p. 14-17.

Detterman, R. L., Reiser, H. N., Brosge', W. P., and Dutro Jr., J. T., 1975, Post-Carboniferous stratigraphy, northeastern Alaska: U.S. Geological Survey Professional Paper 886, p. 1-46.

Dingus, A.S., 1984, Paleoenvironmental reconstruction of the Shublik Formation on the North Slope of Alaska: Master's Thesis, University of California, Berkeley, California, p. 108.

Donovan, A. D., Staerker, T. S., Pramudito, A., Li, W., Corbett, M. J., Lowery, C. M., Romero, A. M., and Gardner, R. D., 2012, The Eagle Ford Outcrops of West Texas: A Laboratory for Understnding Heterogeneities within Unconventional Mudstone Reservoirs: Gulf Coast Associations of Geological Societies, v. 1,p. 162-185

Droser, M. L., and Bottjer, D. J., 1986, A semiquantitative field classification of ichnofabrics: Journal of Sedimentary Research, v. 56, n. 4, p. 558-559.

Droser, D M.L., and Bottjer, D.J., 1989, Ichnofabric of sandstones deposited in high-energy nearshore environ-ments: measurement and utilization: Palaios, v. 4, p. 598-604.

Dunham, R. J., 1962, Classification of carbonate rocks according to depositional texture: AAPG Memoir, v. 1, p. 108-121.

Embry III, A. F. and Klovan, J. E., 1971, A Late Devonian reef tract on northeastern Banks Island, NWT: Bulletin of Canadian Petroleum Geology, v. 19, n. 4, p. 730-781.

Filippelli, G. M., 2011, Phosphate rock formation and marine phosphorus geochemistry: the deep tme perspective: Chemosphere, v. 84, n. 6, p. 759-766.

Flügel, E., 2004, Microfacies of carbonate rocks: analysis, interpretation, and application: Springer Verlag.

Föllmi, K. B., 1996, The phosphorus cycle, phosphogenesis and marine phosphate-rich deposits: Earth-Science Reviews, v. 40, p. 55-124.

Folk, R. L., 1959, Practical petrographic classification of limestones: AAPG Bulletin, v. 43, p. 1-38.

Folk, R. L., 1965, Some aspects of recrystallization in ancient limestones, *in* L. C. Pray, and R.S. Murray, eds., Dolomitization and Limestone diagenesis: Tulsa, OK, SEPM Special Publication, n. 13, p. 14-48.

Hart, B. S., Macquaker, J. H. S., and Taylor, K. G., 2013, Mudstone ("shale") depostional and diagenetic processes: Impications for seismic analyses of source-rock reservoirs: Interpretation, v. 1, n. 1, p. B7-B26.

Haskett, W. J., and Brown, P. J., 2005, Evaluation of Unconventional Resource Plays: Society of Petroleum Engineers presented at SPE Annual Technical Conference and Exhibition, Dallas, Texas, Paper SPE-96879-MS, p.1-11.

Houseknecht, D. W., Rouse, W. A., Garrity, C. P., Whidden, K.J., Dumoulin, J. A., Schenk, C. J., Charpenter, R. R., Cook, T. A., Gaswirth, S. B., Kirschbaum, M. A., and Pollastro, R. M., 2012, Assement of potential oil and gas resources in source rocks of the Alaska North Slope, 2012: US Geologic Survey, n. 2012-2013.

Houseknecht, D. W., and Bird, K. J., 2005, Oil and Gas Resources of the Arctic Alaska Petroleum Province: U.S. Geological Survey Professional Paper 1732-A, p. 11.

Hubbard, R. J., Edrich, S. P., and Rattey, R. P., 1987, Geologic evolution and hydrocarbon habitat of the 'Arctic Alaska Microplate': Marine and Petroleum Geology, v. 4, no. 1, p. 2-34.

Hulm, E. J., 1999, Subsurface facies architecture and sequence stratigraphy of the Eileen Sandstone, Shublik Formation, and Sag River Sandstone, Arctic Alaska [Master of Science: University of Alaska Fairbanks, 105 p.

Hutton, E. M., 2014, Surface to subsurface correlation of the Shublik Formation: Implications for Triassic paleoceanography and source rock accumulation [Master's of Science: University of Alaska Fairbanks, 123 p.

Jarvie, D. M., 2012a, Shale Resource Systems for Oil and Gas: Part 1-Shale-Gas Resource Systems: AAPG Memoir, J. A. Breyer, ed., Shale reservoirs-Giant resources for the 21st century, v. 97, p. 69-87.

Jarvie, D. M., 2012b, Shale Resource Systems for Oil and Gas: Part 2-Shale-Oil Resource Systems: AAPG Memoir, J. A. Breyer, ed., Shale reservoirs-Giant resources for the 21st century, v. 97, p. 89-119.

Jarvie, D. M., Hill, R. J., Ruble, T. E., and Pollastro, R., M., 2007, Unconventional shale-gas systems: The Mississippian Barnett Shale of north-central Texas as on model for themogenic shale-gas assessment: AAPG Bulletin, v. 91, n. 4, p. 475-499.

Johnson, K.J., Riordan, J.A., Papp, K.R., Johnson, K.A., Skutca, J.E., Mansavage, H.L., and Hartman, D., 2010, The Alaska Geological Materials Center Inventory: State of Alaska, Department of Natural Resources, Division of Geological & Geophysical Surveys, Eagle River, Alaska - USA

Kelly, L. N., 2004, High resolution sequence stratigraphy and geochemistry of middle and upper triassic sedimentary rocks, northeas and central Brooks Range, Alaska [Master's of Science: University of Alaska Fairbanks, 224 p.

Kelly, L. N., Whalen, M. T., McRoberts, C. A., Hopkin, E., and Tomsich, C. S., 2007, Sequence stratigraphy and geochemistry of the upper Lower through Upper Triassic of Northern Alaska: Implications for paleoredox history, source rock accumulation and paleoceanography: Division of Geological and Geophysical Surveys, Alaska, Report of Investigations, n. 2007-1, p. 1-50.

Kupecz, J. A., 1995, Depositional setting, sequence stratigraphy, diagenesis, and reservoir potential of a mixed-lithology, upwelling deposit, Upper Triassic Shublik Formation, Prudhoe Bay, Alaska: AAPG Bulletin, v. 79, p. 1301-1319.

Loucks, R. G., Reed, R. M., Rupple, S. C., and Hammes, U., 2012, Spetrum of pore types and networks in mudrocks and a descriptive classification for matrix-related mudrock pores: AAPG Bulletin, v. 96, n. 6, 1071-1098.

MacQuaker, J. H. S., and Adams, A. E., 2003, Maximizing Information from Fine-grained Sedimentary Rocks: An Inclusive Nomenclature for Mudstones: Journal of Sedimentary Research, v. 73, n. 5, p. 735-744.

McRoberts, C. A., 2008, Rhaetian (Late Triassic) *Monotis* (Bivalvia:Pectinoida) from the Eastern Northern Calcareous Alps (Austria and the End-Norian crisis in pelagic faunas: Palaeontology, v. 51, part 3, p. 721-735.

McRoberts, C. A., 2010, Biochronology of Triassic bivalves, *in* Lucas, S.G., ed., The Triassic TImescale, Geological Society of London Special Publications, v. 334, p. 201-219.

McRoberts, C. A., 2011, Late Triassic Bivalvia (Chiefly Halobiidae and Monotidae) From the Pardonet Formation, Williston Lake Area, Northeastern British Columbia, Canada: Journal of Paleontology, v. 85, n. 4, p. 613-664

Milliken, K. L., Esch, W. L., Reed, R. M., and Zhang, T., 2012, Grain assemblages and strong diagentic overprinting in siliceous mudstones, Barnett Shale (Mississippian), Fort Worth Basin, Texas: AAPG Bulletin, v. 96, n. 8, p. 1553-1578

Milliken, K. L., and Reed, R. M., 2010, Multiple causes of diagenetic fabric anisotropy in weakly consolidated mud, Nankai accretionary prism, IODP Expedition 316: Journal of Sturctural Geology, v. 32, n. 12, p. 1887-1898.

Mitchum Jr., R. M., and Van Wagoner, J. C., 1991, High-frequency sequences and their stacking patterns: sequence-stratigraphic evidence of high-frequency eustatic cycles: Sedimentary Geology, v. 70, p. 131-160.

Moore, T. E., Wallace, W. K., Bird, K. J., Karl, S. M., Mull, G. C., and Dillon, J. T., 1994, Geology of Northern Alaska, *in* Plafker, G., and Berg, H. C., eds., The Geology of Alaska, Volume G-1: Boulder, Colorado, Geological Society of America, p. 49-140.

Parrish, J. T., 1982, Upwelling and Petroleum Source Beds, With Reference to Paleozoic: AAPG Bulletin, v. 66, no. 6, p. 750-774.

Parrish, J. T., Droser, M. L., and Bottjer, D. J., 2001a, A Triassic upwelling Zone: the Shublik Formation, Arctic Alaska, U.S.A.: Journal of Sedimentary Research, no. 71, p. 272-285.

Parrish, J. T., Whalen, M. T., and Hulm, E. J., 2001b, Shublik Formation Lithofacies, Environments, and Sequence Stratigraphy, Arctic Alaska, U.S.A., *in* Houseknecht, D. W., ed., Petroleum Plays and Systems in the National Petroleum Reserve-Alaska: SEPM Core Workshop, p. 89-110.

Passey, Q. R., Bohacs, K. M., Esch, R. K., and Sinha, S., 2010, From Oil-Prone Source Rock to Gas-Produding Shale Reservoir- Geologic and Petrophysical Characterization of Unconventional Shale-Gas Reservoirs: Society fo Petroleum Engineers, n. 131350, p. 1-29.

Peters, K. E., Magoon, L. B., Bird, K. J., Valin, Z. C., and Keller, M. A., 2006, North Slope, Alaska: Source rock distribution, richness, thermal maturity, and petroleum charge: AAPG Bulletin, v. 90, no. 2, p. 261-292.

Piper, D. Z., and Link, P. K., 2002, Upwelling model for the Phosphoria sea: A Permian ocean-margin sea in the northwest United States: AAPG Bulletin, v. 86, no. 7, p. 1217-1234.

Ratcliffe, K. T., Wright, A. M., Schmidt, K., 2012, Application of Inorganic Whole-Rock Geochemistry to Shale Resource Plays: An Example from the Eagle Ford Shale Formation, Texas: The Sedimentary Record, v.10, no. 2, p. 4-9.

Robison, V. D., Liro, L. M., Robison, C. R., Dawson, W. C., and Russo, J. W., 1996, Integrated geochemistry, organic petrology, and sequence stratigraphy of the Triassic Shublik Formation, Tenneco Phoenix # 1 well, North Slope, Alaska, U.S.A.: Organic Geochemistry, v. 24, n. 2, p. 257-272.

Scheirer, A. H., Magoon, L. B., Bird, K. J., Duncan, E., and Peters, K. E., 2014, Toward Successful Petroleum Production from Unconventional and Conventional Reservoirs in the Central Alaska North Slope.

Slatt, R. M., 2011, Important Geological Properties of Unconventional Resource Shales: Central European Journal of Geosciences, v. 3, n. 4, p. 435-448

Slatt, R. M., 2013, Unconventional Resource Shales. In *Stratigraphic Reservoir Characterization for Petroleum Geologists, Geophysiscists, and Engineers,* v. 61, (p. 554-616) Oxford, UK: Elsevier.

Slatt, R. M., and Abousleiman, Y., 2011, Merging sequence stratigraphy and geomechanics for unconventional gas shales: The Leading Edge, n. 30, p. 274-282.

Slatt, R. M., and O'Brien, N. R., 2011, Pore types in the Barnett and Woodfor gas shales: Contribution to understanding gas storage and migration pathways in fine-grained rocks: AAPG Bulletin, v. 95, n. 12, p. 2017-2030.

Van Wagoner, J. C., Mitchum, R. M., Campion, K. M., and Rahmanian, V.D., 1990, Siliciclastic sequence stratigraphy in well logs, cores, and outcrops: concepts for high-resolution correlation of time and facies: AAPG Methods in Exploration Series, no., 7, p. 1-55.

White, S. H., Shaw, H. F., and Hugget, J. M., 1984, The Use of Back-Scatter Electron Imaging for the Petrographic Study of Sandstones and Shales: Journal of Sedimentary Petrology, v. 54, n. 2, p. 487-494.

Wingall, P. B. and Simms, M. J., 1990, Psuedoplankton: Palaeontology, v. 33, n. 2, p. 359-378.

Wright, A. M., Spain, D., and Ratcliffe, K. T., 2010, Application of Inorganic Whole Rock Geochemistry to Shale Resource Plays: Society of Petroleum Engineers, n. 137946, p. 1-18.

Yurchenko, I. A., 2017, Stratigraphic and depositional controls on source rock heterogeneity and composition of expelled petroleum in the Triassic Shublik Formation of Arctic Alaska: Doctorate of Philosophy dissertation, Stanford Universtiy, p. 192.